

AD-A059 905

NAVAL POSTGRADUATE SCHOOL MONTEREY CALIF
TESTS OF A MESOSCALE MODEL OVER EUROPE AND THE UNITED STATES. (U)
AUG 78 R A ANTHES
NPS-63-78004

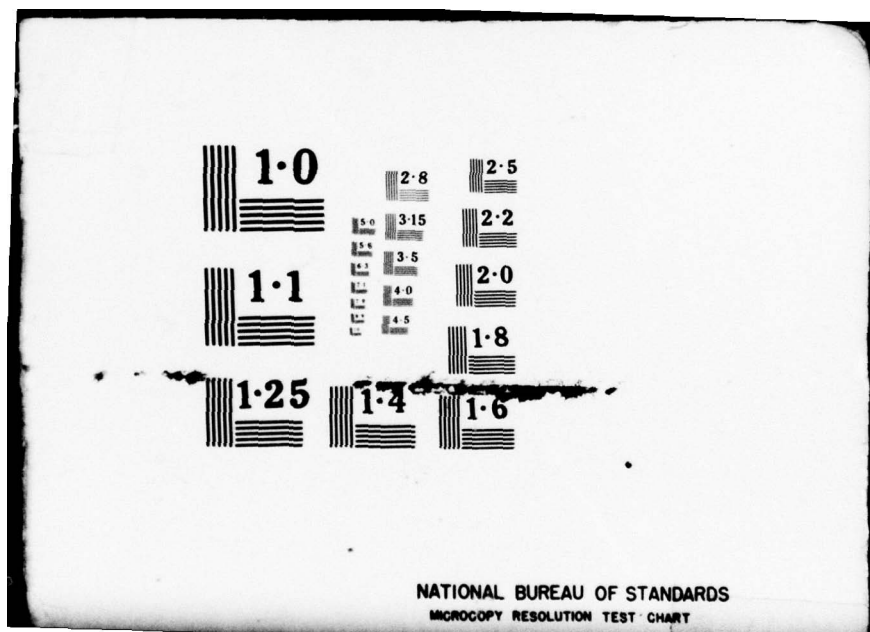
F/G 4/2

UNCLASSIFIED

NL

1 OF 2
ADA
069905





AD A0 59905

LEVEL II
NAVAL POSTGRADUATE SCHOOL
Monterey, California



DDC FILE COPY

TESTS OF A MESOSCALE MODEL
OVER EUROPE AND THE UNITED STATES

Richard A. Anthes

August 1978

Technical Report
Period:

1 October 1977 to
22 September 1978

Approved for public release; distribution unlimited.

Prepared for:
Commander, Naval Air Systems Command,
Department of the Navy
Washington, D. C. 20361

78 10 06 013

NAVAL POSTGRADUATE SCHOOL
Monterey, California

Rear Admiral Tyler F. Dedman
Superintendent

Jack R. Borsting
Provost

ABSTRACT

A total of 32 twenty-four-hour forecasts using a six-layer, 60-km mesh model have been run over western Europe and the eastern United States. The forecasts showed considerable skill in forecasting cyclogenesis over the Mediterranean and the U.S. The average 24-hour S_1 score for sea-level pressure was 39.1 compared to an average of 45.9 for the FNWC operational model and 73.4 for persistence.

Three forecasts were discussed in detail. The first was a case of cyclogenesis in the Gulf of Genoa which was forecast well by the model. The second was a forecast of the intense Ohio blizzard of January 26, 1978, which was also reasonably successful. The third forecast greatly overpredicted the intensity of a cyclone along the southern coast of the U.S. Latent heat and the parameterization of cumulus convection were dominant factors in producing this fictitious intensification.

The major conclusion from this study is that significant improvements in 24-hour sea-level pressure forecasts were obtained by a model with high horizontal resolution, even though the vertical resolution was coarse and the physics in the model was simple. It appears likely, therefore, that further increases in forecast accuracy are possible by refining the vertical resolution and improving the physics.

Richard A. Anthes

Richard A. Anthes
Professor of Meteorology

Approved by:

G. J. Haltiner

G. J. Haltiner, Chairman
Department of Meteorology

Released by:

William M. Tolles

W. M. Tolles
Dean of Research

This task was supported by:

Naval Air Systems Command
Department of the Navy
Washington, D. C. 20361

UNCLASSIFIED

SECURITY CLASSIFICATION OF THIS PAGE (When Data Entered)

REPORT DOCUMENTATION PAGE		READ INSTRUCTIONS BEFORE COMPLETING FORM
1. REPORT NUMBER NPS-63-78004	2. GOVT ACCESSION NO.	3. RECIPIENT'S CATALOG NUMBER
4. TITLE (and subtitle) Tests of a Mesoscale Model over Europe and the United States.		5. TYPE OF REPORT & PERIOD COVERED Technical Report 1 Oct 1978 - 31 Jul 1978
6. PERFORMING ORG. REPORT NUMBER		7. AUTHOR(s) Richard A. Anthes
8. CONTRACT OR GRANT NUMBER(s)		9. PERFORMING ORGANIZATION NAME AND ADDRESS Naval Postgraduate School Monterey, California 93940
10. PROGRAM ELEMENT, PROJECT, TASK AREA & WORK UNIT NUMBERS 61153N; N00019-78-WR-81002		11. CONTROLLING OFFICE NAME AND ADDRESS Naval Air Systems Command Washington, D. C. 20361
12. REPORT DATE August 1978		13. NUMBER OF PAGES 107
14. MONITORING AGENCY NAME & ADDRESS (if different from Controlling Office)		15. SECURITY CLASS. (of this report) Unclassified
16. DISTRIBUTION STATEMENT (of this Report) Approved for public release; distribution unlimited.		15a. DECLASSIFICATION/DOWNGRADING SCHEDULE
17. DISTRIBUTION STATEMENT (of the abstract entered in Block 20, if different from Report) Technical rept. 1 Oct 77-22 Sep 78		
18. SUPPLEMENTARY NOTES		
19. KEY WORDS (Continue on reverse side if necessary and identify by block number) Forecasting Cyclogenesis; FNWC Operational Model: Cumulus Convection;		
20. ABSTRACT (Continue on reverse side if necessary and identify by block number) A total of 32 twenty-four-hour forecasts using a six-layer, 60-km mesh model have been run over western Europe and the eastern United States. The forecasts showed considerable skill in forecasting cyclogenesis over the Mediterranean and the U.S. The average 24-hour S_1 score for sea-level pressure was 39.1 compared to an average of 45.9 for the FNWC operational model and 73.4 for persistence. → next page		

UNCLASSIFIED

SECURITY CLASSIFICATION OF THIS PAGE(When Data Entered)

Three forecasts were discussed in detail. The first was a case of cyclogenesis in the Gulf of Genoa which was forecast well by the model. The second was a forecast of the intense Ohio blizzard of January 26, 1978, which was also reasonably successful. The third forecast greatly overpredicted the intensity of a cyclone along the southern coast of the U.S. Latent heat and the parameterization of cumulus convection were dominant factors in producing this fictitious intensification.

The major conclusion from this study is that significant improvements in 24-hour sea-level pressure forecasts were obtained by a model with high horizontal resolution, even though the vertical resolution was coarse and the physics in the model was simple. It appears likely, therefore, that further increases in forecast accuracy are possible by refining the vertical resolution and improving the physics.

ACCESSION for *W. E. Johnson*

NTIS	Classification	<input type="checkbox"/>
DOC	Ref. Ser. No.	<input type="checkbox"/>
UNANNOUNCED		
Justification		
By		
DISTRIBUTION/AVAILABILITY COPIES		
SPECIAL		
Dist.		
<i>[Handwritten Signature]</i>		

UNCLASSIFIED

3 SECURITY CLASSIFICATION OF THIS PAGE(When Data Entered)

List of Figures

<u>Fig #</u>	<u>Caption</u>
1	Horizontal domain and terrain elevations (m) for European forecasts. Spacing between tick marks is approximately 60 km.
2	As in Fig. 1 for U.S. domain
3a(top)	Plot of vertical velocity ω at level six ($\sigma = 0.925$) along a west-east line through the middle of the domain in a preliminary experiment with ($v = 0.1$) and without ($v = 0$) temporal filtering.
3b(bottom)	$p_s - p_t$ at a particular grid point every time step for the last 25 minutes of a 12-h forecast with ($v = 0.1$) and without ($v = 0$) temporal filtering.
4	Horizontal variations of erroneous temperature changes and vertical velocities at 1, 2 and 3 hours at $\sigma = 0.925$ across a mountain in a preliminary experiment. Top: temperature change. Middle: vertical velocity. Lower: terrain elevation. The width of the mountain top is 1 grid length (60 km); the total horizontal domain shown in figure is 1140 km.
5	Noise in a <u>typical forecast</u> as shown by the temporal variation of $ \frac{\partial p^*}{\partial t} $ and $ \frac{\partial^2 p^*}{\partial t^2} $ in forecast US06.
6	24-h forecast of (SLP-1000 mb) VT 78011300. Contour interval is 4 mb. (a) Unsmoothed; central pressure is 991 mb. (b) Smoothed using smoothing operator 5 (see Table 6 and Eq. 13). Central pressure is 993 mb.
7	(a) FNWC analysis of SLP at 78011300. Isobaric interval is 4 mb. Central pressure is 998 mb. (b) Simplified operational surface analysis for 78011300 produced by U.S. Navy at Rota, Spain. (c) 24-h forecast of (SLP-1000 mb) VT 78011300 by FNWC operational model. Central pressure is 990 mb.
8	24-h forecast vs. observed minimum pressures of cyclones over the interior of the domain (at least 5 grid points or 300 km from the lateral boundary) for the 32 control forecasts.
9	Balanced (a) and 24-h forecast (b) D-values (m) and temperatures ($^{\circ}$ C) at 500 mb for 78011300. The contour interval for the D-values (solid lines) is 60 m; the isotherm (dashed lines) interval is 5° C.

<u>Fig #</u>	<u>Caption</u>
10	24-h forecast winds ($m s^{-1}$) and relative vorticity (solid lines in $10^{-5} s^{-1}$) at 300 mb for 78011300. The maximum value of the relative vorticity along the coast of France is $18 \times 10^{-5} s^{-1}$. The maximum wind speed associated with the jet streak over the Bay of Biscay is $65 m s^{-1}$.
11	Vertical cross section along a line oriented approximately NW to SSE across the middle of the European domain constructed from a 24-h model forecast VT 78011300. Solid lines are potential temperature in K; dashed lines are wind component ($m s^{-1}$) normal to cross section with negative values out of figure and positive values into figure.
12	Forecast precipitation (cm) for 24 hours ending 78011300.
13	(a) Observed SLP-1000 mb VT 78012612. The minimum pressure is 958 mb. (b) 24-h forecast SLP-1000 mb and winds ($m s^{-1}$) at $\sigma = 0.925$ VT 78012612. The central pressure is 955 mb. (c) 24-h forecast SLP-1000 mb VT 78012612 by FNWC model. Central pressure is 985 mb. (d) As in 13(b) except surface friction present over entire domain. The minimum pressure is 978 mb.
14	Balanced (a) and 24-h forecast (b) D-values (m) and temperatures ($^{\circ}C$) at 850 mb for 78012612. The contour interval for the D values (solid lines) is 30 m; the isotherm (dashed lines) interval is $5^{\circ}C$.
15	As in Fig. 9 for 78012612.
16	(a) Balanced winds ($m s^{-1}$) at 300 mb for 78012612. Solid lines (isotachs) are in $m s^{-1}$. (b) 24-h forecast winds ($m s^{-1}$) at 300 mb for 78012612. Solid lines are relative vorticity with a contour interval of $4 \times 10^{-5} s^{-1}$. Maxima over southwestern Illinois and central Virginia are 25 and $30 \times 10^{-5} s^{-1}$ respectively.
17	Vertical cross section along $80^{\circ}W$ through the center of the model cyclone constructed from a 24-h forecast VT 78012612. Solid lines are potential temperature in K(leading 3 or 2 omitted); dashed lines are wind components ($m s^{-1}$) normal to cross section with negative values out of figure and positive values into figure.
18	As in Fig. 17 except for an approximate west to east section.
19	Precipitation (cm) for 24 hours ending 78012612. (a) Observed (b) Forecast

<u>Fig. #</u>	<u>Caption</u>
20	Vertical profiles of wind component (u) parallel to isobars and liquid water potential temperature (θ_L) for a point (47.6°N , 80.0°W) at 78012612 as computed by Burk's PBL model. The ordinate is height in m above the surface. Initial and boundary conditions were provided by the fine-mesh forecast as described in text.
21	As in Fig. 20 except for a point (36.5°N , 80.0°W) south of the storm center. The initial and geostrophic u profile is given by u^* .
22	(a) Observed (SLP - 1000 mb) for 78030300. The minimum pressure is 1003 mb. (b) Balanced D-values (m) and temperatures ($^\circ\text{C}$) at 500 mb for 78030300. The contour interval for the D-values (solid lines) is 60 m; the isotherm (dashed lines) interval is 5°C .
23	(a) Observed SLP-1000 mb for 78030312. The minimum pressure is 1002 mb. (b)-(e) 12-h forecast SLP-1000 mb VT 78030312 and winds (m s^{-1}) at $\sigma = 0.925$ for control forecast (b), forecast with latent heating suppressed (c), forecast with cumulus parameterization suppressed (d), and forecast with revised vertical partitioning of convective heating (e). The minimum pressures in (b)-(e) are: 986 mb (b), 1002 mb (c), 983 mb (d) and 998 mb (e).
24	Precipitation (cm) for 24 hours ending 78030400. (a) Observed (b) Forecast (control model) (c) Forecast (latent heating suppressed) (d) Forecast (cumulus convection suppressed) (e) Forecast (revised vertical partitioning of convective heating)
25	Temperature soundings in center of model cyclone, initial conditions 78030300. 1: 12-h forecast using control model 2: 24-h forecast using control model 3: 12-h forecast using model with revised vertical partitioning of convective heating. 4: 24-h forecast using model with revised vertical partitioning of convective heating. Observed sounding was constructed from NMC analyses at 78030400.

Acknowledgments

The research was supported by the Naval Air Systems Command through their sponsorship of the Meteorology Research Chair at the Naval Postgraduate School, Monterey, California. I thank Professor George Haltiner for his support.

The encouragement and substantial assistance by Tom Rosmond, Ed Barker, and Richard Hodur of the Naval Environmental Prediction Research Facility (NEPRF) is gratefully acknowledged. Without their help, this research would have been impossible.

The computer support was provided by the Fleet Numerical Weather Facility, under the command of Captain Ronald F. Hughes. His support was also essential to the project. Steve Burk of NEPRF kindly provided his PBL model for the diagnostics discussed in section 4.2. Fleet Weather Central, Rota, Spain kindly provided their operational analyses of the European cases. L. R. Brody, R. L. Elsberry, and R. T. Williams reviewed the manuscript and made helpful comments. Marion Marks capably typed the manuscript.

1. Introduction

With a rapid increase in computer power, it has recently become possible to make numerical forecasts on horizontal scales much finer than the operational models that have been in use for the past 10 years. At the National Meteorological Center (NMC), for example, a substantial improvement in forecast accuracy of the 500-mb and surface pressure gradients over the United States (U.S.) occurred when the 6-level limited fine mesh (LFM) model was introduced in 1975 (Miyakoda, 1975). This model has a horizontal resolution of about 174 km at 45°N compared to the old 6-level model's resolution of 349 km at 45°N. Recent tests with still finer meshes by Hovermale and Phillips at NMC have demonstrated a potential for continued improvement as the horizontal resolution is decreased (Phillips, 1978). Other researchers (Perkey, 1976; Bleck, 1977; Miyakoda and Rosati, 1977) have reported encouraging results with experimental models using grid sizes of less than 100 km. However, these forecasts have been made in a research environment and the number of cases tested has been small. Furthermore, quantitative verification of very fine mesh models (grid size less than 100 km) is a problem which has received little attention. Thus the question of how useful mesoscale models might be to operational forecasting is only partially answered.

The development of mesoscale models is not simply a matter of decreasing the horizontal grid size on well-tested large-scale models. As the horizontal resolution increases by a factor of five or more from synoptic-scale models, solutions corresponding to more energetic and transient circulations become possible. Interactions of the flow with condensation heating and cooling, terrain variations, and land-sea contrasts as well as nonlinear interactions between longer waves produce energy in short wavelengths, even if little

energy exists in these small scales at the beginning of the forecast. Parameterization schemes designed and tested on large meshes may prove inadequate on small meshes. The verification of these parameterizations on fine meshes requires testing on a large number of cases, since the relative importance of nonconservative physical processes such as latent heating, radiation, or friction varies greatly from one synoptic situation to the next.

This paper describes the results of a fairly large number (32) of 24-h forecasts made with a simplified version of the model described by Anthes and Warner (1978), hereafter referred to as AW. The study differs from the results mentioned above mainly in the large number of cases; however, a unique aspect of this study is a simple quantitative comparison of forecast accuracy with a well-tested large-scale operational model (the 5-layer primitive equation hemispheric model at the Fleet Numerical Weather Facility; Kesel and Winninghoff, 1972).

The tests were carried out on (50 x 50) grids with horizontal resolutions of about 60 km over two regions. Nineteen control¹ forecasts were made over a region centered at 45°N 5°E which contains portions of northern Africa, the western Mediterranean and western Europe (Fig. 1). This region was chosen because of the presumed importance of terrain in generating mesoscale perturbations to synoptic scale flows. In particular, a number of scientists have shown that the Alps and Pyrenees play important roles in generating cyclones in the Gulf of Genoa (Radinović, 1965 a,b; Egger, 1972; Bleck, 1977).

In addition to the Mediterranean forecasts, 13 control forecasts were made over a domain centered at 40°N 90°W, which includes the eastern two-thirds of the U.S. (Fig. 2). This region was chosen because of the high

¹A control forecast is one made with the basic model structure presented in this paper. All verification statistics pertain to these forecasts.

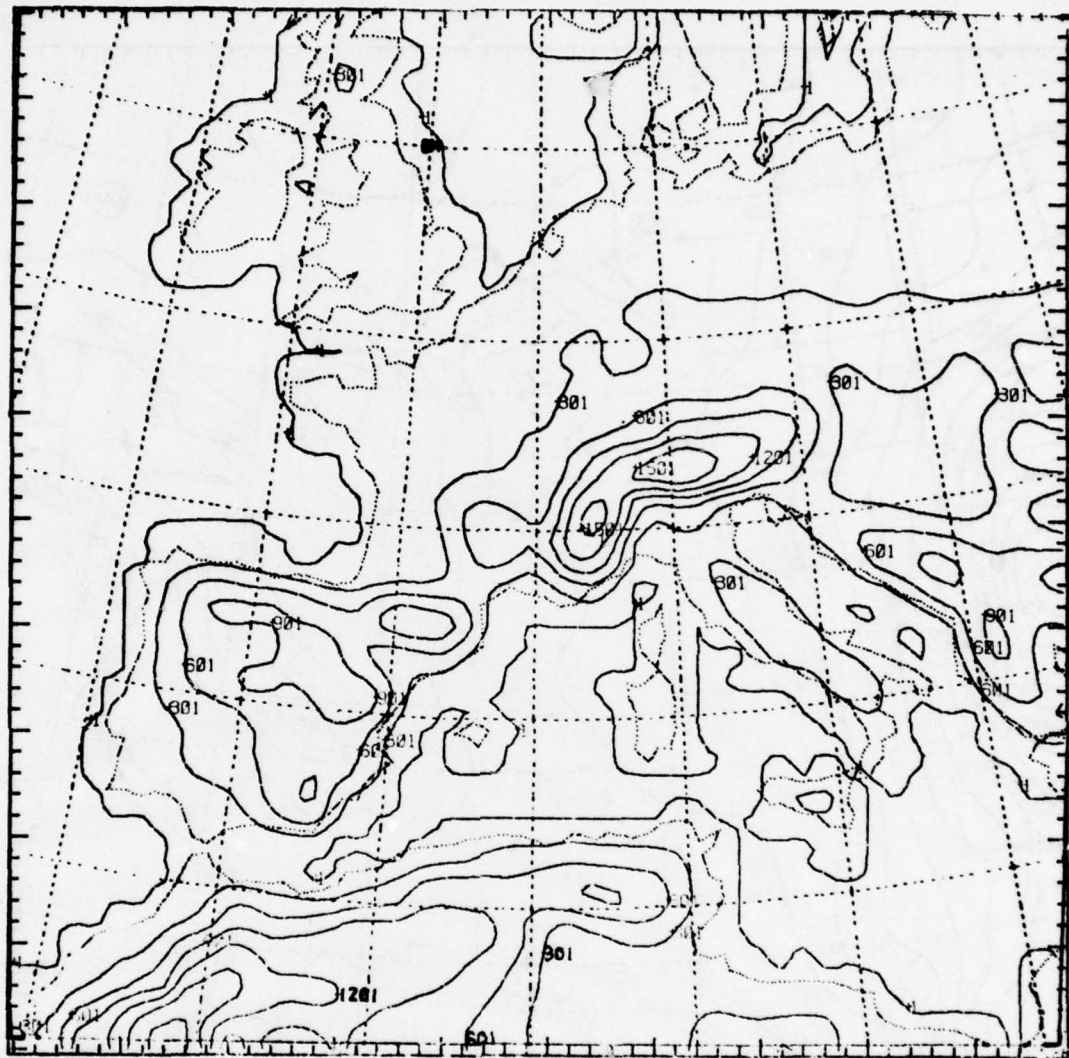


Fig. 1. Horizontal domain and terrain elevations (m) for European forecasts. Spacing between tick marks is approximately 60 km.

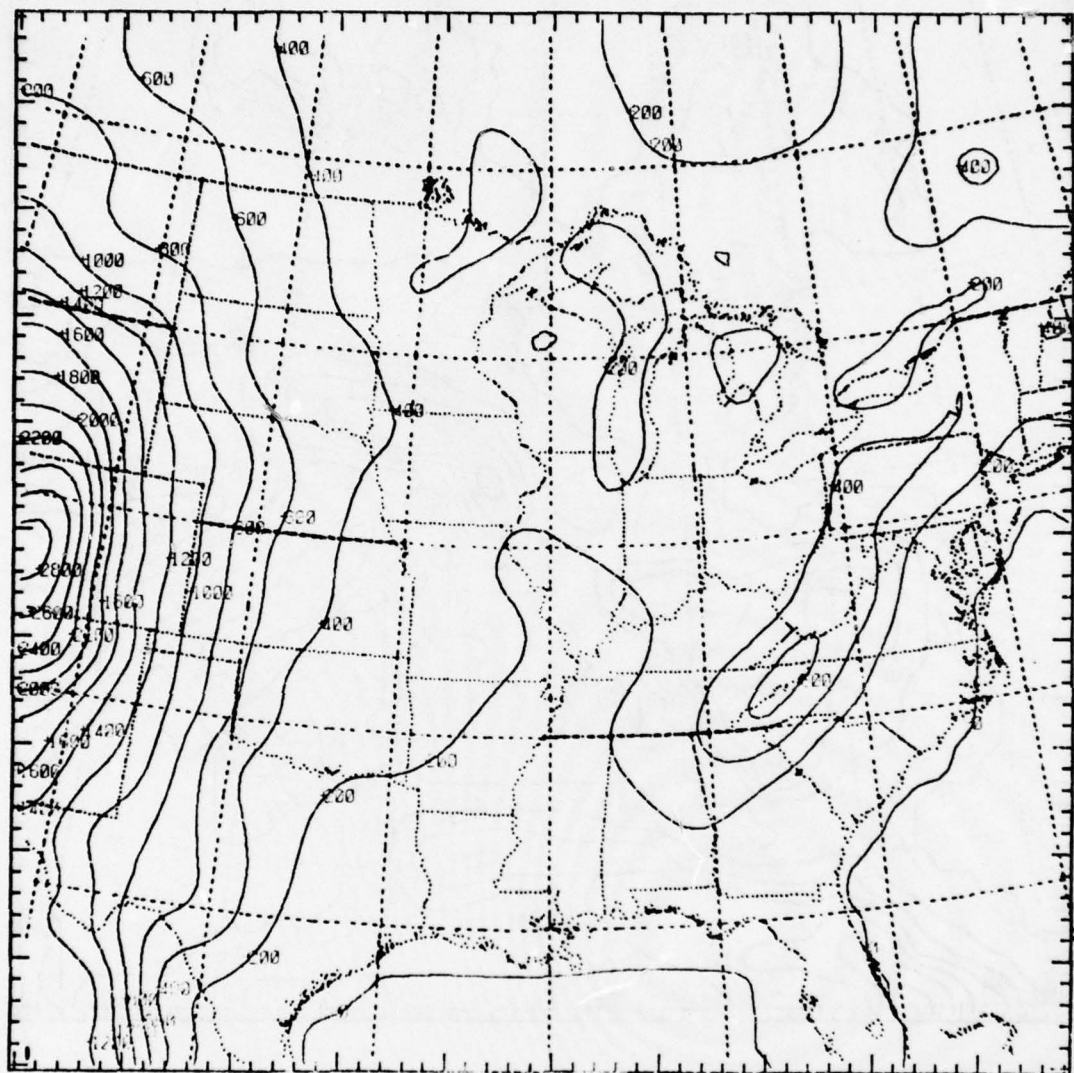


Fig. 2. As in Fig. 1 for U.S. domain.

frequency of winter storms and to study the role of latent heating in cyclogenesis along the Gulf Coast.

The 32 control cases are summarized and verified quantitatively by computing S_1 scores (Teweles and Wobus, 1954) of 12- and 24-h forecasts of sea-level pressure. These scores are compared to persistence and to the S_1 scores computed for the same points by the FNWC model. In addition, the intensities of the forecast cyclones are compared quantitatively with the observed intensities.

To help understand the properties of the model, three forecasts are examined in detail. These include a forecast of cyclogenesis in the Gulf of Genoa during the period of 00 GMT January 12 to 00 GMT January 13, 1978 (78011200 to 78011300)² and a forecast of a record-breaking intense winter storm that affected the eastern U.S. during the period 78012512 to 78012612. Both of these forecasts were reasonably successful. The third forecast examined, however, overdeveloped a low along the Gulf Coast during the period 78030300 to 78030400. Subsequent forecasts during this period in which the moisture cycle and cumulus parameterization were modified establish the importance of condensation heating and cumulus transports of heat and moisture in the model.

² Dates and times are given by the last two digits of the year followed by the month, day, and hour (GMT).

2. Cyclogenesis in the western Mediterranean

The complex terrain surrounding the Mediterranean modifies the low-level flow and affects strongly the development and movement of cyclones in this region. Radinović (1965a) identified no fewer than eight different cyclogenetic regions in southern Europe. Many of the cyclones that form in these areas are small in horizontal extent and short-lived compared to extratropical cyclones in other parts of the world. In some instances, two lows may form and decay over such short time-scales that they give the appearance of a single retrograding center.

Of all the cyclogenetic regions in southern Europe, the center of maximum frequency is in the Gulf of Genoa. Over the period 1951 to 1960, 48 cyclone centers formed in a 1° latitude by 1° longitude quadrangle in the Gulf of Genoa north of Corsica. A little less than half of the Genoa cyclones have lifetimes of less than 24 hours, and some persist less than 6 hours. Although many of these cyclones are not intense, even the weak depressions produce important effects on the weather (Radinović, 1965a).

The blocking effect of the high terrain associated with Alps to the north, the Massif Central to the northwest, and the Pyrenees to the west of the Gulf of Genoa are apparently responsible for a significant number of the cases of Genoa cyclogenesis. The major effect appears to be the blocking of a low-level cold air flow from the northwest as an upper-level trough moves over the region. This blocking induces a thermal wave in the lower troposphere of a wavelength that is favorable for cyclogenesis by the "self-development" mechanism (Sutcliffe, 1947; Palmén and Newton, 1969). Surface pressure falls begin as a trough approaches and warm advection occurs over Italy. Without the blocking effect of the Alps, the low-level cold advection would tend to offset the pressure falls before a closed surface low could form.

The above sequence of events can also be interpreted in terms of the divergence patterns associated with vorticity advection. While the high-level divergence associated with positive vorticity advection in advance of the trough passes with little impedance over the Alps, the lower-level flow, which tends to be convergent, is partially blocked by the mountains. Thus surface pressure falls to the lee of the mountains are enhanced.

The above ideas have been tested in a numerical model by Egger (1972) for an idealized case. Using a coarse mesh (350 km) PE model, Egger found that the surface pressure fall was associated with upper-level warming. In an experiment in which the mountains were removed, low-level cold advection reduced the surface pressure falls and a cyclone did not develop. A somewhat similar study was made by Trevisan (1976), who studied the behavior of a baroclinically unstable flow parallel to a mountain range which contained a gap. Cold air advection through the gap produced a disturbance to the flow and resulted in cyclogenesis downwind of the gap. When the gap in the mountains was doubled in width, this cyclogenesis did not occur.

Although most studies of cyclogenesis in the western Mediterranean have concentrated on the role of the mountains, favorable large-scale circulation patterns are necessary ingredients of cyclogenesis. Buzzi and Rizzi's (1975) study of two cases of cyclogenesis stressed the importance of large-scale forcing in producing strong cyclonic circulations throughout the entire troposphere. Their study suggested that although the Alps, Pyrenees, and Atlas mountains modified the flow somewhat, the dynamics of these two cyclones was similar to that of cyclones in regions without major mountains. In particular, cyclogenesis began in the middle troposphere as a strong jet and baroclinic zone moved into the Mediterranean area. Buzzi and Rizzi speculate that the Alps caused the jet approaching from the northwest across the British

Isles to split, with the southern branch passing to the west of the Alps and producing the cyclogenesis in the Mediterranean.

Because Egger and Trevisan found large effects on model flow by relatively simple terrain, it would be surprising if the actual terrain in Europe did not produce important and more complicated perturbations in the real atmosphere. The above observational and model results suggest strongly that very fine mesh models are necessary to simulate the effect of orography on the atmosphere in this region, at least in many cases of significant weather.

Bleck's (1977) six numerical forecasts during three synoptic periods of cyclogenesis in the Gulf of Genoa continued the study of the role of topography in this region. His forecasts were made with a nested grid; the fine mesh grid length was about 85 km, which allowed for the best resolution of the European terrain in a numerical model up to this time. The results were very encouraging, in spite of the simple physics in the model, which was adiabatic, dry, and contained a simple representation of the planetary boundary layer (PBL). An important result of Bleck's paper is that cyclogenesis in the model was sensitive to the configuration of the terrain. In particular, the original smoothed terrain elevations had to be enhanced by nearly a factor of two to produce cyclogenesis.

Although six forecasts is not a large enough sample to draw general conclusions, Bleck suggested that the underprediction of the cyclone intensity in five out of the six forecasts was due to one or more of three reasons: (1) the neglect of latent heat (2) the inadequate prediction of the large-scale ridging over the Atlantic by the coarse-mesh model and (3) the limited horizontal resolution of the 85-km fine mesh. Because our model contains precipitation and utilizes a 60-km mesh, we can hopefully shed some light on the first and third possibilities.

3. Numerical aspects of the model

The model described by AW was simplified for economic reasons for this large number of tests. The major simplifications include a specification of a constant weighting function for the distribution of latent heating associated with cumulus convection and the use of a simple representation of the PBL. This version of the model requires 3200s of central processing (CP) time on a Control Data CYBER 175 to make a 24-h forecast.

The model used in the control experiments discussed in this paper consists of 7 levels at which σ is defined, given by $\sigma = 0.0, 0.25, 0.4, 0.55, 0.70, 0.85$ and 1.0. All other variables are defined halfway between these levels, so that the model contains 6 layers. The pressure p_t at the top of the model is 200 mb. Further details of the vertical and horizontal grid structures are given by AW.

3.1 Simplifications to the cumulus parameterization

In the model described by AW, the vertical partitioning of the cumulus convective heat release was determined as a function of the model's thermodynamic and moisture structures by utilizing a one-dimensional cloud model (Anthes, 1977, hereafter designated I). To save time and memory requirements for these tests, this scheme was greatly simplified by specifying a spatially and temporally constant vertical distribution function $N(\sigma)$ (see Eq. 27 of I). The values of N for the control experiments as well as modified values used in a sensitivity test are given in Table 1. The weights in the control cases were determined by considering the vertical distribution of latent heating in an entraining one-dimensional cumulus cloud which reaches a pressure of about 300 mb.

In addition to specifying constant values of N , we also simplified the calculation of the vertical eddy flux of moisture $\bar{w}'q'$ due to cumulus clouds

by specifying constant values of the vertical velocity (ω_c) in the cloud and ($q_c - q$), where q is specific humidity and the c subscript refers to the cloud updraft (Table 1). The percent (a) of area covered by this representative updraft is the remaining variable needed to compute $\overline{\omega'q'}$ (see Eq. 18 of I) and is given by a simplified form of Eq. 51 in I.

$$a = (1-b)g M_t / (4.3 \times 10^{-3} \text{ cb s}^{-1}) \quad (1)$$

where b is the fraction of water vapor convergence M_t which is not precipitated and the constant 4.3×10^{-3} is a representative value of the denominator of Eq. 45 in I. Finally, the vertical eddy flux of heat $\overline{\omega'T'}$ associated with cumulus convection is neglected. The term is normally much smaller than the condensation term in the thermodynamic equation. In these forecasts, convection occurs whenever M_t exceeds $3.0 \times 10^{-6} \text{ g H}_2\text{O m}^{-2} \text{ s}^{-1}$.

In retrospect, the simplification of the cumulus parameterization probably did not have much effect on most of the forecasts, because of the relatively dry air masses affecting the domains. However, in one or two of the U.S. forecasts, latent heating was a dominant factor and the above parameterization may have been inadequate. The third case discussed in this paper is an example of one of these cases.

3.2 Parameterization of the PBL

The surface stress is given by

$$\tau = \rho C_D |\tilde{v}_6| \tilde{v}_6 \quad (2)$$

where ρ is density (1.1 kg m^{-3}) and \tilde{v}_6 is the wind in the lowest layer.

The drag coefficient C_D over land varies according to terrain elevation z_s (expressed in km) in a manner similar to that of Bleck (1977)

$$C_D = 5.0 \times 10^{-3} + (6.45 \times 10^{-3}) [z_s / (1+z_s)] . \quad (3)$$

Over water, C_D equals 1.5×10^{-3} . Sensible and latent heat fluxes are allowed only over water; here they are modeled according to conventional bulk aerodynamic formulas with the exchange coefficients equal to 1.5×10^{-3} .

Over the right half of the domain, C_D was inadvertently zero in all of the control forecasts. Rerunning several of the forecasts with C_D given by (3) everywhere produced significantly weaker cyclones over the right half of the domain. An analysis of the PBL structure (presented later) indicates that a more realistic drag coefficient would be about 2.0×10^{-3} . Thus the low-level circulations on the left half of the domain are probably overdamped while on the right half they are definitely underdamped.

3.3 Horizontal diffusion

In some preliminary experiments in which the horizontal diffusion of any variable α was proportional to $\nabla_p^2 \alpha$, the solutions were excessively smooth after 12 hours of integration. In particular, wind maxima in jet streams became weaker than those in nature and the moisture patterns did not show realistic streaky patterns. Williamson (1978) found better results in a general circulation model when the diffusion proportional to $\nabla \cdot K_H \nabla \alpha$ was replaced by the more scale-selective $\nabla^2 K \nabla^2 \alpha$ diffusion, where K_H is a horizontal eddy viscosity and $K = \Delta s^2 K_H$. Therefore, in an effort to reduce the damping of waves with wavelength greater than $6\Delta s$, where Δs is the grid size, while retaining the strong damping of shorter waves, a horizontal diffusion proportional to $\nabla_p^4 \alpha$ was introduced.

The damping rate of various wavelengths can be calculated from the finite difference analog to

$$\frac{\partial \alpha}{\partial t} = -K \nabla_p^4 \alpha \quad (4)$$

which is

$$\frac{\alpha^{n+1} - \alpha^n}{\Delta t} = - \frac{K}{\Delta s^4} [\alpha_{ij+2} - 4(\alpha_{ij+1} + \alpha_{ij-1} + \alpha_{i+1j} + \alpha_{i-1j}) + 12\alpha_{ij} + \alpha_{ij-2} + \alpha_{i+2j} + \alpha_{i-2j}] \quad (5)$$

where n refers to the time level and i and j are the horizontal indices.

If the wavelength in the x -direction is $m\Delta s$ and the wavelength in the y direction is $n\Delta s$, the damping per time step is given by

$$\alpha^{n+1} = [1 - \frac{K\Delta t}{\Delta s^4} (2 \cos \frac{4\pi}{m} - 8(\cos \frac{2\pi}{m} + \cos \frac{2\pi}{n}) + 12 + 2 \cos \frac{4\pi}{n})] \alpha^n \quad (6)$$

From (6) we see that computational stability requires that

$$\frac{K\Delta t}{\Delta s^4} \leq \frac{1}{32} . \quad (7)$$

The horizontal eddy viscosity K_H in these experiments is

$$K_H = A(4.0 \times 10^4 + 0.08 \Delta s^2 |D|) \text{ m}^2 \text{ s}^{-1} \quad (8)$$

where the deformation D is

$$D = \left[\left(\frac{\partial u}{\partial x} - \frac{\partial v}{\partial y} \right)^2 + \left(\frac{\partial v}{\partial x} + \frac{\partial u}{\partial y} \right)^2 \right]^{\frac{1}{2}} . \quad (9)$$

The parameter A in (8) is an amplification factor that is used to increase K_H near the boundaries and is given by

$$A(r) = \begin{cases} 1 & r < r_o \\ 1 + 3(r-r_o)/\Delta s & r \geq r_o \end{cases} \quad (10)$$

where r is the radial distance from the center of the grid and $r_o = 20\Delta s$.

Finally, K_H is restricted to be less than $30 \times 10^4 \text{ m}^2 \text{ s}^{-1}$ to insure computational

stability. In a typical forecast, K_H varies between 5 and $8 \times 10^4 \text{ m}^2 \text{ s}^{-1}$ over the interior of the grid, and up to the maximum value of $30 \times 10^4 \text{ m}^2 \text{ s}^{-1}$ near the boundaries. Table 2 lists the fraction of the original amplitude of horizontal waves in one direction only of wavelength $m\Delta s$ remaining after 24 hours. These calculations assume a value of K_H equal to $5 \times 10^4 \text{ m}^2 \text{ s}^{-1}$ and a Δt of 135s.

3.4 Temporal filter

In order to reduce the amount of energy in waves with high frequencies, all variables are filtered according to

$$\hat{\alpha}^n = (1-v)\alpha^n + \frac{v}{2}(\alpha^{n+1} + \hat{\alpha}^{n-1}) \quad (11)$$

where $\hat{\alpha}$ is the filtered variable (Asselin, 1972). The filter coefficient v in these experiments is 0.1, which does not appreciably affect waves with periods longer than 15 minutes over a 24-hour forecast.

The beneficial effect of the weak filter (11) is illustrated by the temporal behavior of $p^* = (p_s - p_t)$ at a particular grid point on the interior of the domain over the last 25 minutes of a 12-h forecast (Fig. 3b). The initial conditions in this preliminary experiment consisted of an unbalanced 5 m s^{-1} wind over a domain which included a long mountain of maximum elevation 1 km. As shown in Fig. 3b, the $2\Delta t$ oscillation in the experiment with $v=0$ (no smoothing), is eliminated with $v=0.1$, whereas the variations associated with the lower frequencies are nearly unaffected. A plot of the horizontal variation of vertical velocity, ω , at level 6 in the same experiment at 12 hours (Fig. 3a) shows that the weak temporal filter also reduces spatial noise, since high temporal frequencies generally have short wavelengths. The disadvantage of using the filter (11) is the necessity of reducing the time step by a factor of 0.95 in order to maintain computational stability. These forecasts used a Δt of 135s.

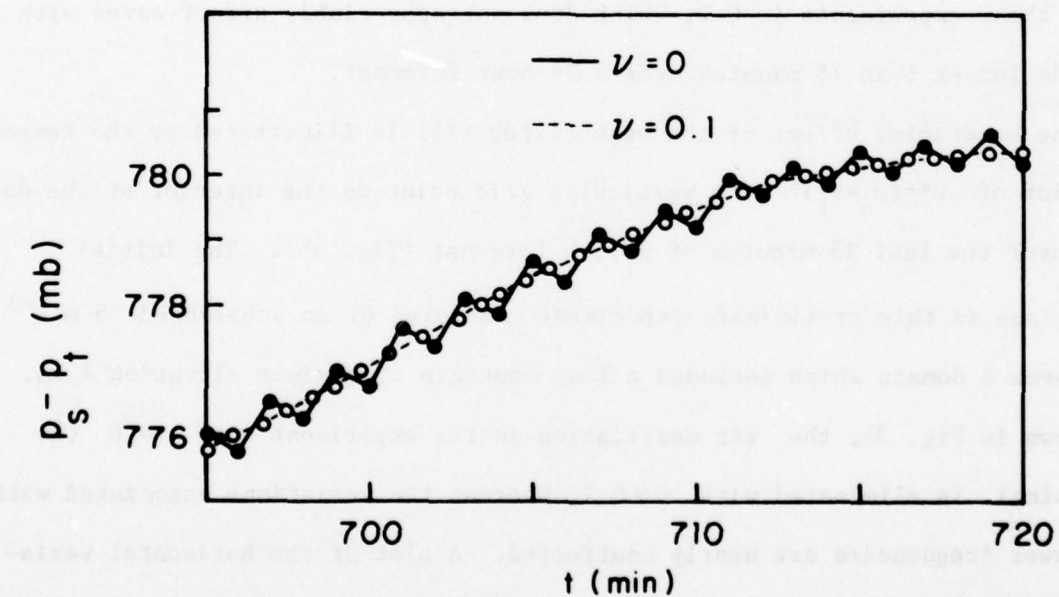
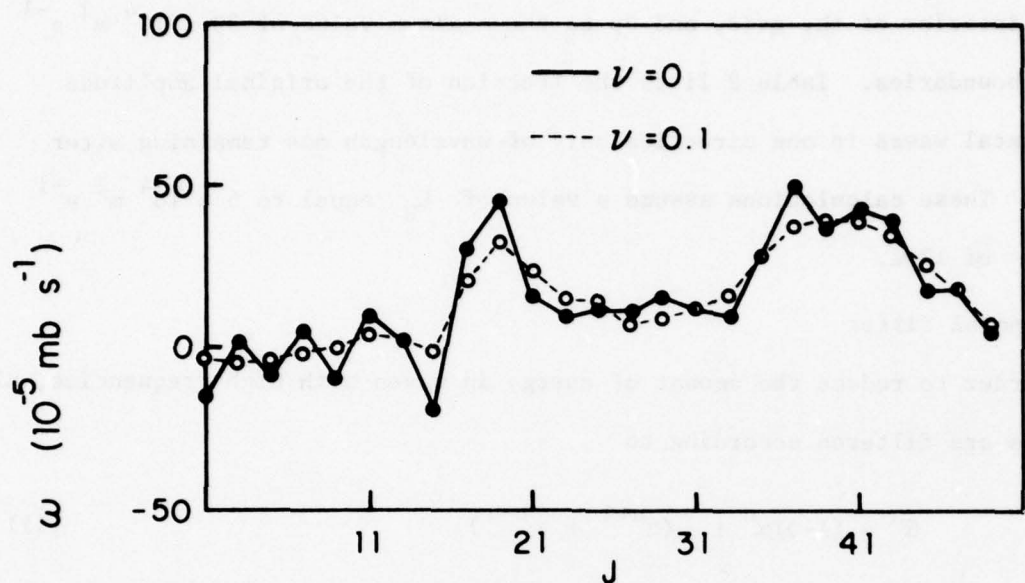


Fig. 3a (top) Plot of vertical velocity ω at level six ($\sigma = 0.925$) along a west-east line through the middle of the domain in a preliminary experiment with ($\nu = 0.1$) and without ($\nu = 0$) temporal filtering.

3b (bottom) $p_s - p_t$ at a particular grid point every time step for the last 25 minutes of a 12-h forecast with ($\nu = 0.1$) and without ($\nu = 0$) temporal filtering.

3.5 Truncation errors over steep terrain

The horizontal pressure gradient force in σ -coordinates over sloping terrain consists of two large terms of opposite sign (see Eq. 4 of AW). Truncation errors in these terms may lead to erroneous pressure gradients. Furthermore, the interpolation of temperature to constant pressure surfaces in the computation of the horizontal diffusion of temperature may lead to erroneous diabatic effects. To demonstrate the magnitude of the fictitious accelerations resulting from these truncation errors, a 3-hour forecast was made over a domain which included the 500-m mountain shown in Fig. 4. The initial conditions consisted of zero winds and horizontally homogeneous temperature and pressure fields. The vertical stratification was equal to that in the standard atmosphere.

With zero terrain, the forecast fields remained unperturbed. With the mountain shown in Fig. 4, however, horizontal velocities of maximum value 1.0 m s^{-1} were generated in the vicinity of the slopes. These winds produced vertical velocities of order $0.2 \times 10^{-5} \text{ mb s}^{-1}$, with subsidence over the peak (Fig. 4). The maximum temperature changes associated with these vertical motions were 0.2°C (Fig. 4). These erroneous perturbations did not grow with time; in fact, by 3-h the amplitudes of the perturbations were less than they were at 1 h (Fig. 4). Mutual adjustments between the mass and momentum fields occurred to compensate for the truncation errors in the horizontal pressure gradient force and diffusion terms.

Another preliminary experiment exactly like the one above except that horizontal diffusion was eliminated, produced virtually identical results. Thus errors associated with the horizontal diffusion calculation are negligible compared to those associated with the pressure gradient force calculation.

3.6 Noise in a typical forecast

Bleck (1977) discusses several objective measures of noise in primitive equation models. He presented the temporal behavior of the domain-averaged

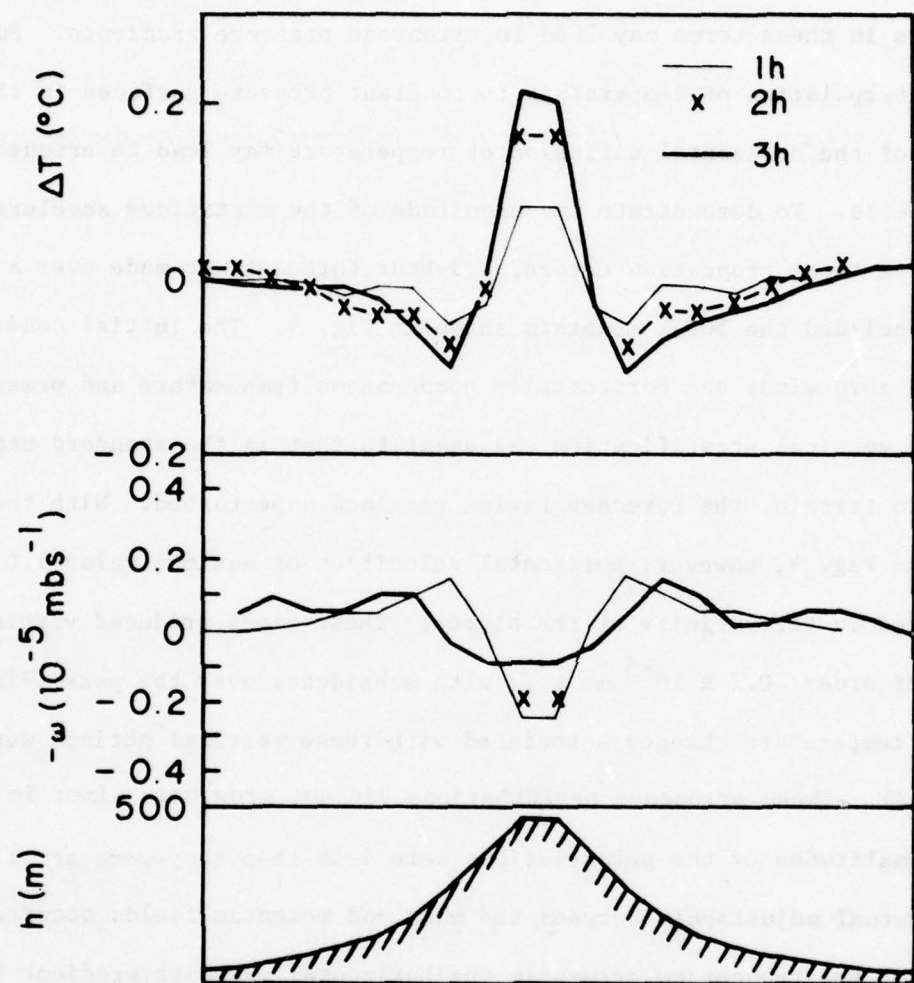


Fig. 4. Horizontal variations of erroneous temperature changes and vertical velocities at 1, 2 and 3 hours at $\sigma = 0.925$ across a mountain in a preliminary experiment. Top: temperature change. Middle: vertical velocity. Lower: terrain elevation. The width of the mountain top is 1 grid length (60 km); the total horizontal domain shown in figure is 1140 km.

absolute value of the second derivative of surface pressure with respect to time as an indication of the noise level in his isentropic model. This noise is primarily associated with external gravity waves. With mountains, $|\frac{\partial^2 p}{\partial t^2} s|$ averaged around $4 \times 10^{-7} \text{ mb s}^{-2}$ for the last 12 hours of a 24-hour forecast over his 85 km mesh.

Fig. 5 shows the temporal variation of $|\frac{\partial^2 p^*}{\partial t^2}|$ for a typical control model forecast in our set of experiments (US06)³. During the 24-h forecast, this measure of noise decreases from about $50 \times 10^{-7} \text{ mb s}^{-2}$ to about $4.5 \times 10^{-7} \text{ mb s}^{-2}$ at the end of the forecast. This behavior is very similar to what Bleck observed. The slow decrease with time is a result of the model gradually achieving a better dynamic balance during the forecast.

Fig. 5 also shows the temporal variation of $|\frac{\partial p^*}{\partial t}|$. Bleck states that this variable is probably not as good a measure of noise as $|\frac{\partial^2 p^*}{\partial t^2}|$ because it is affected more by the synoptic situation. The more gradual decrease of $|\frac{\partial p^*}{\partial t}|$ over time compared to the decrease of $|\frac{\partial^2 p^*}{\partial t^2}|$ indicates that the second derivative of pressure is indeed a more sensitive indicator of noise.

³Tables 3 and 4 identify the forecasts and provide a brief description of each synoptic situation.

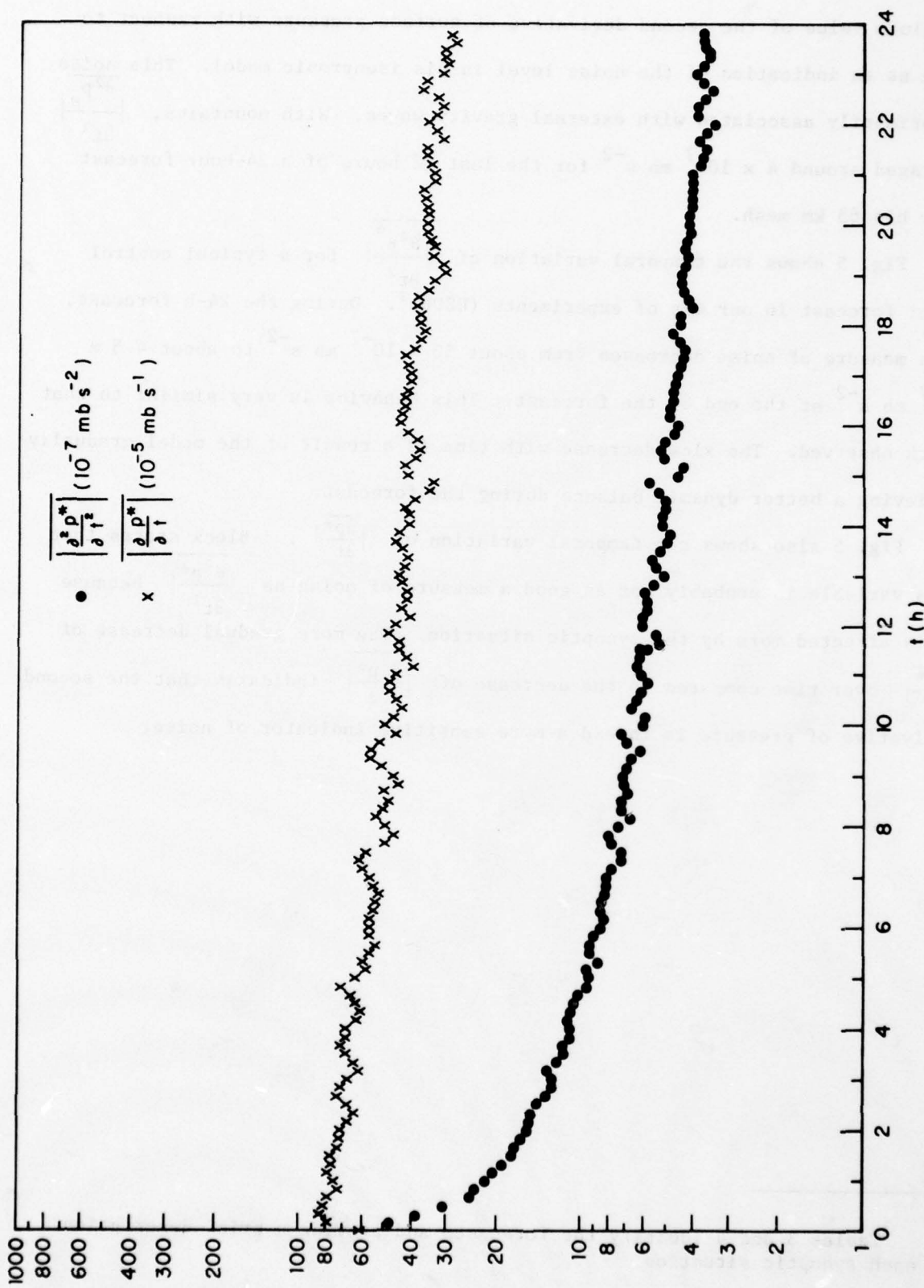


Fig. 5. Noise in a typical forecast as shown by the temporal variation of $\left| \frac{\partial p^*}{\partial t} \right|$ and $\left| \frac{\partial^2 p^*}{\partial t^2} \right|$ in forecast US06.

4. Forecast results

Tables 3 and 4 list the control forecasts and the variations discussed in this report. With the exception of the two U.S. forecasts starting at 78012212 and 78012300, the forecasts involve cyclones over a major portion of the domain. Two of the most intense winter storms ever to affect the U.S. (the Ohio blizzard of 26 Jan. 1978 and the Boston blizzard of 6-7 Feb. 1978) are included in the sample. The European cyclones tend to be weaker and behave more erratically, in agreement with climatology.

4.1 Statistical measures of forecast accuracy

Although it by no means provides a complete description of the "weather", the sea-level pressure (SLP) chart is one of the most important parts of a numerical forecast. An objective measure of the forecast skill of the SLP map that is simple to compute and has been reported often for other models is the S_1 score developed by Teweles and Wobus (1954). The S_1 score for SLP relates horizontal differences in the forecast SLP to the observed differences; it therefore measures the skill of the surface geostrophic wind forecast. In these forecasts, the S_1 score is computed from

$$S_1 = 100 \sum_{i=1}^{17} |\Delta P_f - \Delta P_o|_i / \sum_{i=1}^{17} G_i \quad (12)$$

where ΔP is the difference in SLP between a pair of grid points, f and o subscripts denote forecast and observed values of ΔP respectively, and G_i is the maximum of ΔP_f and ΔP_o for a particular pair of points. The differences in SLP were calculated between all adjacent points in the set of 12 points given in Table 5, which yields 17 pairs of points. The "observed" SLP differences were calculated from the analysis of SLP produced by the FNWC hemispheric analysis and then interpolated to the (50 x 50) fine mesh.

The above procedure was selected for its expediency. However, the use of the FNWC SLP analysis for verification had the disadvantage that the analysis contained no fine-scale information, owing to the interpolation of the coarse mesh analysis to a fine mesh. The model forecasts, on the other hand, did contain fine-scale features and therefore may have been penalized by verifying against a smooth analysis. The forecasts were not smoothed in the computation of the S_1 scores. Figure 6a shows the unsmoothed 24-hour SLP forecast from MED01 (VT 78011300). The FNWC analysis for this time is shown in Fig. 7a and the operational high-resolution analysis produced by the Navy at Rota, Spain is shown in Fig. 7b. For comparison, the FNWC operational model forecast is shown in Fig. 7c. The FNWC analysis and model are incapable of showing the detail present in the fine mesh model forecast and the high resolution analysis. In particular, the packing of the isobars over the Alps is not resolved by the FNWC analysis.

In an effort to determine the sensitivity of the S_1 score to the amount of fine-scale information present, several 24-h forecast SLP maps were smoothed in varying degrees using the smoother-desmoothening discussed by Shuman (1957) and Shapiro (1970). A variable A_{ij} is modified by a number of passes of the operator defined by

$$B_{ij} = (1-\nu)A_{ij} + \frac{\nu}{2} (A_{ij+1} + A_{i,j-1})$$

$$A_{ij} = (1-\nu)B_{ij} + \frac{\nu}{2} (B_{i+1,j} + B_{i-1,j}) \quad (13)$$

where i and j are horizontal indices. The degree of smoothing can be controlled by repeated application of (13) with varying values of ν on each pass.

Table 6 shows the effect of 5 types of smoothing on the S_1 score for six different forecasts. Smoothing type 1 consists of no smoothing; type 2 consists

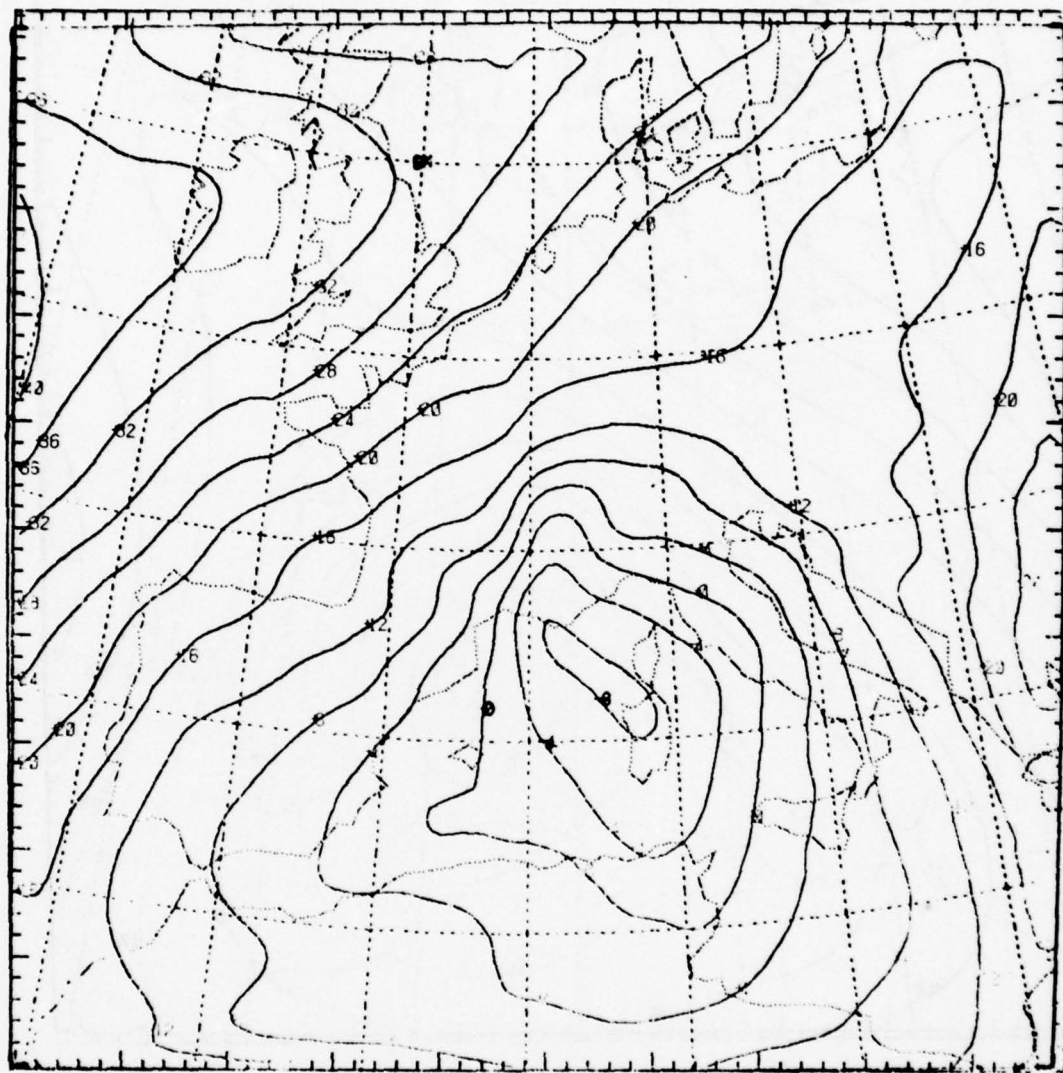


Fig. 6. 24-h forecast of (SLP-1000 mb) VT 78011300. Contour interval is 4 mb.
(a) Unsmoothed; central pressure is 991 mb.

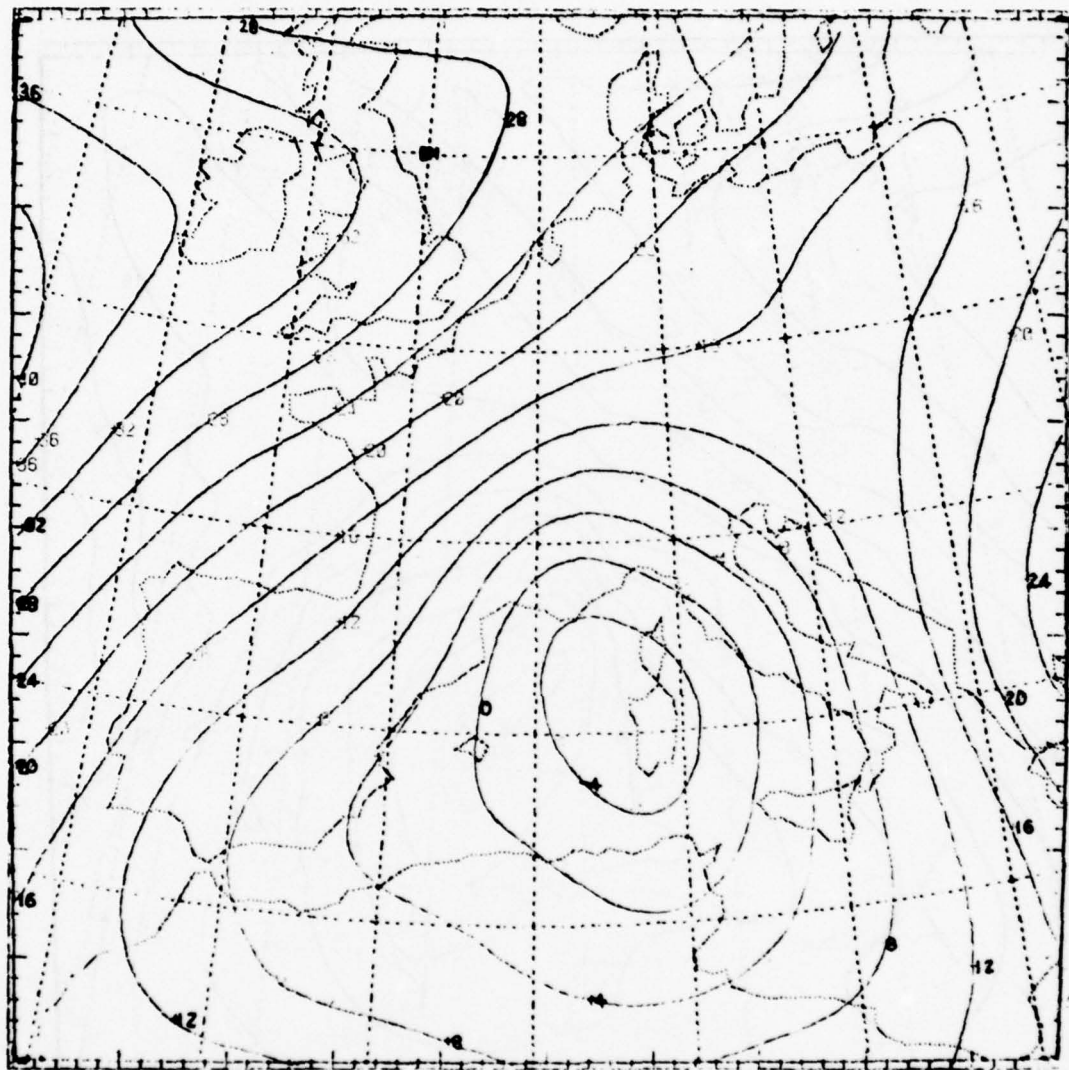
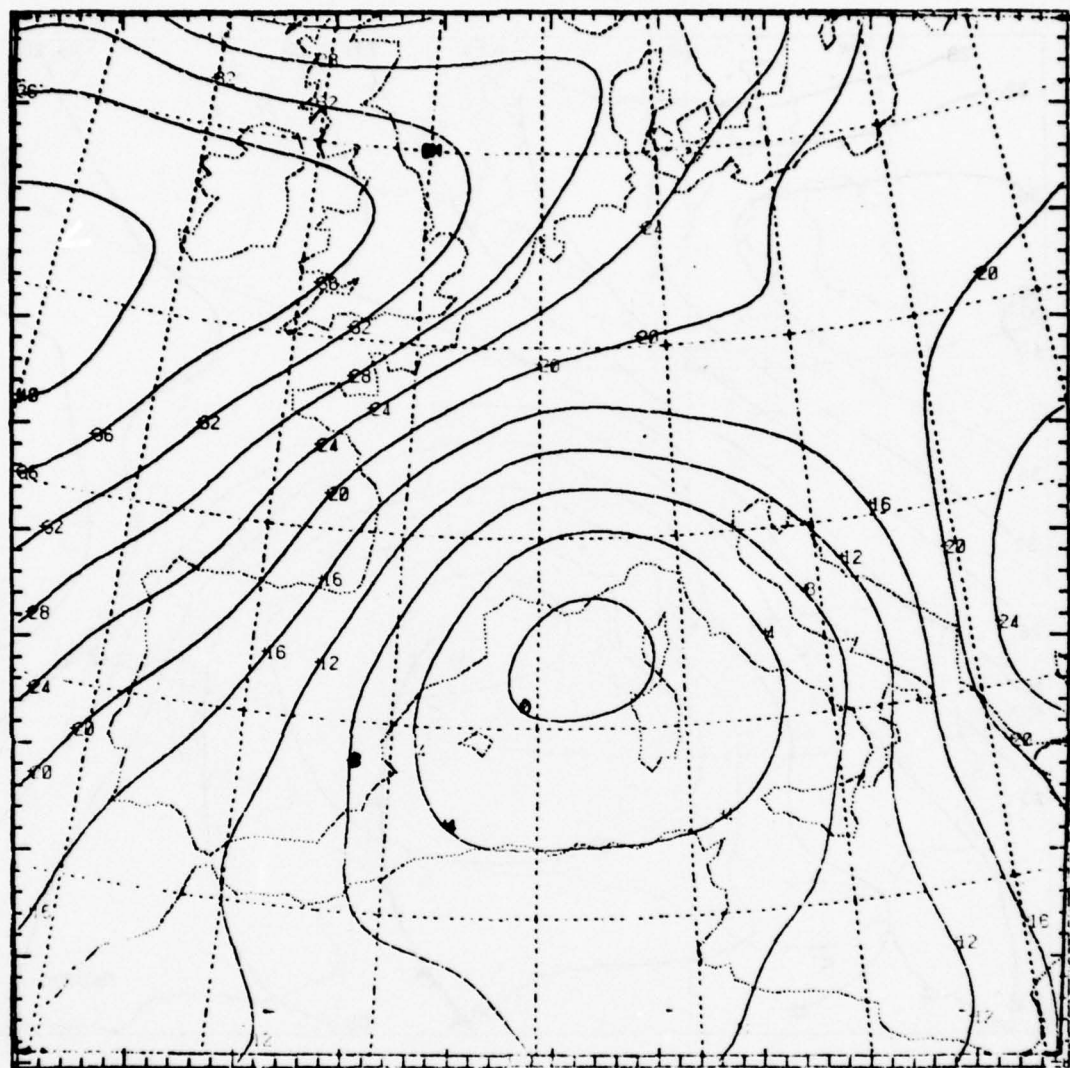


Fig. 6b. Smoothed using smoothing operator 5 (see Table 6 and Eq. 13). Central pressure is 993 mb.



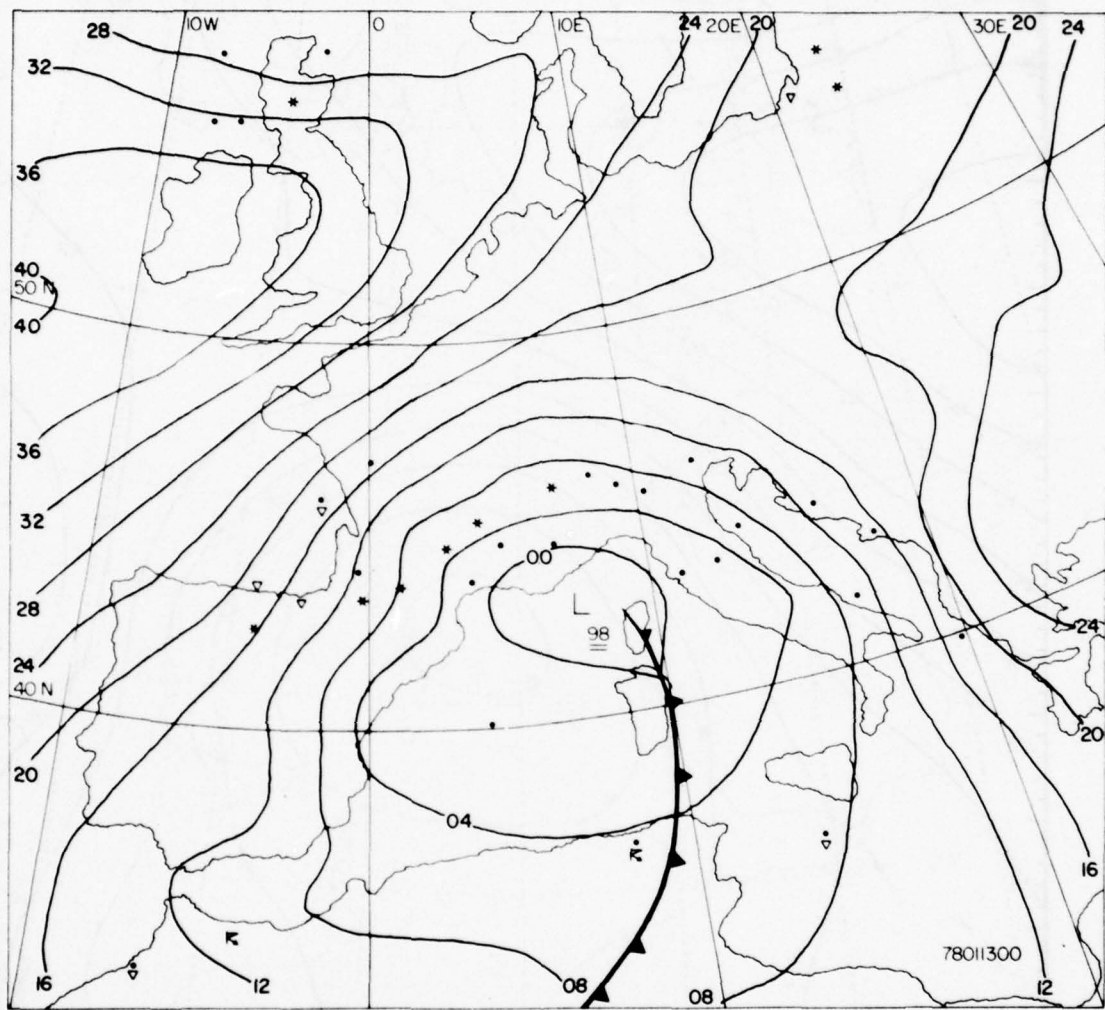


Fig. 7b. Simplified operational surface analysis for 78011300 produced by U.S. Navy at Rota, Spain.

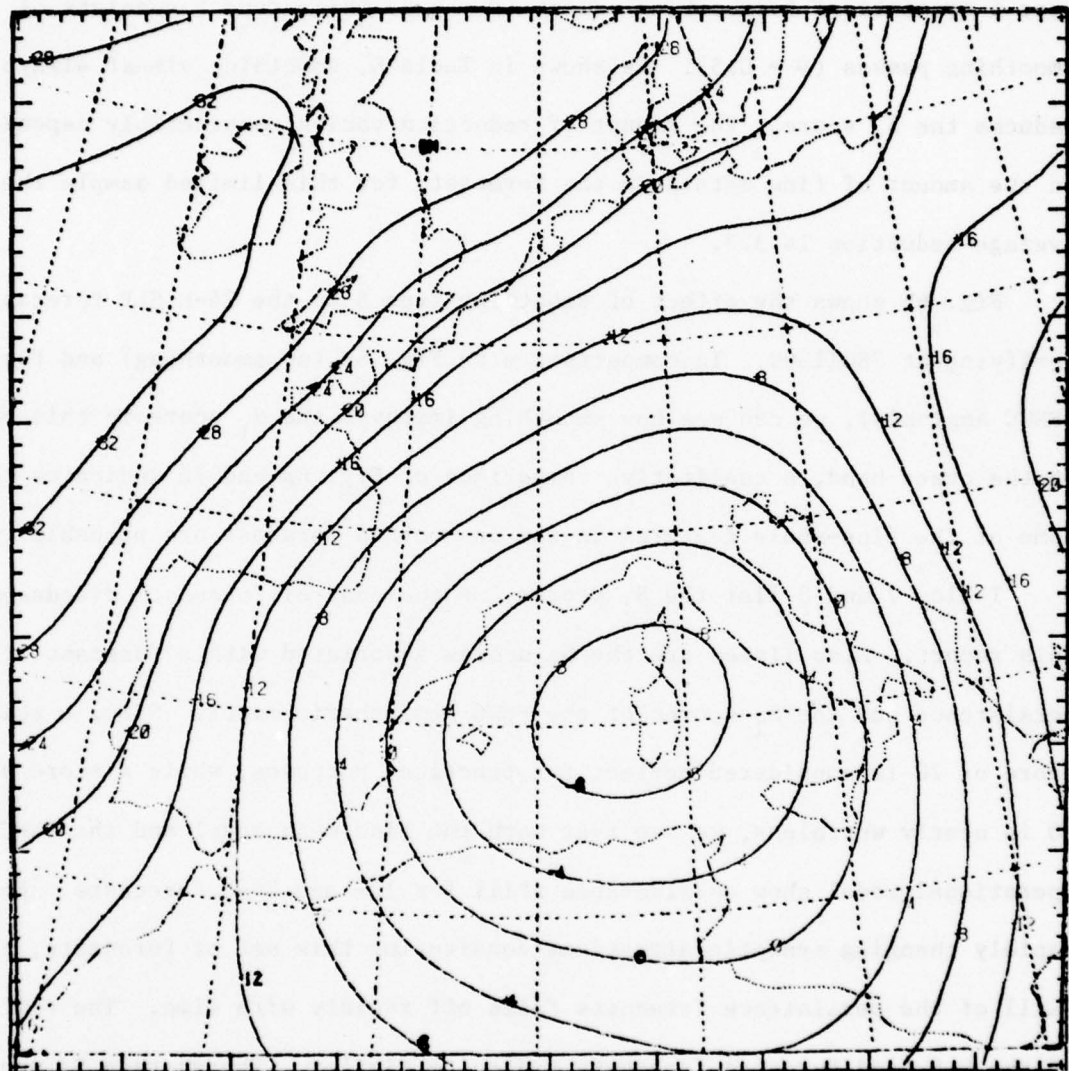


Fig. 7c. 24-h forecast of (SLP-1000 mb) VT 78011300 by FNWC operational model. Central pressure is 990 mb.

of 1 pass of (13) with $\nu = 0.5$; type 3 consists of a smoothing pass ($\nu = 0.5$) followed by a desmoothing pass ($\nu = -0.5$) repeated for a total of 6 times; type 4 consists of 6 smoothing passes ($\nu = 0.5$) while type 5 consists of 12 smoothing passes ($\nu = 0.5$). As shown in Table 6, smoothing almost always reduces the S_1 score. The amount of reduction varies considerably depending on the amount of fine detail in the forecast; for this limited sample the average reduction is 3.3.

Fig. 6b shows the effect of smoothing type 5 on the 24-h SLP forecast verifying at 78011300. In comparison with Fig. 6a (no smoothing) and Fig. 7a (FNWC analysis), we can see how smoothing improves the S_1 score in this case. On the other hand, a qualitative comparison of Fig. 6a and 7b indicates that some of the fine-scale features in the unsmoothed forecast are probably real.

Tables 7 and 8 list the S_1 scores for the control forecasts discussed in this report. Also listed are the S_1 scores associated with a forecast of persistence and the S_1 scores of the FNWC hemispheric model. Since a skill score of 20 is considered perfect for practical purposes, while a score of 70 is nearly worthless, we see that both the fine mesh model and the FNWC operational model show considerable skill for 12- and 24-h forecasts. For the rapidly changing synoptic situations constituting this set of forecasts, the skill of the persistence forecasts falls off rapidly with time. The skills of the U.S. and European forecasts are quite similar. The average S_1 scores for all 32 cases at 12 and 24 hours for the fine mesh model are 33.8 and 39.1 respectively; for the FNWC model the corresponding scores are 37.2 and 45.9. With proper smoothing, the fine-mesh scores would likely be lowered by about 3 points.

In judging the meaning of these comparative scores, it is important to remember that the fine mesh model had the benefit of analyzed lateral boundary conditions. On the other hand, the FNWC operational model did not have the

numerical problems associated with incompatible boundary conditions. It also had the benefit of eight years of tuning (it was implemented in Sept. 1970). On balance, it seems fair to conclude that fine-mesh models can provide significant improvements in SLP forecasts provided they are supplied with reasonable lateral boundary conditions as part of a nested model or from an independent large-scale model. For comparison purposes, we note that the S_1 score for the 30-h surface pressure forecasts at NMC have decreased gradually from approximately 65 in 1947 to the low 50s in 1975 (Miyakoda, 1975). Recent tests of a limited-area model with 250 km horizontal resolution over Australia showed S_1 scores for 24-h forecasts of approximately 49 (McGregor et al., 1978, Table 1).

The S_1 score is affected both by amplitude and phase errors. In order to detect possible biases in the model toward over- or underprediction of the intensity of cyclones, the 24-h forecast minimum pressures of all lows at least 5 grid points from the lateral boundary were plotted versus the observed minimum pressure. The results, shown in Fig. 8, indicate that the model predicts lows that are somewhat more intense than observed. This result is in contrast to Bleck's forecasts which underpredicted the intensity of the cyclones, and is probably due mainly to the absence of surface friction over half the domain. For example, the central pressure of 928 mb (Fig. 8) associated with forecast US09, was 974 mb when friction was included over the entire domain.

In a comparison of forecasts using a coarse-mesh isentropic primitive equation (PE) model with the NMC 6-layer PE model, Bleck (1974) used the median absolute pressure error for surface cyclones as a measure of forecast accuracy. For the 50 cases he tested, the median pressure error at 24 hours was about 5.5 mb for the isentropic PE and 5.0 mb for the NMC PE. A similar distribution for the cyclones summarized in Fig. 8 is given in Table 9.

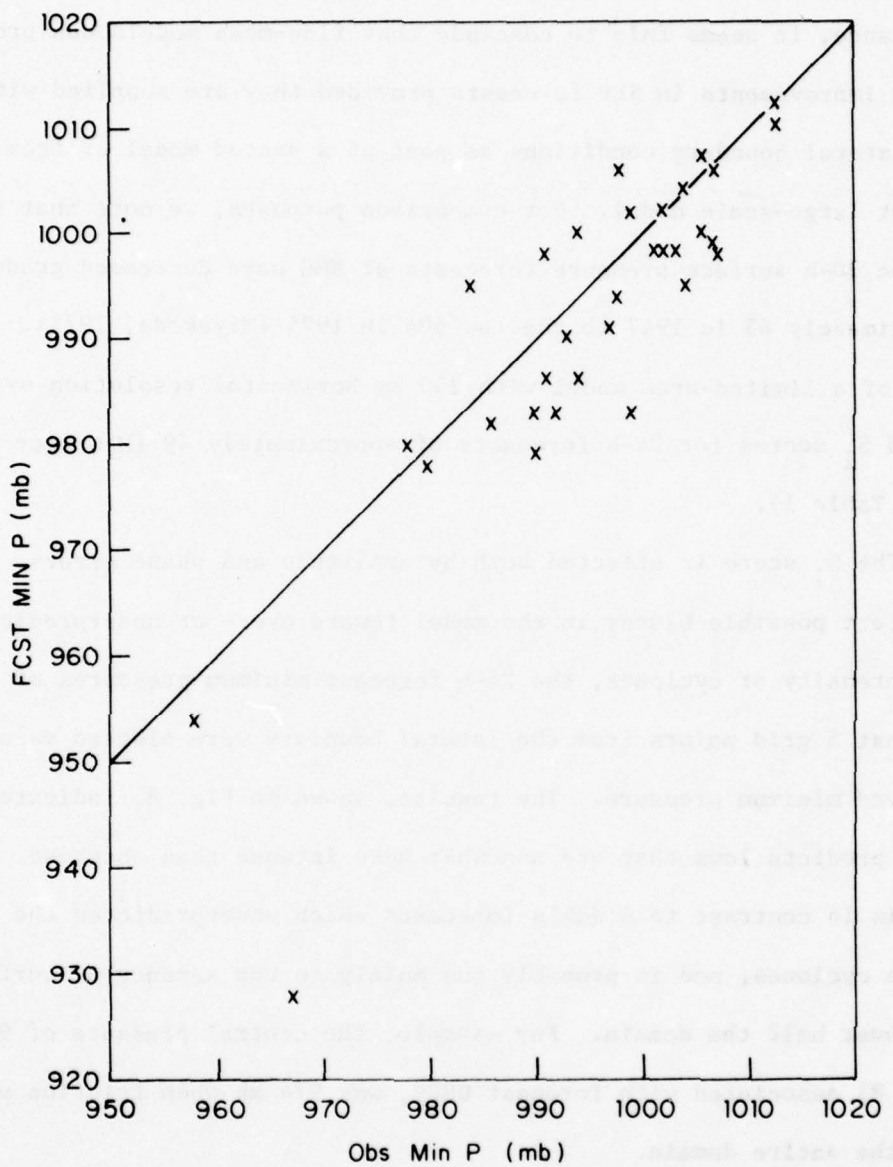


Fig. 8. 24-h forecast vs. observed minimum pressures of cyclones over the interior of the domain (at least 5 grid points or 300 m from the lateral boundary) for the 32 control forecasts.

4.2 A forecast of cyclogenesis in the Gulf of Genoa

The first case to be discussed in detail covers the genesis of a low in the Gulf of Genoa. In many respects the evolution of this cyclone was similar to the Feb. 3-4, 1969 case discussed by Buzzi and Rizzi (1975). At the initial time (78011200) an intense cyclone (990 mb) was centered over the Netherlands. To the west, a 1038 mb high was located about 1300 km northwest of Spain at latitude 45°N 25°W. Surface winds in the strong pressure gradient between these two systems averaged 20 m s^{-1} over the British Isles and North Sea. A cold front extended from the Netherlands low southward across France into a developing (997 mb) low on the southeast coast of France. Cold air behind this front was already covering most of Spain, with temperatures in northern Spain averaging several degrees below freezing.

Fig. 2 in Keyser (1978)⁴ shows the FNWC SLP analysis for this time.

At 500 mb, a high-amplitude short-wave trough extended from the North Sea southward across the Pyrenees and into northern Africa (Fig. K3b). A pool of cold ($< -35^\circ\text{C}$) air was being advected rapidly southward in the strong (30 m s^{-1}) northerly flow behind the trough over western France. At 300 mb, a 70 m s^{-1} jet streak was moving southward across the northwest coast of Spain (Fig. K4c). The flow at 300 mb was strongly diffluent over the Balearic Sea. Therefore the upper-level flow pattern was very favorable for cyclogenesis in the northwestern Mediterranean.

During the next 12 hours, cyclogenesis over the Ligurian Sea proceeded rapidly, so that by 78011212 a 992 mb low was located off the west coast of Corsica. The Netherlands low was rapidly decaying and the surface winds over

⁴Hereafter figures in Keyser (1978) will be prefixed by K.

the North Sea, British Isles and France were veering into the northeast as a strong geostrophic easterly flow developed north of the Mediterranean low. A cold front extended southward from the new cyclone, penetrating several hundred kilometers into Africa. Behind the front and north of the low, light snow was falling over northern Spain, the Pyrenees, southern France, and the Alps. Along the front thunderstorms were scattered over northern Morocco and Algeria. Ahead of the front, southerly winds of 15 m s^{-1} carried warm ($+15^\circ\text{C}$) air over Italy.

The upper-level trough cut off by 78011212 and was centered over southern France. The strongest winds aloft were located west of the low over Spain; at 500 mb the winds were 50 m s^{-1} while at 300 mb winds exceeded 70 m s^{-1} .

During the following 12 hours, the closed low at 500 mb maintained its intensity as it drifted southward to a position over the Balearic Sea. The circulation aloft became more nearly symmetric by this time (78011300). Very cold⁵ air filled the center of the circulation at 500 mb (Fig. 9a).

As the upper-level circulation became more symmetric and the cold air was carried into the circulation, the surface cyclone remained stationary and began to decay; by 78011300 the minimum pressure had risen to 998 mb. Light snow and rain continued over the Pyrenees and Alps and over most of northern Italy. Thunderstorms and showers were reported north of the cold front in Northern Africa (Fig. 7b).

During the first 12 h, the model weakened the Netherlands low from 990 to 1006 mb as observed and developed a low of 994 mb (2 mb too high) over the Ligurian Sea about 120 km east of the observed position. At 24 h

⁵The balanced temperatures in Fig. 9a are about 5°C lower than the first guess temperatures in the center of the cyclone, which is typical of the cold bias in the balanced temperatures at middle levels of cyclonic systems (Keyser, 1978).

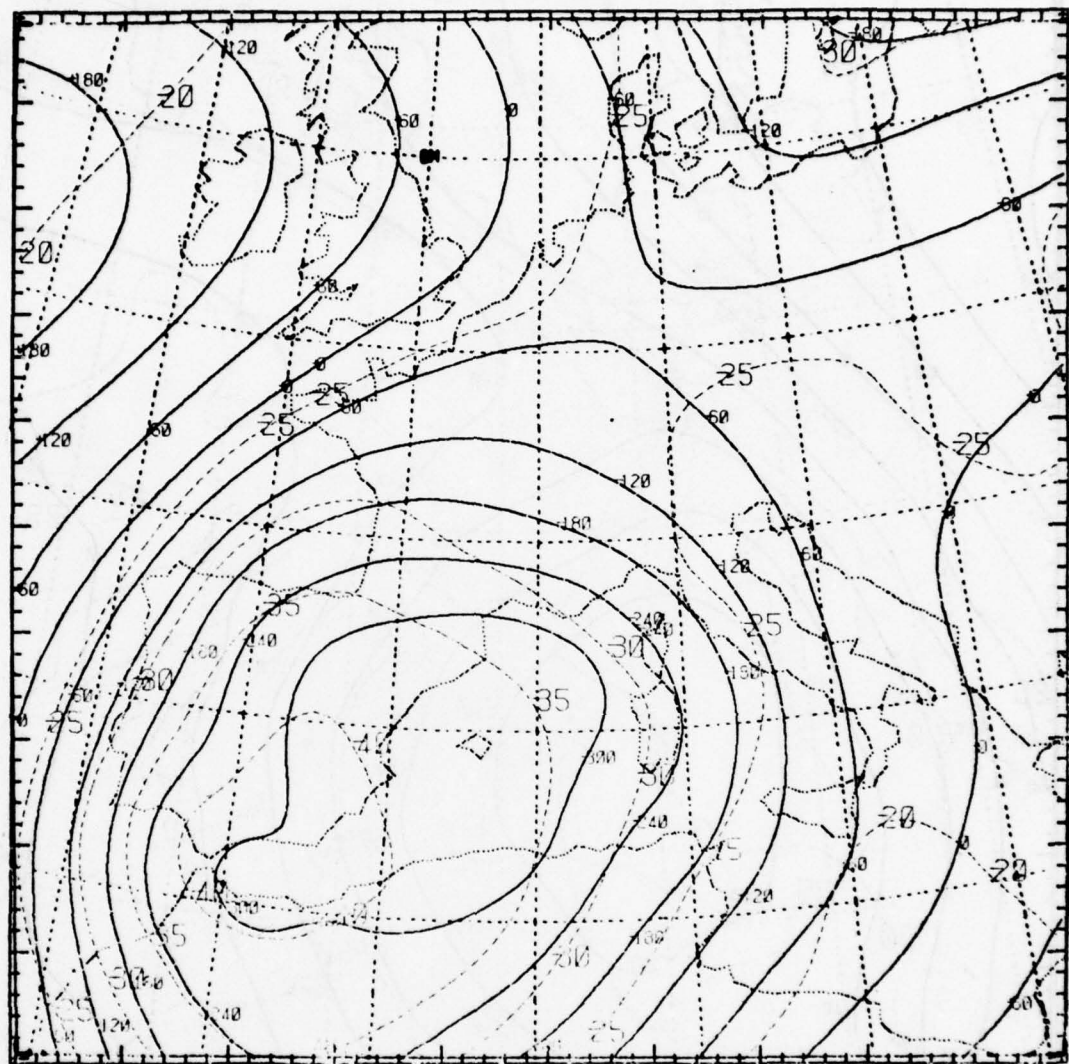


Fig. 9a. Balanced D-values (m) and temperatures ($^{\circ}\text{C}$) at 500 mb for 78011300. The contour interval for the D-values (solid lines) is 60 m; the isotherm (dashed lines) interval is 5°C .

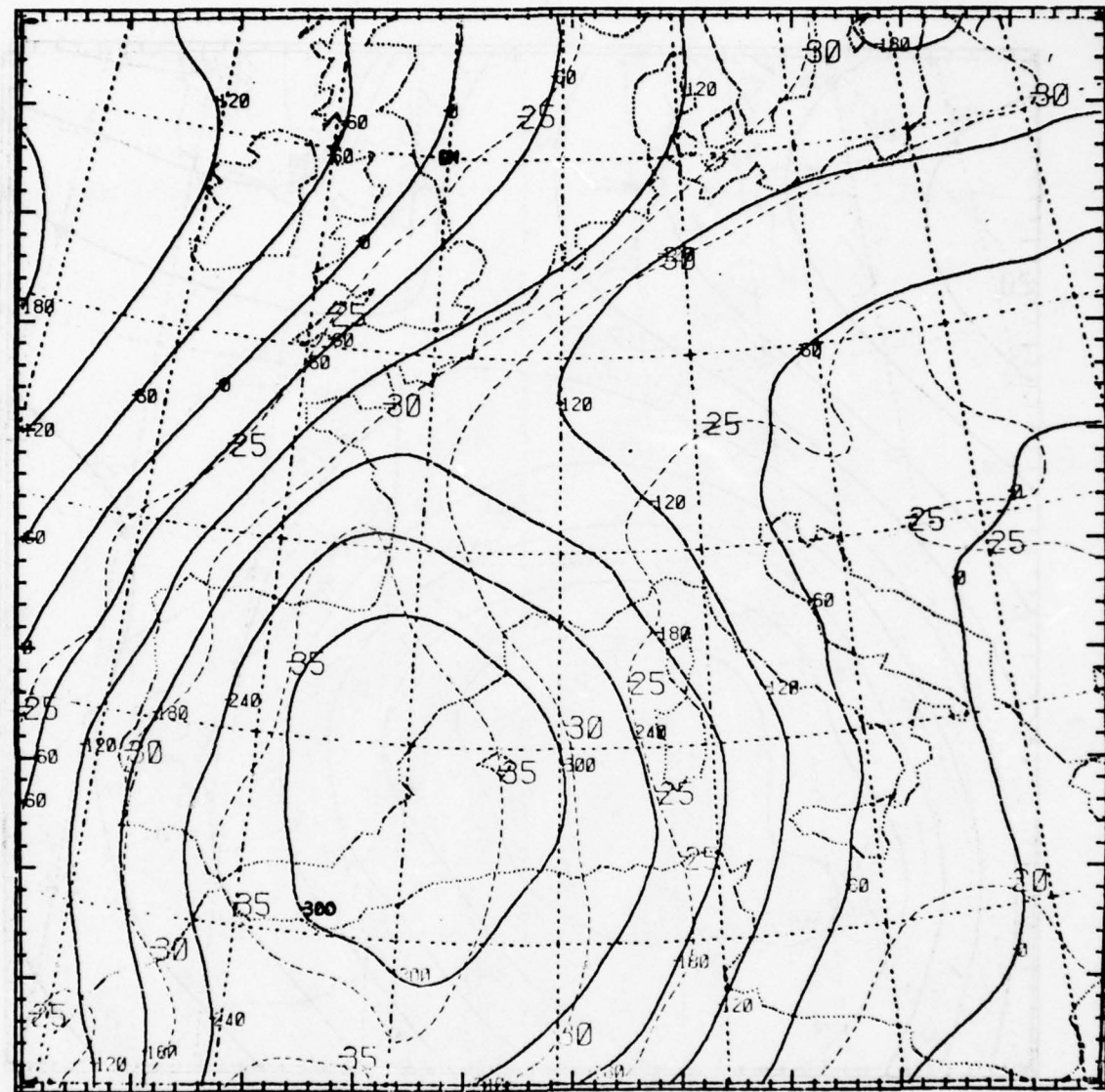


Fig. 9b. 24-h forecast D-values (m) and temperatures ($^{\circ}$ C) at 500 mb for 78011300. The contour interval for the D-values (solid lines) is 60 m; the isotherm (dashed lines) interval is 5° C.

(78011300) the predicted central pressure was 991 (7 mb too low) and the location was about 100 km south of the observed position (Fig. 6a). The strong SLP gradient north and east of the cyclone is well forecast by the model, and regions of strong winds in the PBL over the Ionian Sea and the Bay of Biscay correspond well with reports of surface winds $20-25 \text{ m s}^{-1}$ in these areas.

The upper-level circulation and temperature patterns are also well predicted by the model. At 500 mb (Fig. 9b) the low has cut off in about the right position (compare with Fig. 9a) and the forecast temperatures are close to the first guess values (see footnote 5).

Fig. 10 shows the forecast 300 mb winds (m s^{-1}) and the relative vorticity fields (10^{-5} s^{-1}). The jet streak with maximum speeds of over 65 m s^{-1} over the Bay of Biscay agrees well with observations (not shown) in this region. It is interesting to note that the jet has become smaller in horizontal scale during the 24 h (compare Fig. K4c with Fig. 10), indicating that the model dynamics and thermodynamics have produced a more realistic mesoscale structure from a larger scale analysis. Relative vorticity values on the cyclonic side of the jet exceed $18 \times 10^{-5} \text{ s}^{-1}$, compared to a maximum of about $13 \times 10^{-5} \text{ s}^{-1}$ in the initial conditions. This magnitude is quite comparable to the values of $25 \times 10^{-5} \text{ s}^{-1}$ and $18 \times 10^{-5} \text{ s}^{-1}$ diagnosed by Shapiro (1976) from aircraft data across a strong frontal zone over the Great Plains of the United States and to the maximum value of relative vorticity of 2.4 f in Hoskins' (1971) theoretical model of fronts. However, it is less than the extreme value of $60 \times 10^{-5} \text{ s}^{-1}$ found in an upper-level front over Colorado by Shapiro (1974).

Figure 11 shows a vertical cross section extending along a northwest-southeast line from a point northwest of Lands End (U.K.) to the Albanian Coast (Fig. 10). The analyses of potential temperature and isotachs of the

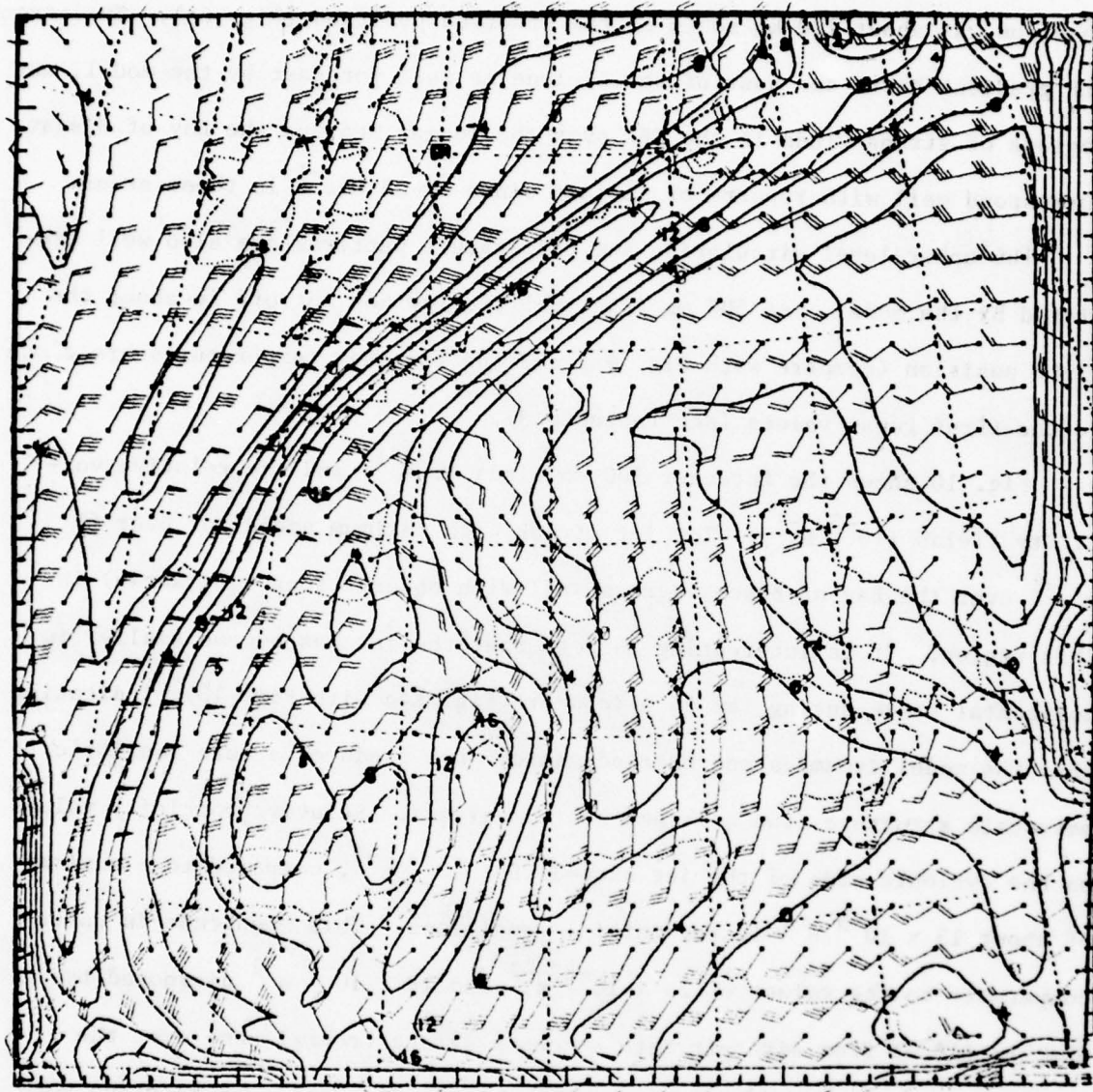


Fig. 10. 24-h forecast winds (m s^{-1}) and relative vorticity (solid lines in 10^{-5}s^{-1}) at 300 mb for 78011300. The maximum value of the relative vorticity along the coast of France is $18 \times 10^{-5} \text{s}^{-1}$. The maximum wind speed associated with the jet streak over the Bay of Biscay is 65 m s^{-1} .

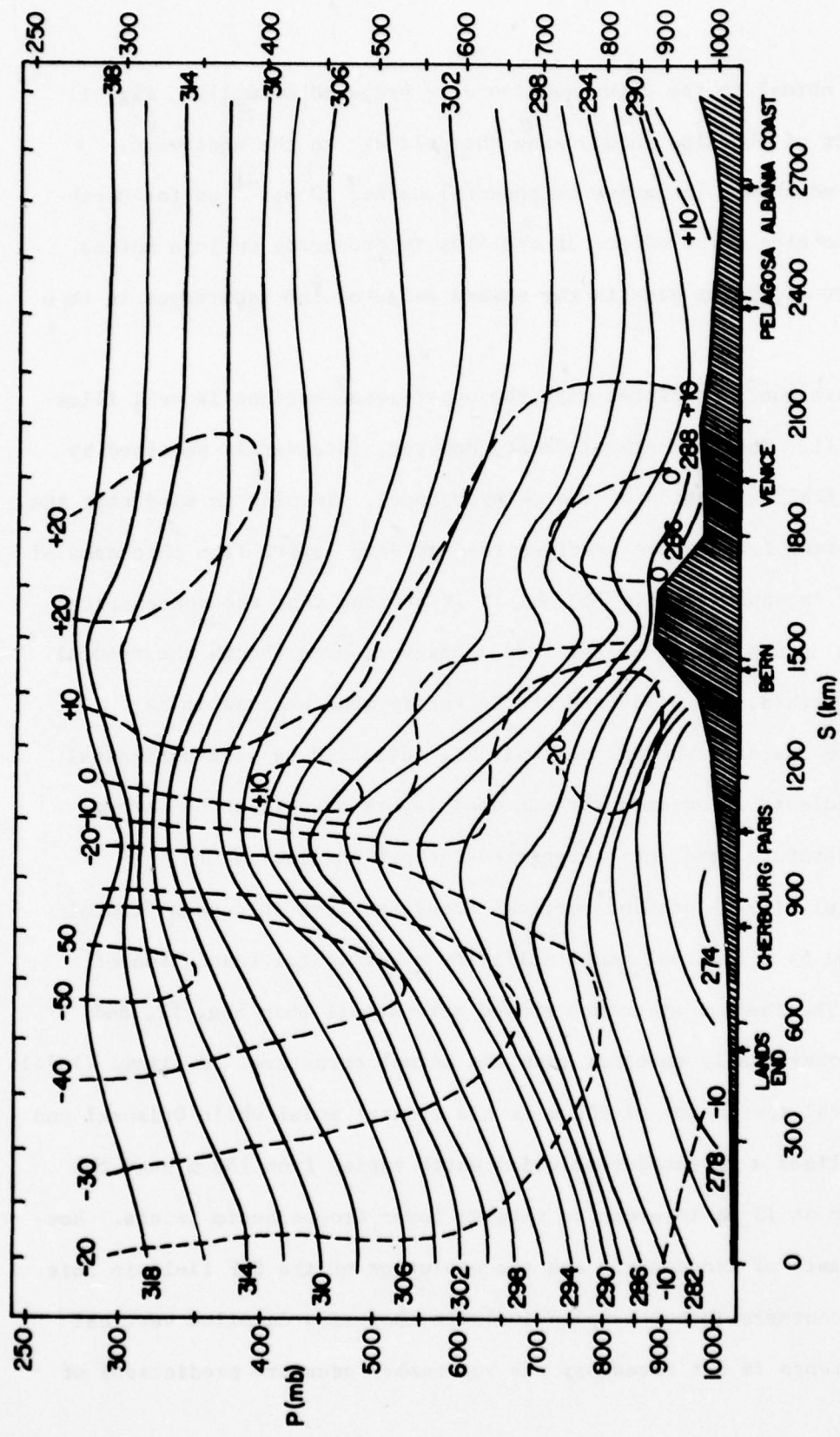


Fig. 11. Vertical cross section along a line oriented approximately NNW to SSE across the middle of the European domain constructed from a 24-h model forecast VT 78011300. Solid lines are potential temperature in K ; dashed lines are wind component ($m s^{-1}$) normal to cross section with negative values out of figure and positive values into figure.

wind component normal to the cross section were prepared manually. Fig. 11 shows the effect of the Alps in blocking the cold air to the northwest. Winds from the northeast (negative components) exceed 20 m s^{-1} on the northwest side of the Alps. The effect of the Alps in producing upslope motion on the southeast slopes is seen in the upward bulge of the isentropes in this region.

The cold air pool associated with the upper-level cyclone is well illustrated by Fig. 11. The upper-level front, however, is severely smoothed by the coarse vertical resolution of the 6-layer model. Keeping in mind that the model is predicting temperature averages through deep layers (the thickness of the upper layer is approximately 200 mb), it is obvious that the concentrated fronts found in nature cannot be resolved. However, even though the frontal structure is smoothed, the wind forecast is fairly good because it is possible to have the same thermal wind balance satisfied by weak horizontal temperature gradients integrated through deep layers as well as by strong horizontal temperature gradients integrated through shallow layers.

Keyser et al. (1978) present vertical cross sections through a frontal system predicted by a 15-level model utilizing a horizontal resolution of about 100 km. The thermal structure showed more detail than Fig. 11, and yet was still considerably smoother than the actual structure. Williams (1974) adopted a vertical resolution of 200 m in his frontal model while Orlanski and Ross (1977) utilized a vertical resolution which varied from 150 m near the surface to 400 m at 15 km in order to resolve lower tropospheric fronts. However, the forecasts of winds aloft and the evolution of the SLP field in this case (as well as others in our sample) indicate that such detailed vertical resolution of fronts is not necessary for reasonably accurate predictions of these fields.

Finally, the forecast 24-h precipitation forecast is presented in Fig. 12. Because much of the precipitation is over water, a quantitative verification is not possible. However, the main band associated with the cold front extending across the western Mediterranean is realistic, and the maxima over the Pyrenees and Atlas mountains are consistent with surface reports of precipitation in these regions during the 24 hour period.

4.3 Forecast of the Ohio blizzard of 26 January 1978

The second case selected for detailed study covers the development of the "worst blizzard on record in the Ohio Valley" (Wagner, 1978). Between 78012512, the start of the forecast, and 78012612, a 998 mb low over Mississippi deepened to 958 mb as it moved northeastward to Cleveland, Ohio. Shortly thereafter the storm moved into southwestern Ontario where Sarnia measured a pressure of 955.5 mb. Toronto, which began keeping records in 1840, broke its all time record for lowest pressure with a reading of 962 mb (Ludlam, 1978).

Gusts of near hurricane force winds were reported at many locations (Cleveland, 82 mph; Erie, PA, 78 mph; Blue Hill Observatory, Boston, 72 mph). Gusts of 90 mph were measured on the Chesapeake Bay Bridge. Snowfall amounts to the west of the storm track exceeded 30 cm in several locations.

The cyclogenesis was a result of the phasing of two intense shortwave troughs, one moving into the U.S. from Canada across North Dakota and the other moving into the Lower Mississippi Valley from New Mexico. Strong low-level southerly and southeasterly winds ahead of the southern trough (Fig. K5) brought very warm, moist air inland across the Appalachians. This warm air was drawn into the developing low, forming an unusual warm-core cyclone and allowing for the extremely low pressure.

Fig. K7c shows the 300 mb winds at 78012512. Two strong jets associated with the phasing troughs are moving into the domain. The northern jet has

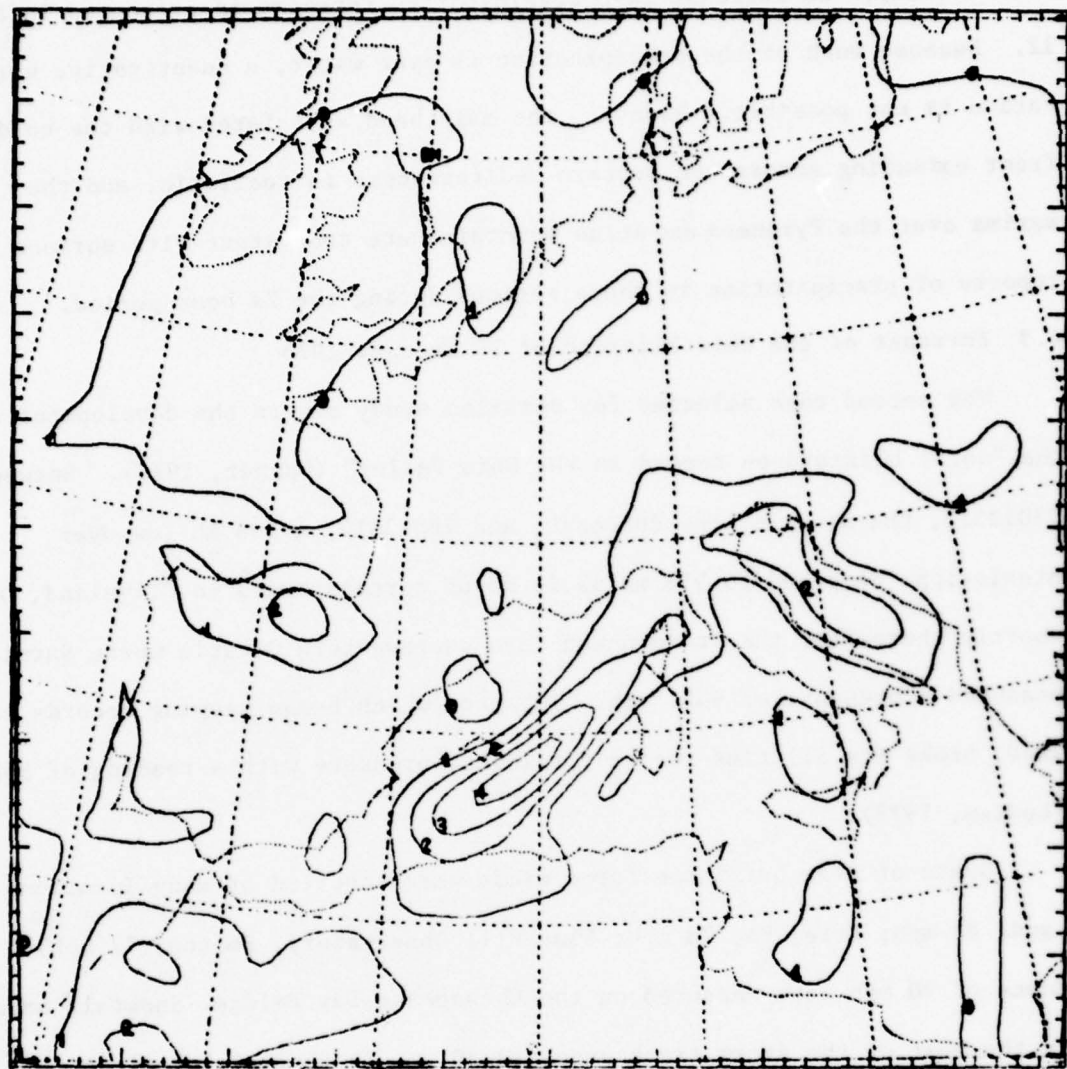


Fig. 12. Forecast precipitation (cm) for 24 hours ending 78011300.

speeds greater than 65 m s^{-1} ; the maximum wind in the southern jet exceeds 75 m s^{-1} . At 500 mb the northern jet with a maximum speed of 50 m s^{-1} was stronger than the southern jet, which had a maximum speed of about 40 m s^{-1} .

The 850 mb map of D values and temperature (not shown) shows a broad baroclinic zone oriented in a southwest-northeast direction from the Gulf Coast to New England and a small pool of extremely cold air entering the U. S. over North Dakota. Warm advection was occurring over the eastern states with cold advection over Texas and Louisiana. This differential advection was favorable for deepening the southern trough while building the ridge off the East Coast by Sutcliffe's self-development mechanism. Later, the cold air over North Dakota moved into the rear of the combined trough, producing further intensification.

In summary, the synoptic conditions were extremely favorable for cyclogenesis. A strong large-scale temperature gradient existed; there were two jet streaks with maximum winds in excess of 60 m s^{-1} moving into the same region, and there was an abundant moisture supply available to the system from the east and southeast.

In the next 12 hours the southern trough moved rapidly from Texas to Alabama as it phased with the northern system. Winds at 500 mb over the southeastern U.S. ahead of this southern system backed into a more southwesterly direction and doubled in speed. At 850 mb the cold air which was over North Dakota 12 hours earlier moved rapidly southeastward and was entering the rear quadrant of the developing cyclone, which was located over eastern Tennessee.

In the 12 hours ending at 78012612, the surface low deepened to 958 mb as it moved to a position over southwestern Ontario (Fig. 13a). At 850 mb, the center of the low contained very warm air (+ 5°C) for January; the low-level cold air was far to the southwest (Fig. 14a). The trough at 500 mb had formed a closed circulation, although cold advection was still occurring in the southwest quadrant (Fig. 15a).

MODEL FORECAST

The development of the cyclone by the fine mesh model followed the atmosphere fairly closely. Fig. 13b shows the predicted SLP pattern and the winds at the lowest model level ($\sigma = 0.925$). The central pressure of 955 mb is 3 mb lower than the minimum observed pressure of 958 and the center is located about 360 km to the southeast of the actual position. The low-level wind field shows many 40 m s^{-1} winds around the low and several 50 m s^{-1} winds in western Virginia and North Carolina. These winds are much larger (by a factor of 4 or so) than the mean surface winds, due in part to the neglect of surface friction. Also, they pertain to a level of about 600 m above the ground and hence should be greater than the average surface winds even if friction were included. They are comparable in magnitude to the observed winds at 850 mb and to the maximum surface gusts mentioned earlier. A more detailed interpretation of these winds follows in the next section.

The 24-h forecast of SLP by the FNWC model is given in Fig. 13c. This case is one in which the advantage of high horizontal resolution is fairly clear; the coarse mesh FNWC model could not resolve the small scale structure of the cyclone. The smooth forecast was 27 mb too high and the speed was too slow.

Fig. 14b shows the fine mesh model's forecast D-values and temperatures at 850 mb. The warm core nature of the model cyclone is evident; in fact, the model cyclone is warmer than observed by several °C at 850 mb. The

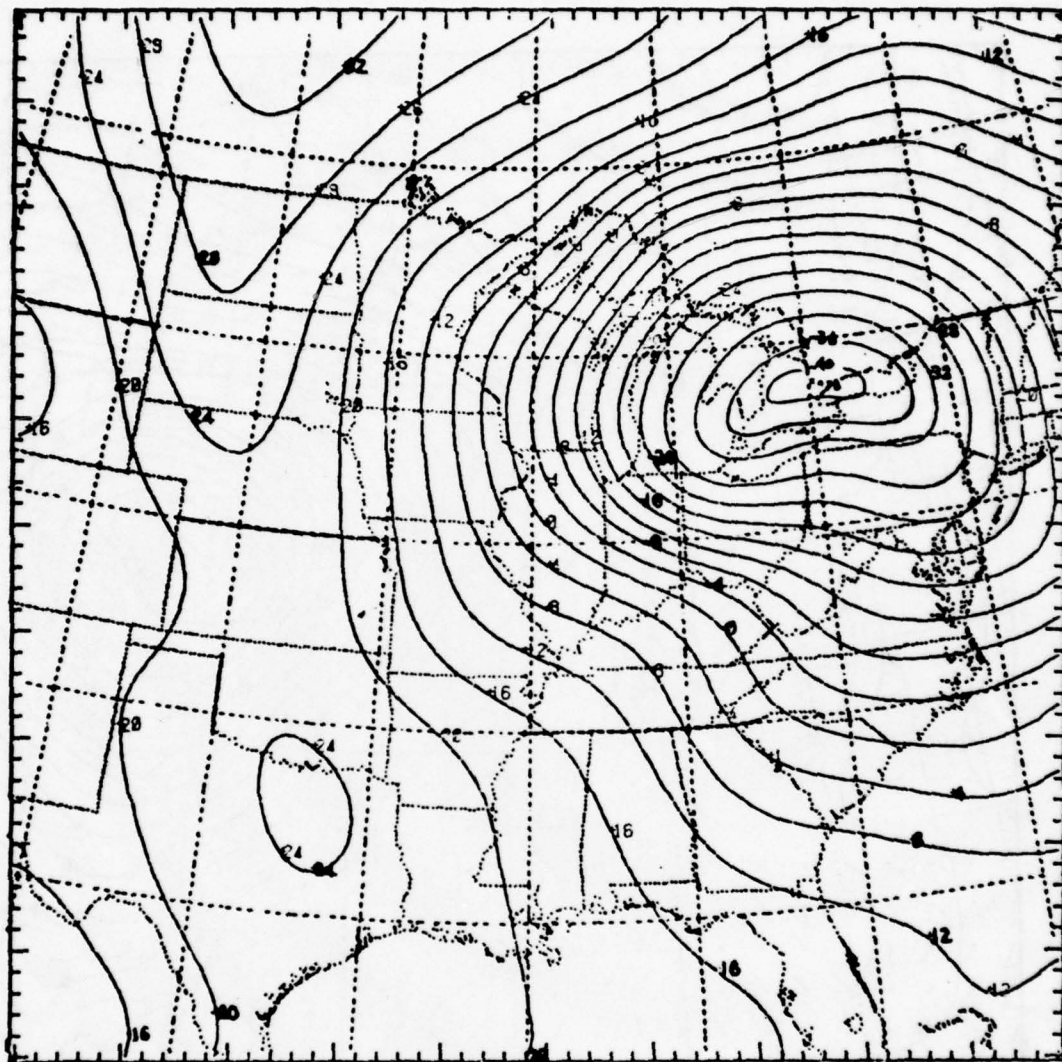


Fig. 13a. Observed SLP-1000 mb VT 78012612. The minimum pressure is 958 mb.

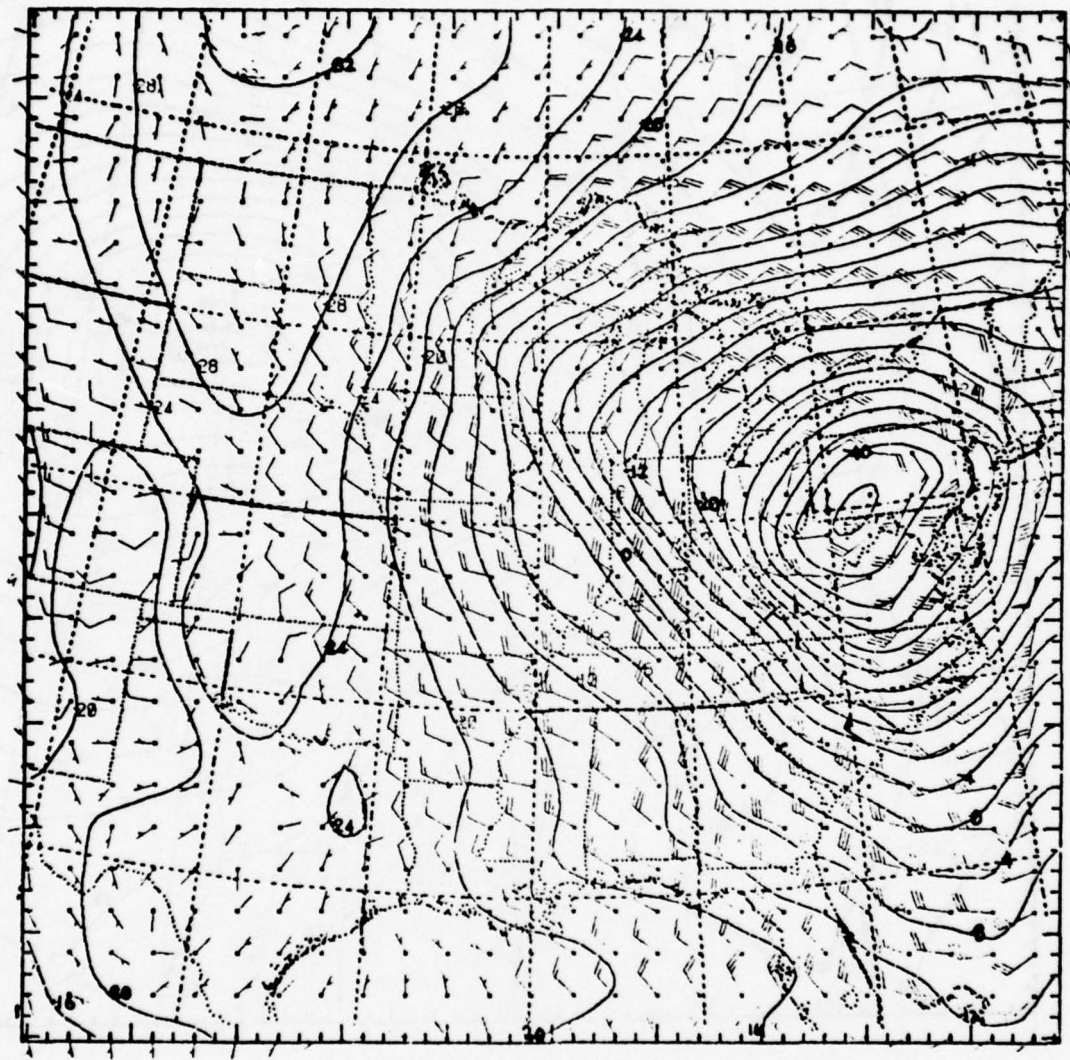


Fig. 13b. 24-h forecast SLP-1000 mb and winds (m s^{-1}) at $\sigma = 0.925$
VT 78012612. The central pressure is 955 mb.

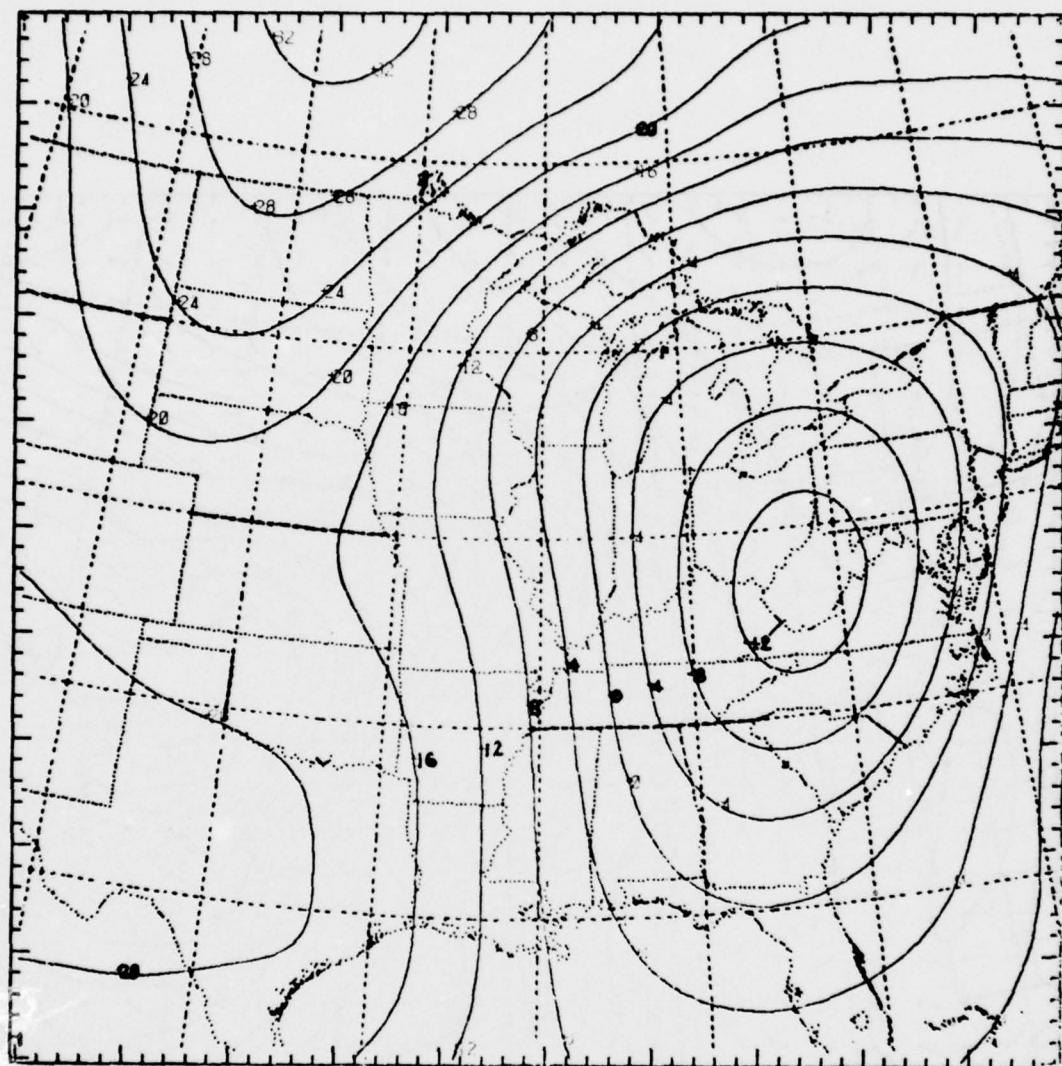


Fig. 13c. 24-h forecast SLP-1000 mb VT 78012612 by FNWC model.
Central pressure is 985 mb.

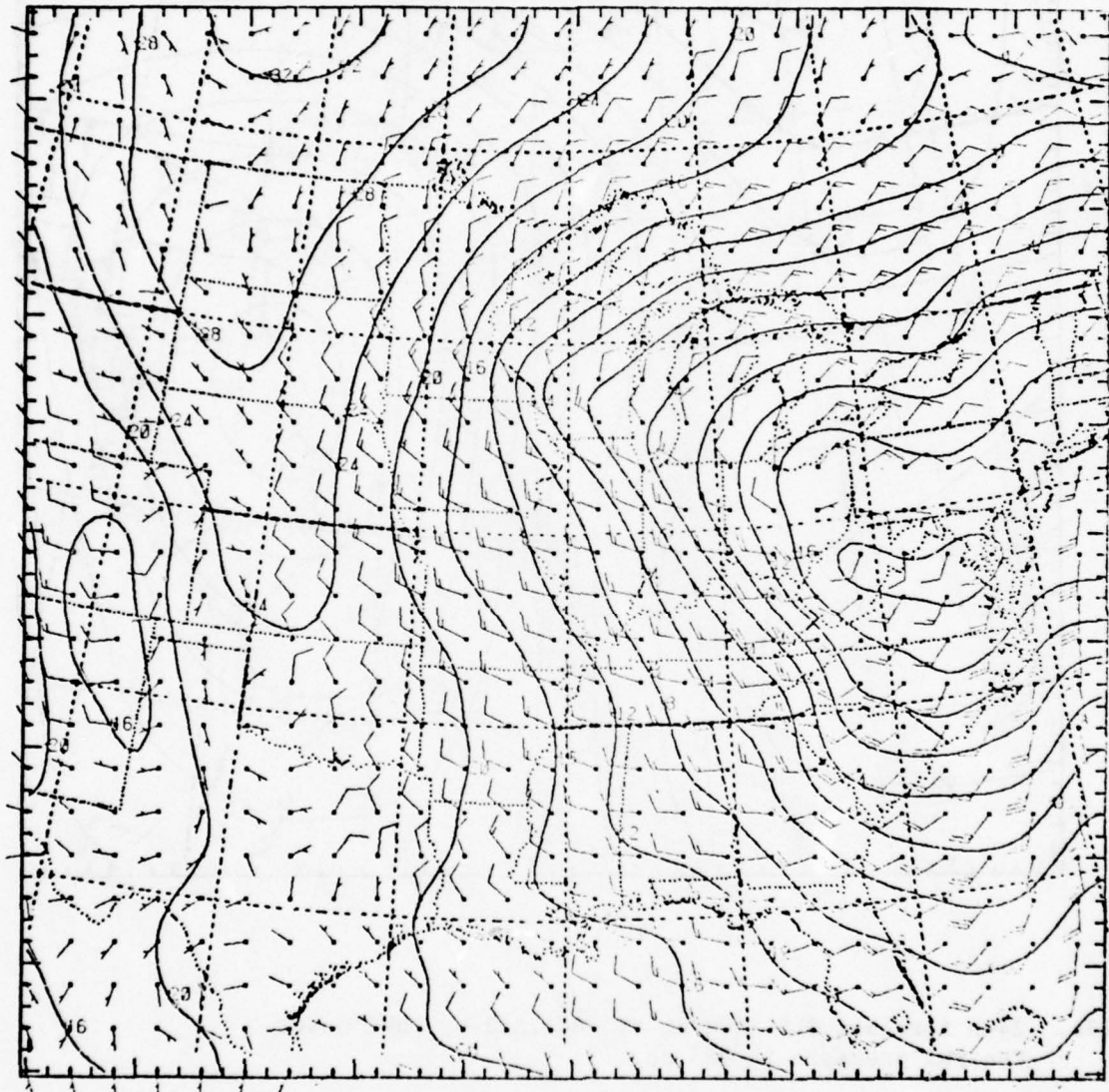


Fig. 13d. As in 13(b) except surface friction present over entire domain. The minimum pressure is 978 mb.

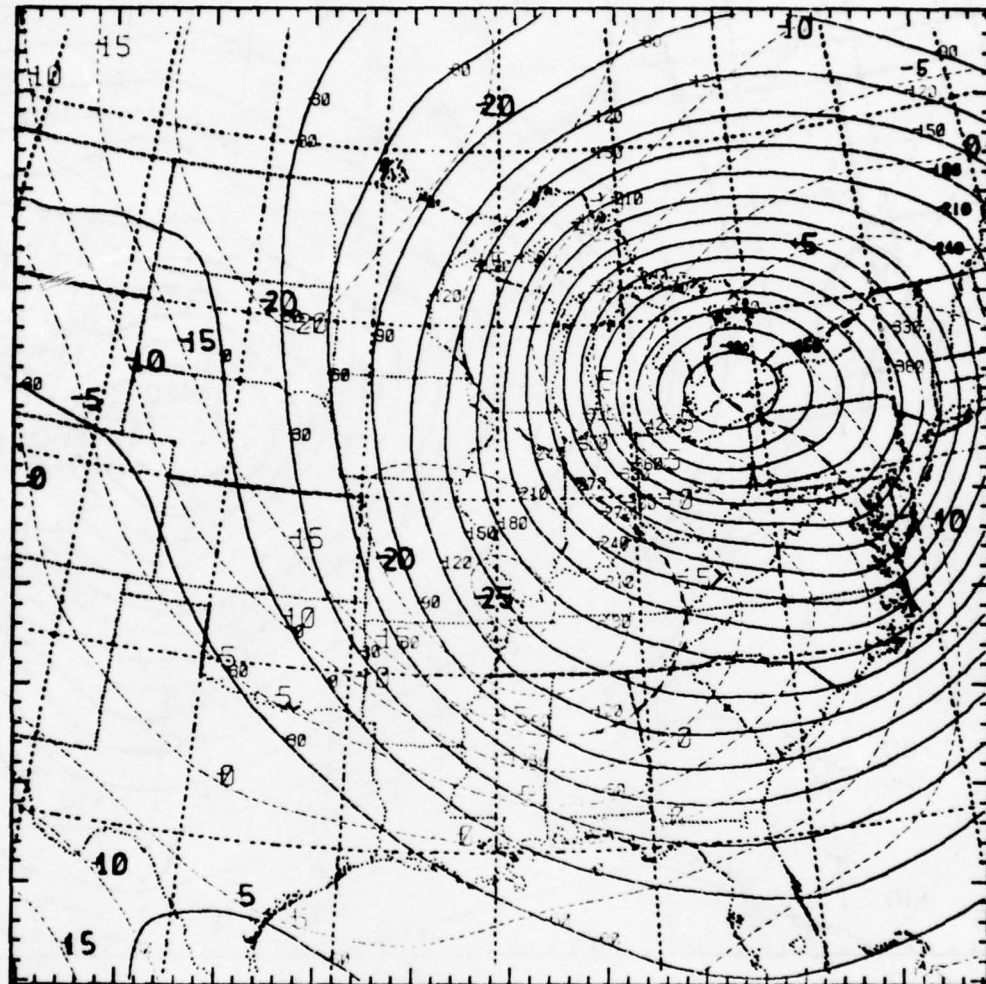


Fig. 14a. Balanced D-values (m) and temperatures ($^{\circ}\text{C}$) at 850 mb for 78012612. The contour interval for the D-values (solid lines) is 30 m; the isotherm (dashed lines) interval is 5°C .

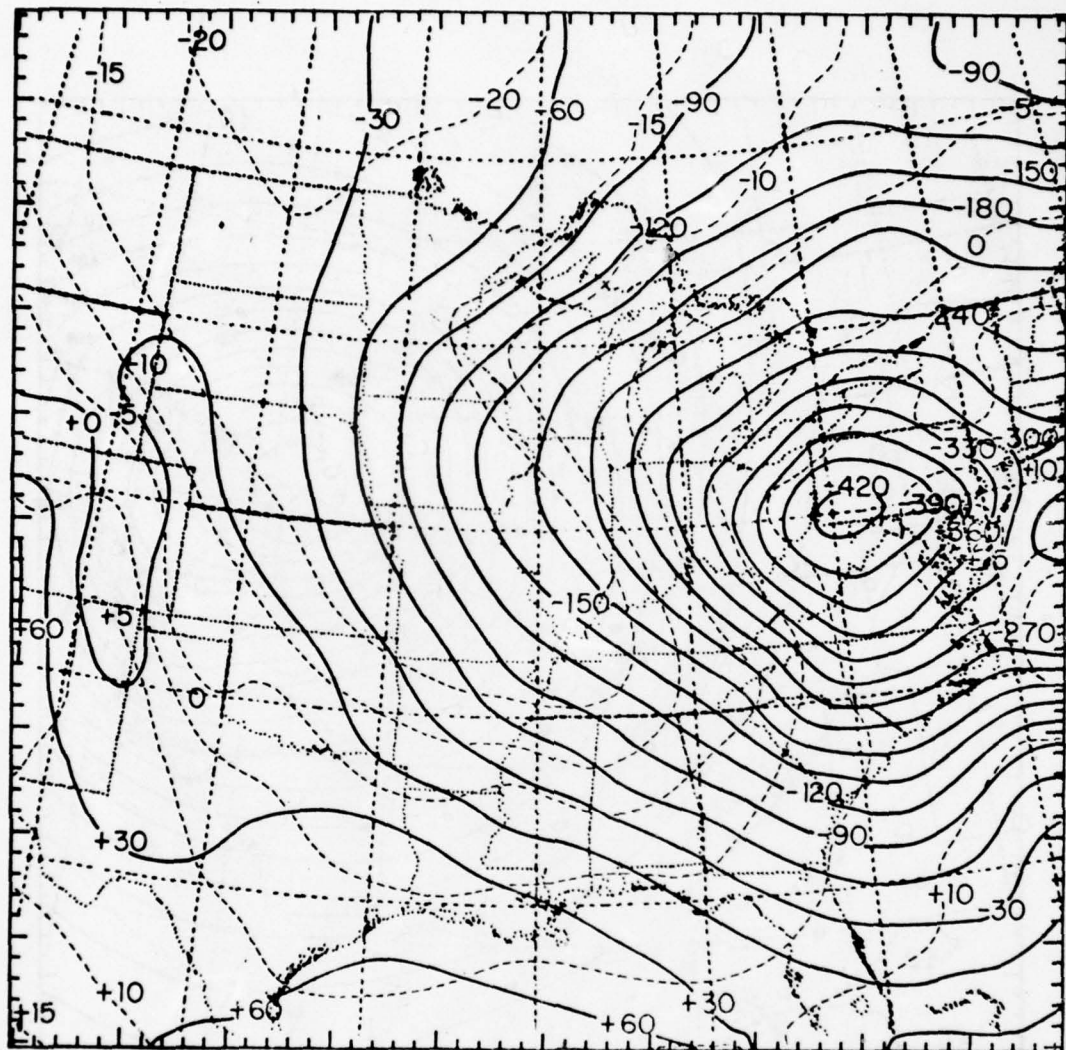
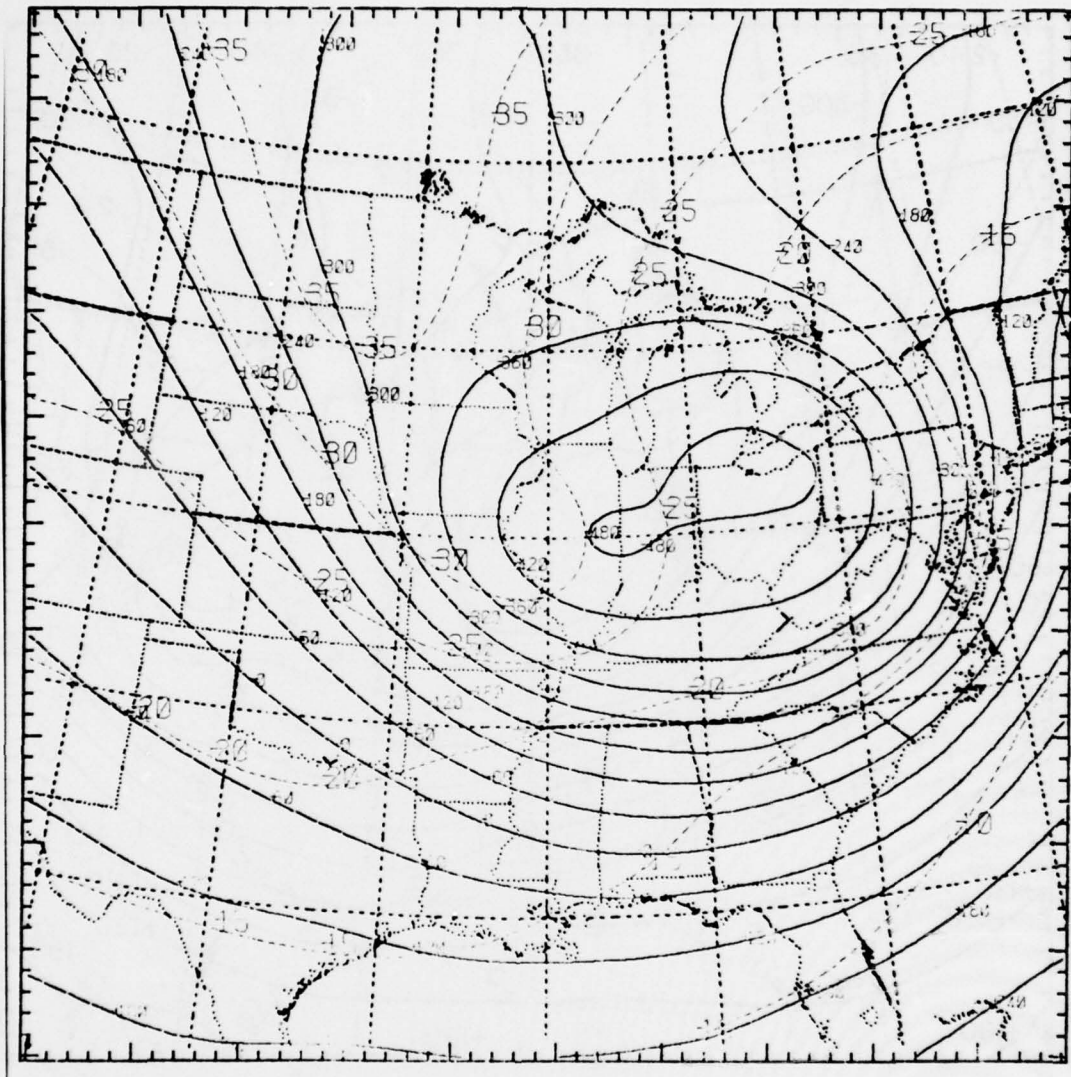


Fig. 14b. 24-h forecast D-values (m) and temperatures ($^{\circ}\text{C}$) at 850 mb for 78012612. The contour interval for the D-values (solid lines) is 30 m; the isotherm (dashed lines) interval is 5°C .



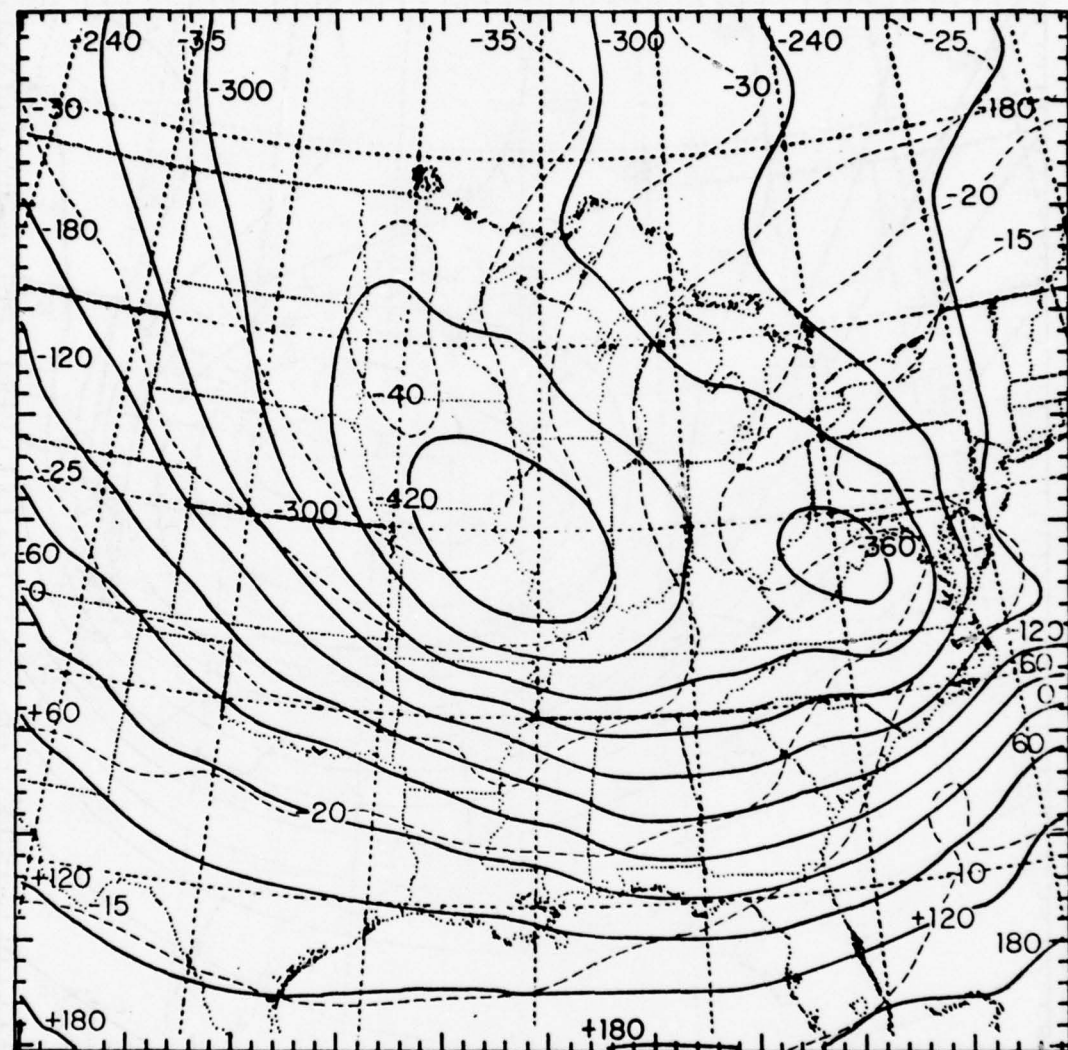


Fig. 15b. As in Fig. 9 for 78012612.

warm pocket over southwestern New Jersey of over 15°C is unrealistic and the air over western Kentucky is not cold enough.

At 500 mb the model forecast (Fig. 15b) is similar to the observed (Fig. 15a) with the exception that the air over the center of the model storm is about 5°C too warm and the air over Minnesota is 5°C too cold. Another discrepancy is the model's forecast of the main 500 mb low center over western Illinois rather than northern Ohio. The excessive tilt of the cyclone is consistent with the model's subsequent overdevelopment after 24 hours.

Fig. 16a shows the analyzed (balanced) winds at 500 mb for 78012612 while Fig. 16b shows the predicted 500-mb winds and relative vorticity. The jet curving in an arc across Nebraska, Arkansas, northern Alabama and Georgia and up the East Coast is fairly well forecast by the model. In addition to the general region of cyclonic vorticity north of the jet, the model has produced 2 shortwave features, with relative vorticity maxima of $25 \times 10^{-5} \text{ s}^{-1}$ and $30 \times 10^{-5} \text{ s}^{-1}$ over western Illinois and Virginia respectively. The rapid variation of the vorticity near the eastern boundary is noise induced by the strong winds normal to the boundary.

Fig. 17 shows a north-south vertical cross section along 80°W longitude which passes very near to the center of the surface low. The warm core nature of the low is evident. In contrast to the cross section through the Genoa low (Fig. 11) the winds normal to the cross section in the vicinity of the low do not satisfy the thermal wind relationship very well. For example, the vertical wind shear between 700 and 300 mb is weak over Pittsburgh (PIT) in spite of a large horizontal temperature gradient. The lack of geostrophic balance apparently reflects accelerations associated with the strongly curved flow in the vicinity of this rapidly deepening cyclone. Shapiro (1974) found that the effects of trajectory curvature were important in determining the

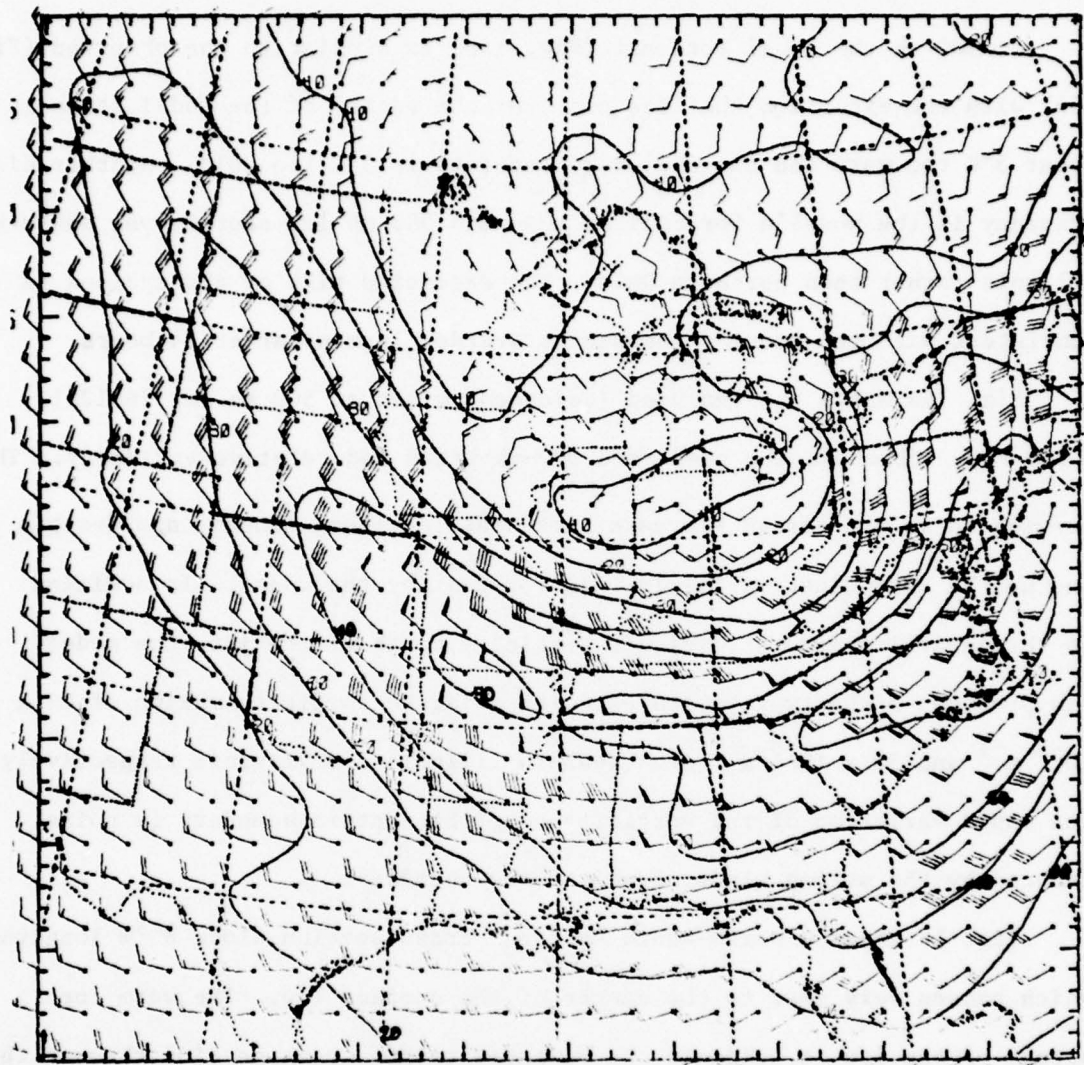


Fig. 16a. Balanced winds (m s^{-1}) at 300 mb for 78012612. Solid lines (isotachs) are in m s^{-1} .

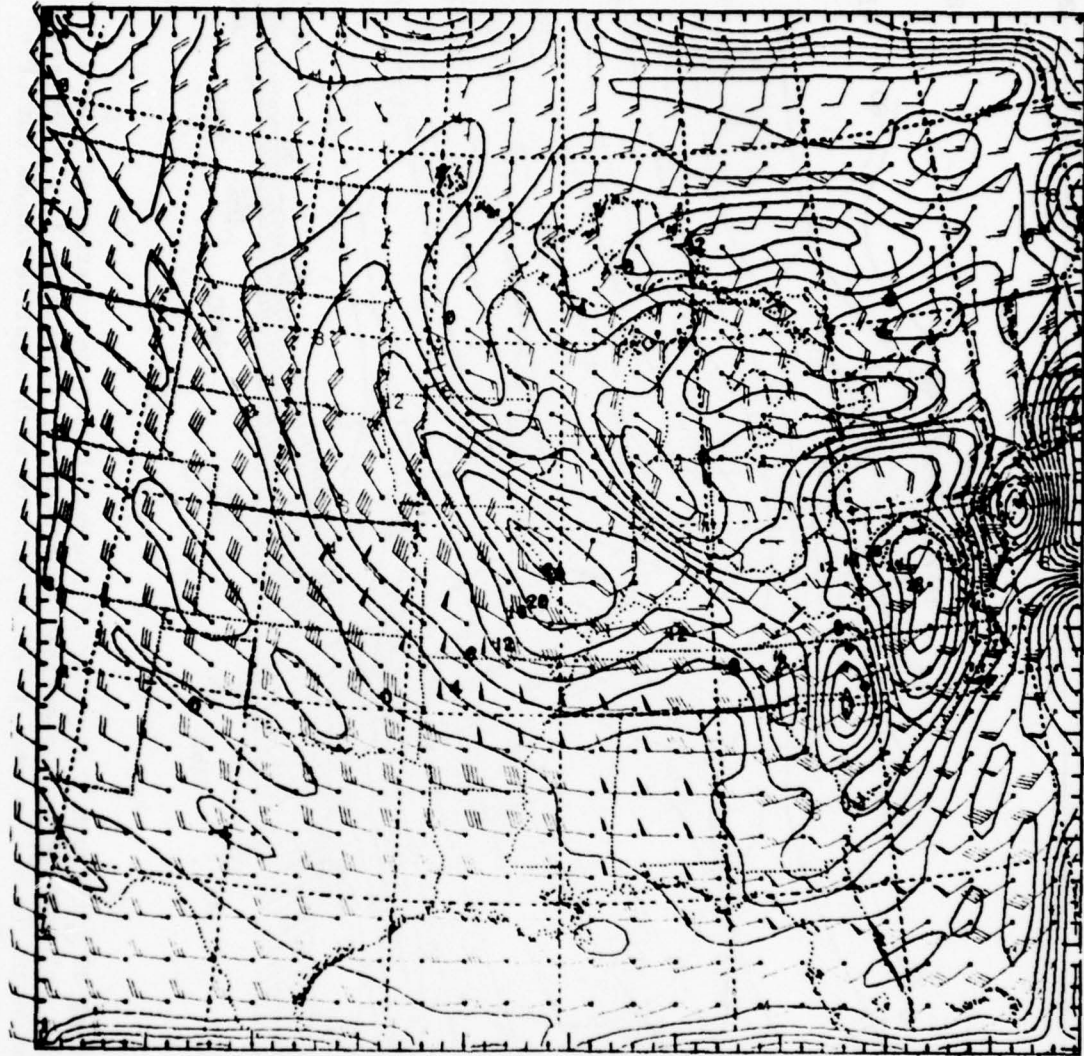


Fig. 16b. 24-h forecast winds (m s^{-1}) at 300 mb for 78012612. Solid lines are relative vorticity with a contour interval of $4 \times 10^{-5} \text{ s}^{-1}$. Maxima over southwestern Illinois and central Virginia are 25 and $30 \times 10^{-5} \text{ s}^{-1}$ respectively.

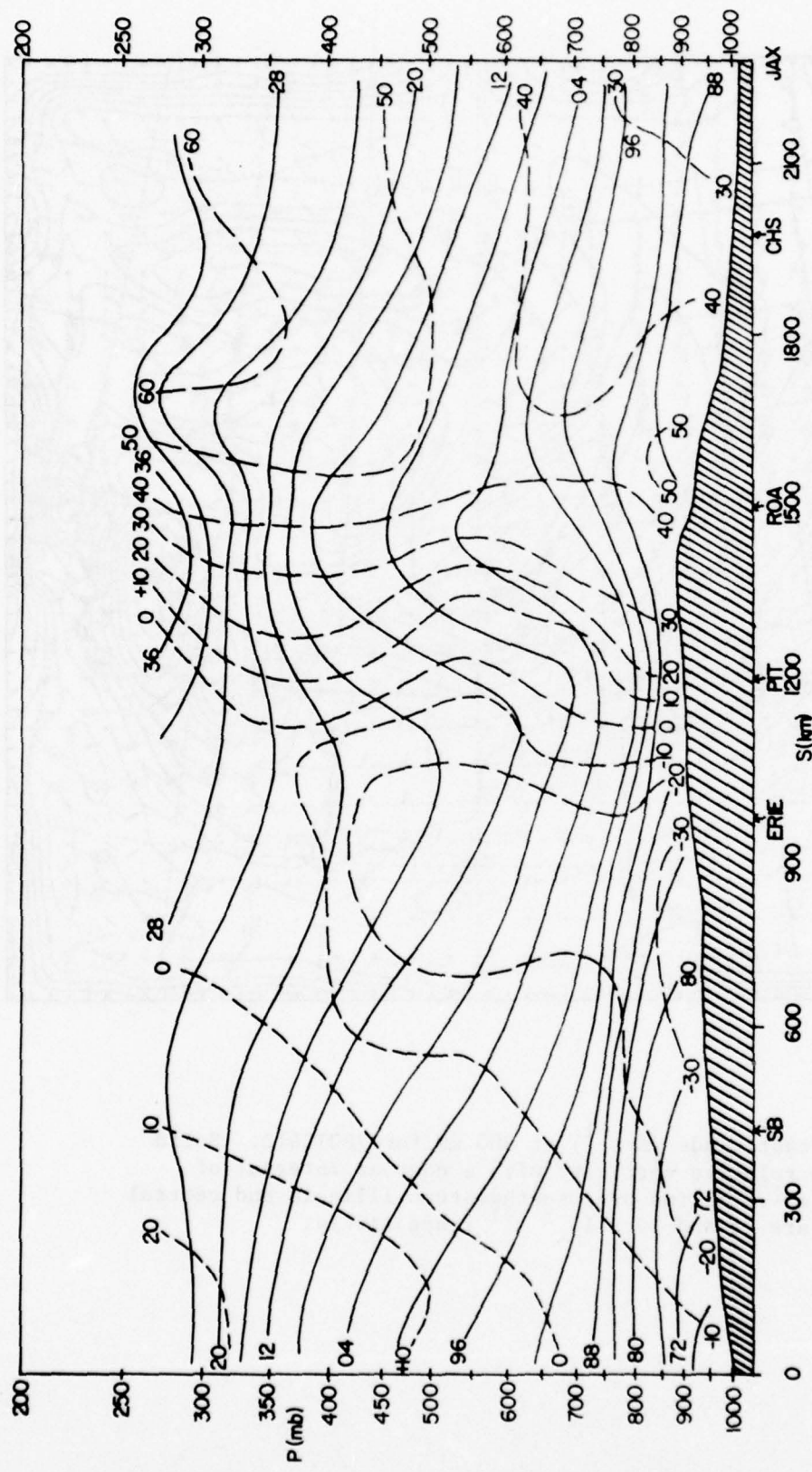


Fig. 17. Vertical cross section along 80°W through the center of the model cyclone constructed from a 24-h forecast VT 78012612. Solid lines are potential temperature in K (leading 3 or 2 omitted); dashed lines are wind components ($m s^{-1}$) normal to cross section with negative values out of figure and positive values into figure.

vertical wind shears in a strong cyclone. For gradient flow, the actual and geostrophic (denoted by subscript g) shears are related by

$$\frac{\partial V}{\partial z} = \frac{f}{\frac{2V}{R} + f} \frac{\partial V_g}{\partial z} + \frac{V^2}{R^2} \frac{\partial R}{\partial z} \quad (14)$$

where V is the component of the horizontal wind tangent to the isobars and R is the radius of curvature (positive for cyclonic flow). For cyclonic flow in which the vertical variation of R is small, the actual wind shear is less than the geostrophic wind shear as indicated in Fig. 17.

Fig. 18 shows a cross section oriented approximately west to east through the cyclone. The cold air mass between the Rockies and the Appalachian shows up clearly. The thermal wind relation is reasonably well satisfied west of Columbus, Ohio (CMH). However, as in the north-south section, the normal wind components are not in geostrophic balance in the vicinity of the storm.

Fig. 19 shows the observed and forecast precipitation for the 24-h period ending 78012612. There is some agreement, but considerable room for improvement. The observed maximum over central Alabama and Georgia is forecast to be a little too far south. The two observed maxima over southeastern Michigan and eastern Kentucky are not resolved; instead the model forecasts one maximum over Ohio. The model places the northern portion of the elongated maximum too far east. Finally, the 20-cm maximum off the Virginia coast is too high because of numerical errors at the lateral boundary.

The effect of surface friction on the development of this intense storm is illustrated by the SLP and level-6 winds (Fig. 13b) in a rerun of forecast US08 which included surface friction over the entire domain. With the large drag coefficient given by (3), the model storm is weaker than observed with a minimum pressure of 978 mb. The low-level winds are weaker by a factor of about 2 and the cross-isobar flow angle has increased markedly compared to

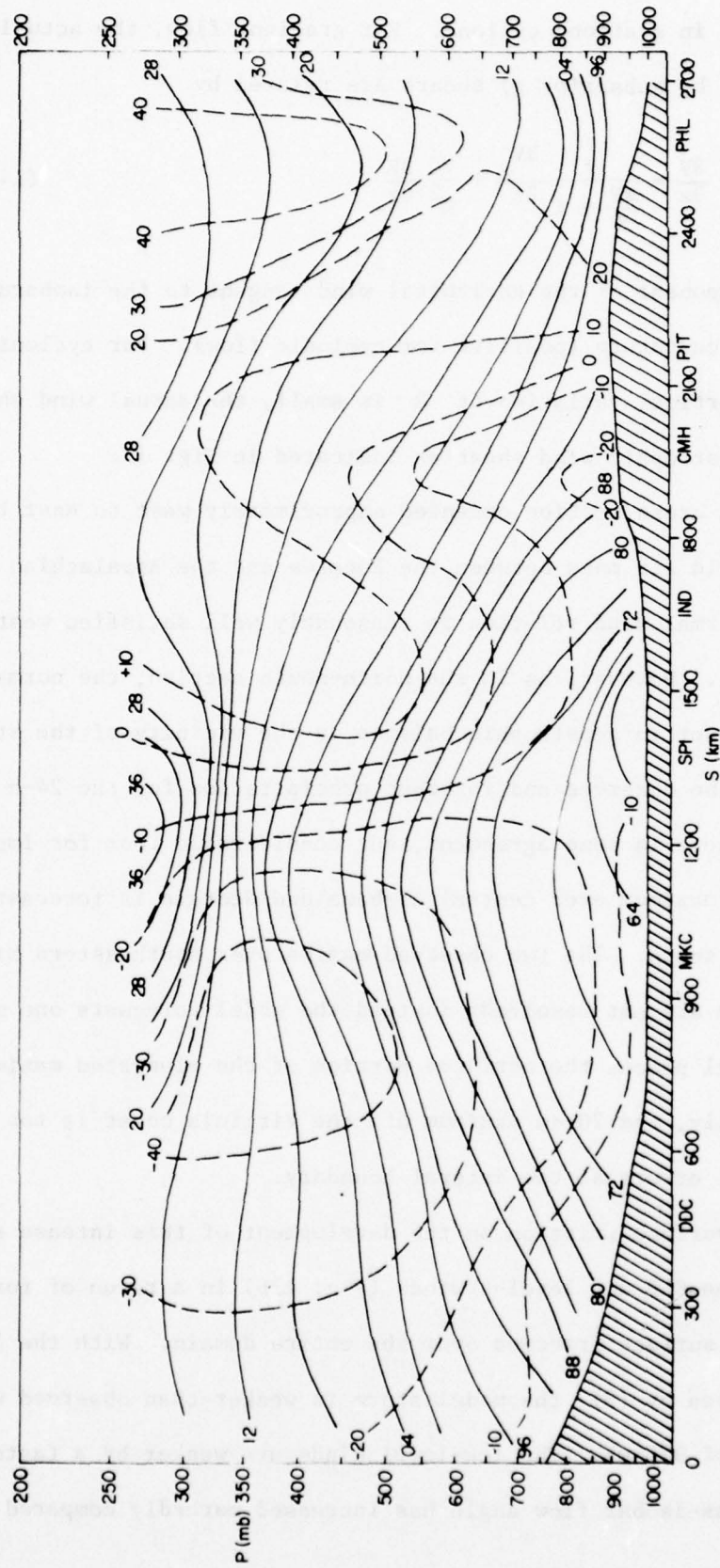


Fig. 18. As in Fig. 17 except for an approximate west to east section.

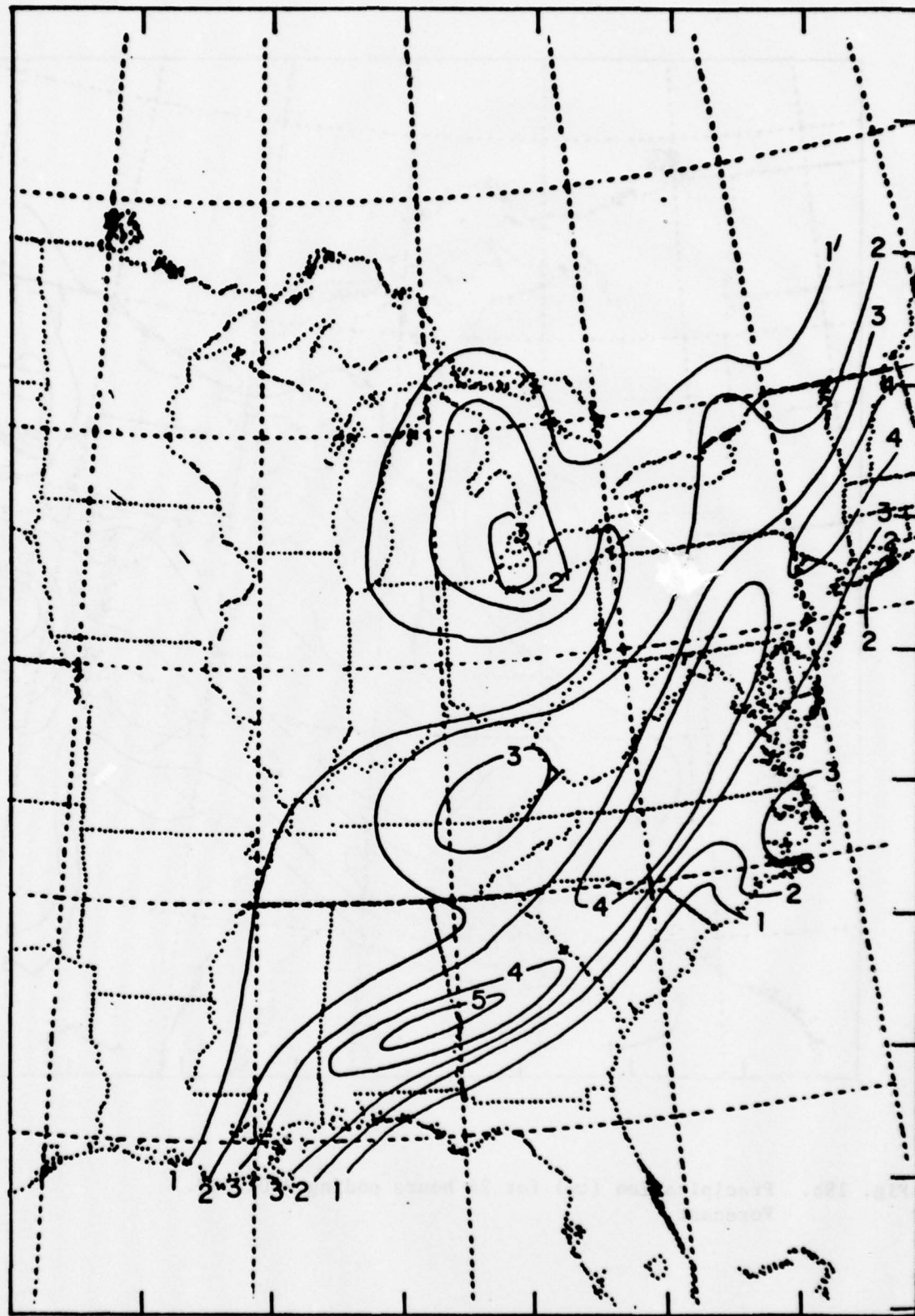


Fig. 19a. Precipitation (cm) for 24 hours ending 78012612.
Observed.

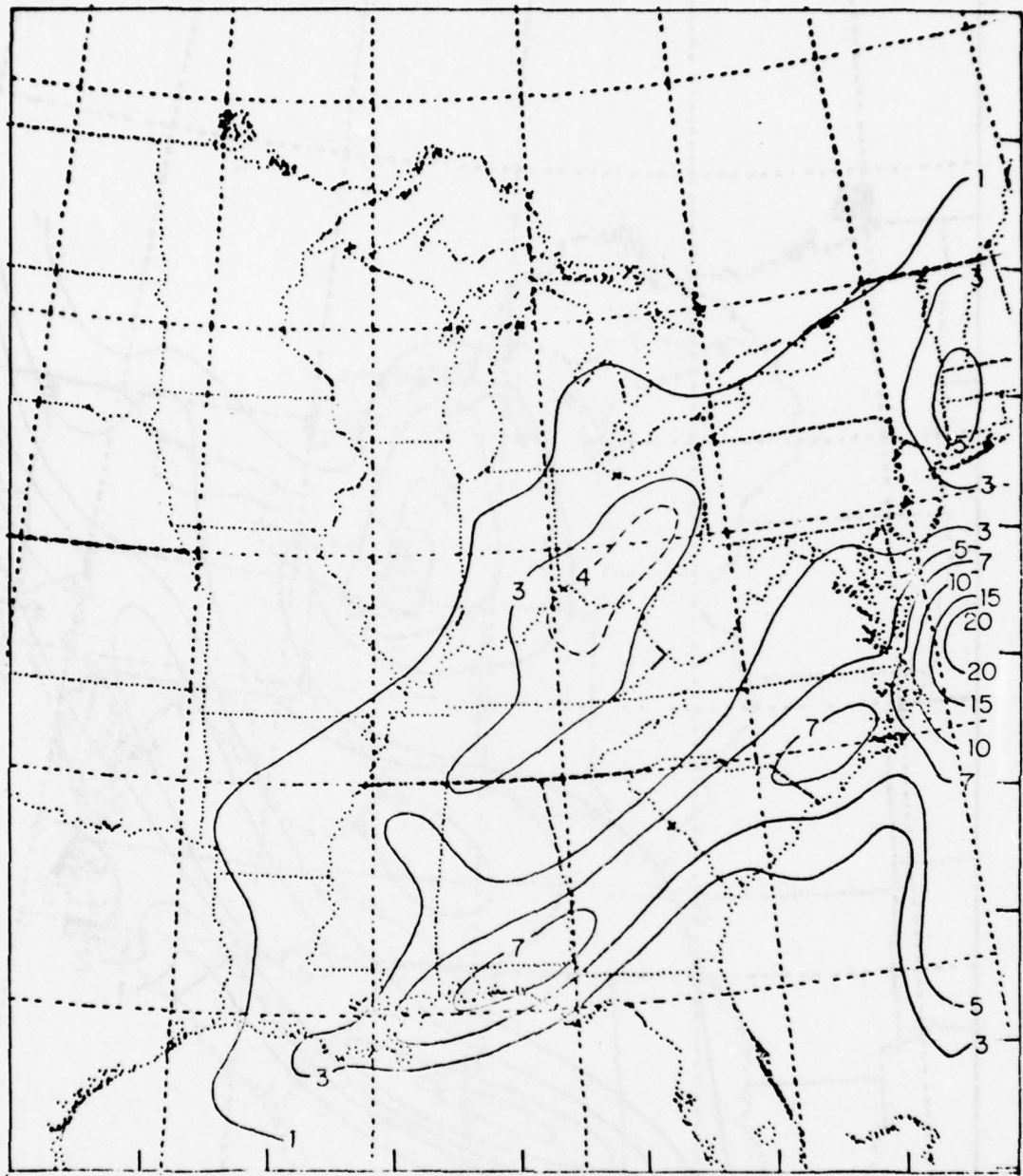


Fig. 19b. Precipitation (cm) for 24 hours ending 78012612.
Forecast.

the control forecast. This comparison probably exaggerates the importance of the PBL on 24-h forecasts in general because of the extreme low-level winds in this case and the large variation in drag coefficient between the two forecasts. Nevertheless, the significant differences suggest that a fine tuning of the PBL model could yield improvements in short-range forecasts of strong cyclones.

BOUNDARY LAYER WINDS

Some applications, including model verification, may require the estimation of mean surface winds from the winds in the lowest layer of the model. Because of the extreme wind speeds in the PBL in this forecast (Fig. 13b), we have applied a one-dimensional high-resolution model of the PBL to two points in the domain in order to relate the winds in the lowest layer of the model (which are essentially inviscid) to winds that would be expected at levels closer to the surface. In addition to providing wind profiles, this procedure also reveals some important diagnostic information on how to improve the treatment of the PBL in the model.

The PBL model is the Level 3 version of the Mellor-Yamada (1974) model as modified by Burk (1977). This model consists of prognostic equations for the 2 horizontal velocity components, liquid water potential temperature, (θ_l), total water mixing ratio (Q_w), turbulent kinetic energy, and the variances of θ_l and Q_w . Diagnostic equations determine the Reynolds stresses ($\overline{u'_i u'_j}$) and the turbulent heat ($\overline{u'_i \theta'_l}$) and water ($\overline{u'_i Q'_w}$) fluxes.

The model consists of 22 levels ($z=1, 10, 25, 50, 90, 150, 250, 400, 600, 800, 1000, 1200, 1400, 1600, 1800, 2000, 2200, 2400, 2600, 2800, 3000, 3200$ m). Initial wind, potential temperature and mixing ratio are provided by the forecast model. Above 600 m, the lowest level in the regional model, the data are obtained by linear interpolation; below 600 m, the data are

assumed to be vertically constant. A roughness length z_0 of 30 cm is chosen as a realistic value for wooded, hilly terrain (Table 3 in Keyser and Anthes, 1977). After 2.5 hours of integration time the PBL profiles reach a slowly varying state, and the results presented here pertain to this time.

Fig. 20 shows the profiles of u and θ_ℓ (which is equal to potential temperature in this case since no liquid water is present) for a point north of the storm (47.6°N 80.0°W). The initial wind and the geostrophic wind speed below 600 m was 24 m s^{-1} . Above 600 m, the initial and geostrophic wind decreased with height to a value of 10 m s^{-1} at 3000 m. The potential temperature increased rapidly with height above 600 m ($\frac{\partial \theta}{\partial z} \approx 14^\circ\text{C km}^{-1}$). Because of the extreme stability, the depth of the PBL was restricted to about 600 m in spite of the strong winds. The profiles above 600 m are virtually unchanged from their initial values. Below 600 m, the wind speed falls off rapidly with decreasing height, so that by 10 m, the speed is about 5 m s^{-1} , or about 5 times lower than the geostrophic wind.

Fig. 21 shows the wind and potential temperature profiles for a point south of the storm (36.5°N , 80.0°W). Here the static stability is less ($\frac{\partial \theta}{\partial z}$ above the PBL $\approx 4^\circ\text{C km}$) and the geostrophic wind is stronger (50 m s^{-1}), so the depth of the PBL increases to 1000 m. For this sounding the 10-m wind is reduced to 9 m s^{-1} , which is again about 5 times lower than the geostrophic wind.

From the above 2 examples, the inviscid forecast winds at the lowest level of the model should be divided by a factor of about 5 to obtain an estimate of the standard level (10-m) mean wind that is reported on surface charts. This reduction brings the winds in Fig. 13b into reasonable agreement with the reported surface winds. The unreduced winds are typical of the maximum gusts reported at many stations.

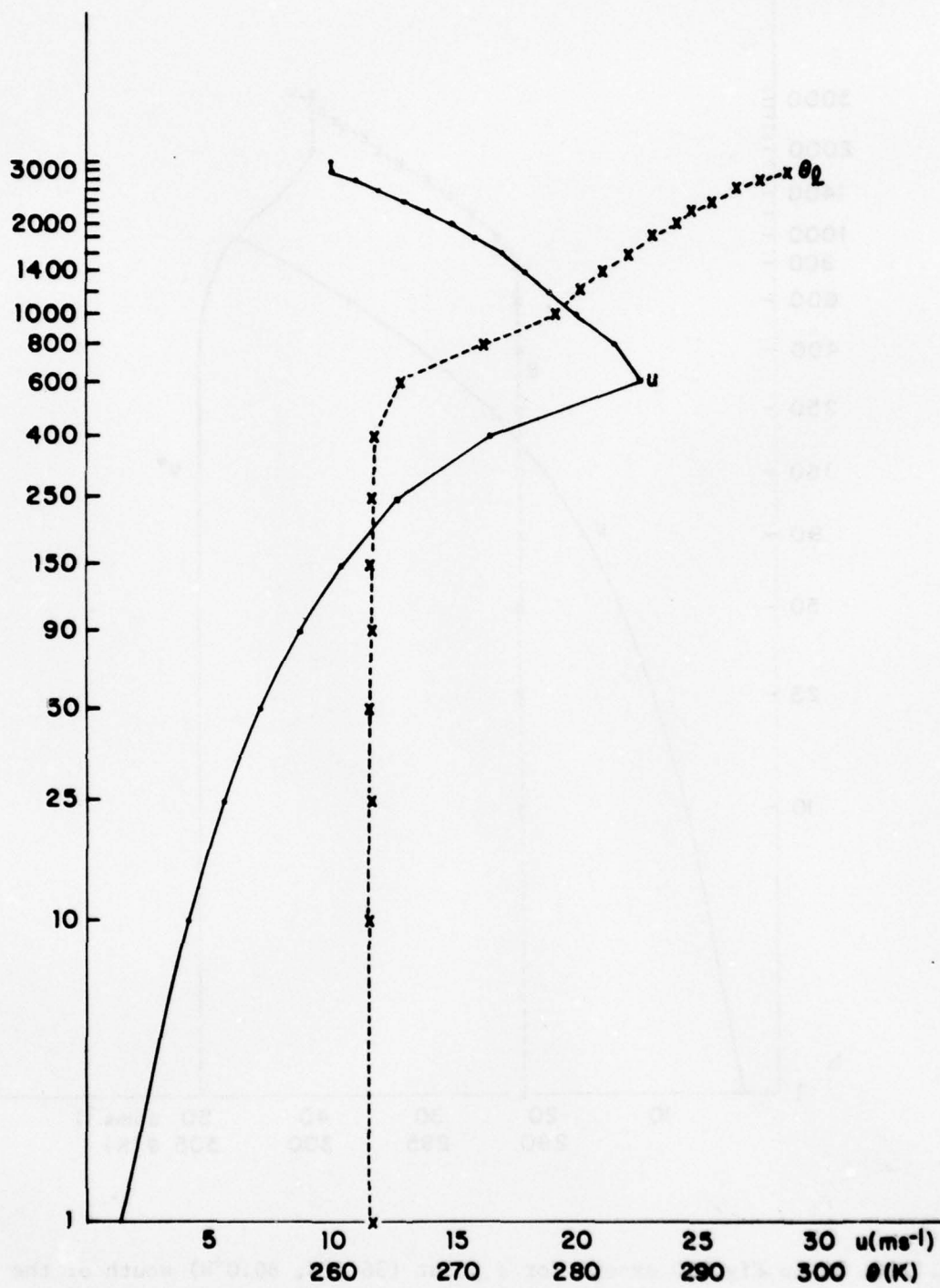


Fig. 20. Vertical profiles of wind component (u) parallel to isobars and liquid water potential temperature (θ) for a point (47.6°N , 80.0°W) at 78012612 as computed by Burk's PBL model. The ordinate is height in m above the surface. Initial and boundary conditions were provided by the fine-mesh forecast as described in text.

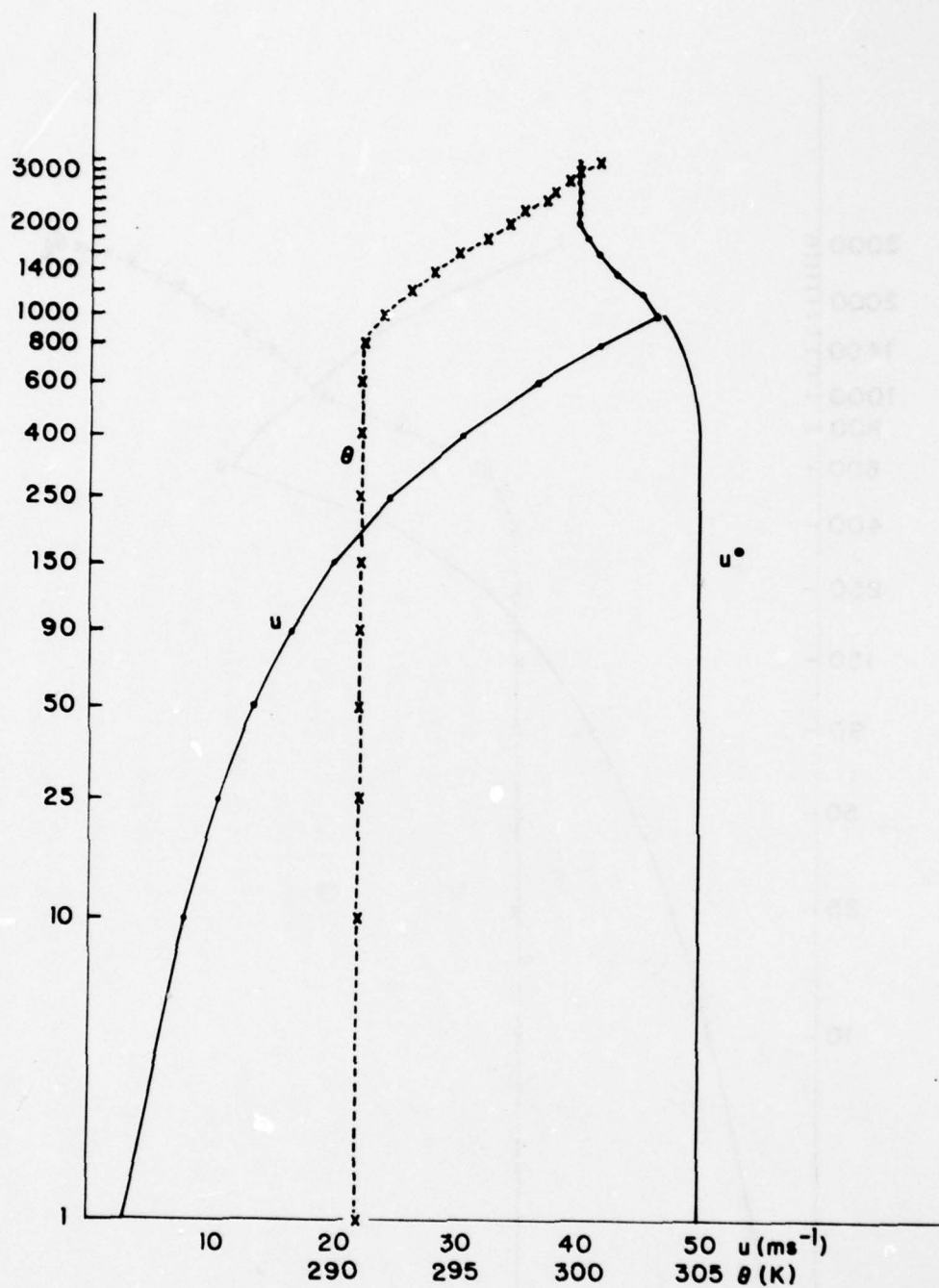


Fig. 21. As in Fig. 20 except for a point (36.5°N , 80.0°W) south of the storm center. The initial and geostrophic u profile is given u^* .

The PBL model provides estimates of the surface stress and depth of the PBL which may be used to estimate drag coefficients appropriate for use with the wind at any level in formulas such as (2), where C_D appropriate to the wind speed V at level z is

$$C_D(z) = u_*^2/V^2 \quad (15)$$

and u_* is the surface friction velocity. Another estimate of C_D appropriate for use with the mean PBL wind speed V_m may be obtained from Deardorff's (1972) method, which relates C_D to a bulk Richardson number and a nondimensional height H/z_0 .

Table 10 lists the surface stress, depth of the PBL, mean frictional acceleration, and drag coefficients appropriate to the 10-m and mean wind in Burk's model and to the mean PBL wind using Deardorff's eq. (33). If we identify the wind at the lowest level in the regional model with V_m predicted by the PBL model, it is clear from Table 10 that the drag coefficients appropriate for the use of (2) should be between 1×10^{-3} and 3×10^{-3} rather than between 5×10^{-3} and 11.45×10^{-3} as given by (3). Therefore, circulations over the portion of the domain which utilize (3) in our forecasts are probably overdamped. This conclusion is consistent with the weak cyclone obtained when the large values of C_D were used over the entire domain (Fig. 13d).

4.4 Role of condensation heating in a model cyclone

The last case to be discussed (US13) is an example of one of the worst forecasts. Starting with initial conditions at 78030300, the control version of the model forecast the development of an intense low over the Florida Panhandle. In reality, only weak intensification occurred. This forecast is instructive because it illustrates that fine mesh models, with their capability of resolving intense small-scale circulations, may require better

physical parameterizations of processes that are associated with sensible or latent energy transfers, since erroneous representation of these processes may produce unrealistic positive feedbacks with the flow. Coarse mesh models tend to average sources and sinks of heat and moisture over large horizontal areas and hence are probably not as sensitive to the parameterization of subgrid-scale processes such as cumulus convection. Fig. 22 shows the SLP and the 500-mb D values and temperatures for the initial time (78030300). A broad area of low pressure existed over Texas and Louisiana with a weak minimum (1003 mb) southwest of New Orleans. A low-amplitude, short-wave trough over Texas disturbed the basically zonal flow across the southern U.S. Heavy precipitation was occurring over the southern U.S. as moist (mixing ratio 10-12 g kg⁻¹) air from the Gulf of Mexico was lifted over a stationary front which extended along the northern Gulf Coast and across northern Florida.

Twelve hours later (78030312) the surface low moved to the Florida Panhandle while deepening only 1 mb (Fig. 23a). Vigorous thunderstorms (tops over 12 km) occurred to the east of the low while more continuous precipitation fell north of the center. The model, which developed strong convective heating immediately after the start of the forecast, deepened the low by 17 mb to a pressure of 986 mb and produced the intense small-scale cyclone shown in Fig. 23b. This cyclone resembled a large tropical cyclone in its symmetric low-level wind structure, its warm core, and heavy precipitation patterns.⁶ In the following 12 h, the low deepened to 971 mb and moved to Wilmington, NC. whereas the actual low had deepened to 994 mb and moved off

⁶ It is interesting to note that the development, which superficially resembles conditional instability of the second kind (Charney and Eliassen, 1964) proceeded without "Ekman pumping."

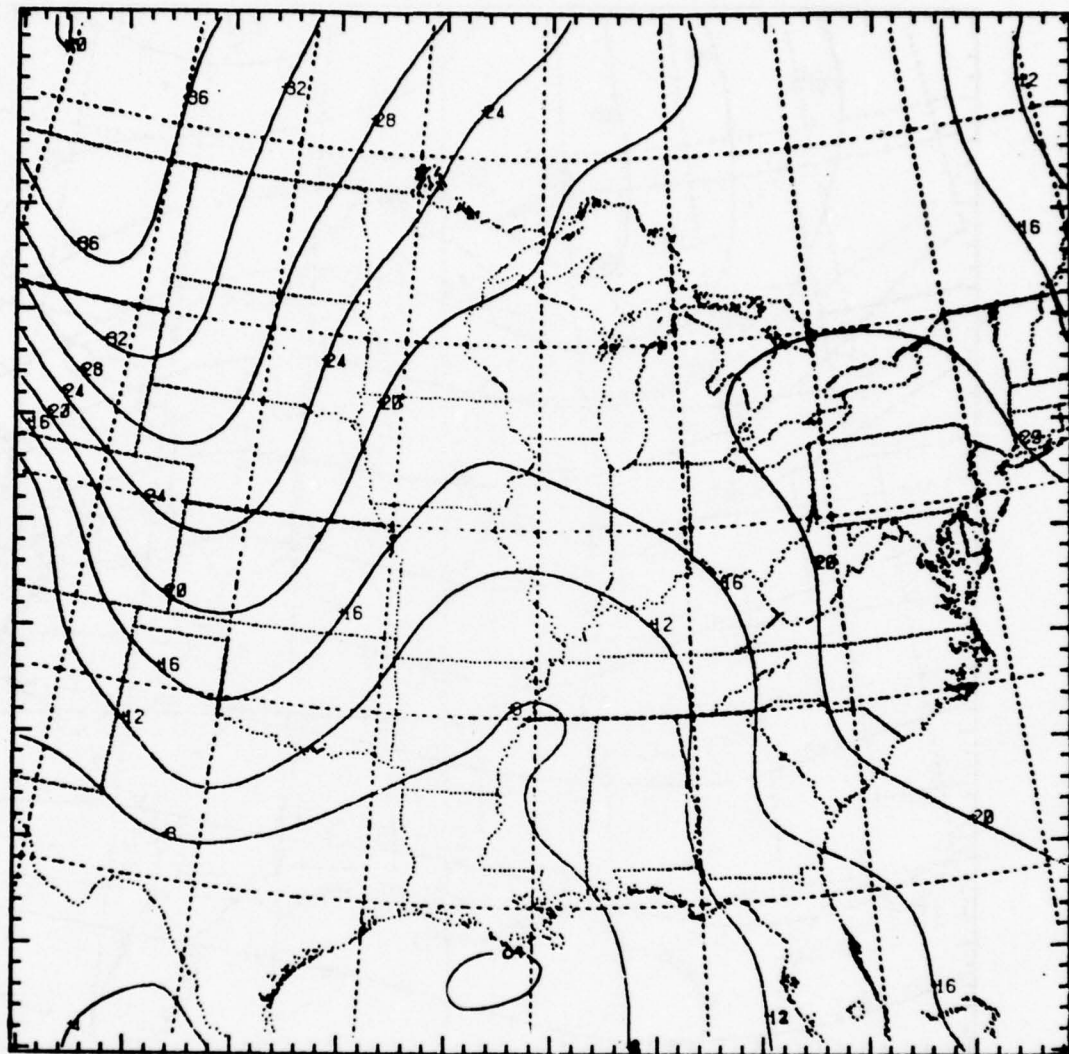


Fig. 22a. Observed (SLP - 1000 mb) for 78030300. The minimum pressure is 1003 mb.

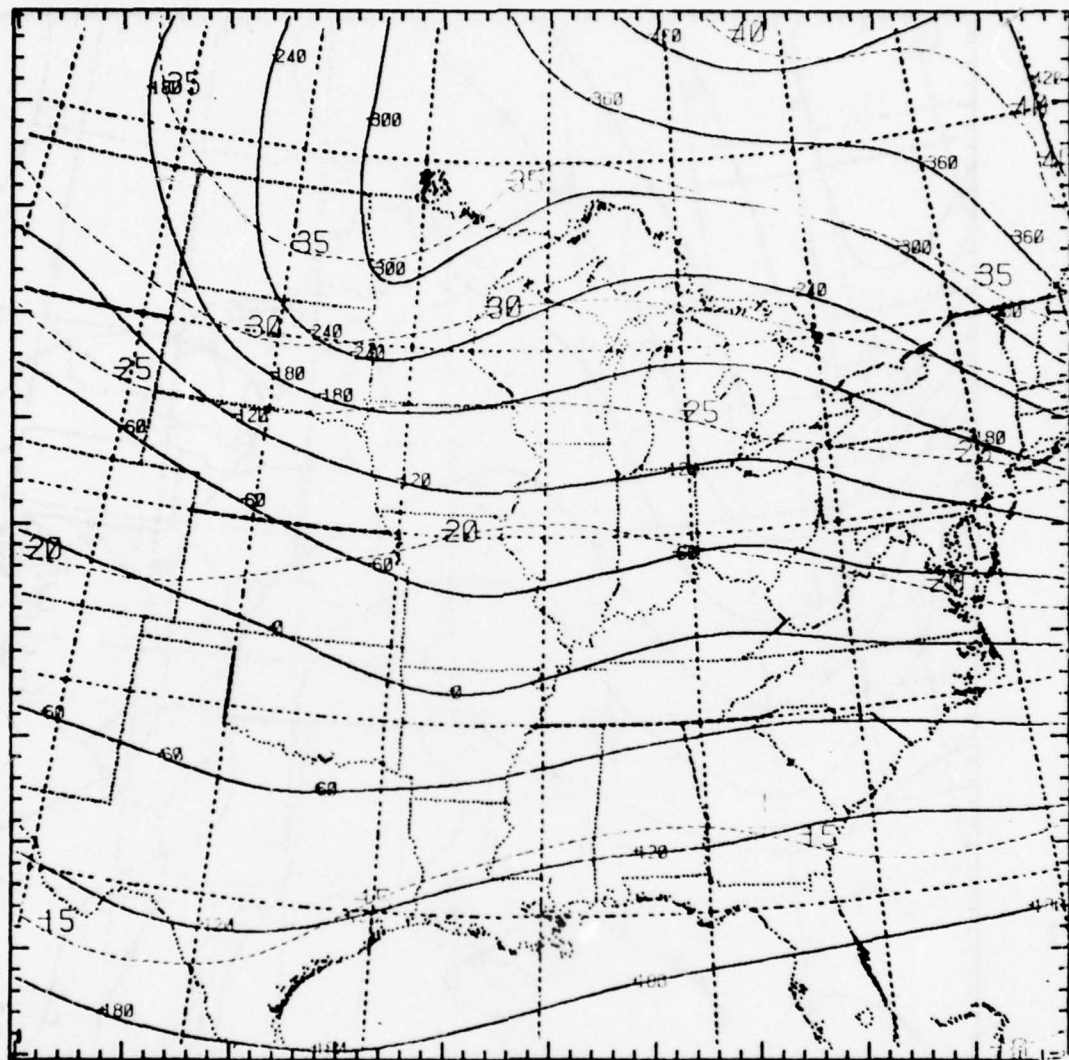


Fig. 22b. Balanced D-values (m) and temperatures ($^{\circ}$ C) at 500 mb for 78030300. The contour interval for the D-values (solid lines) is 60 m; the isotherm (dashed lines) interval is 5° C.

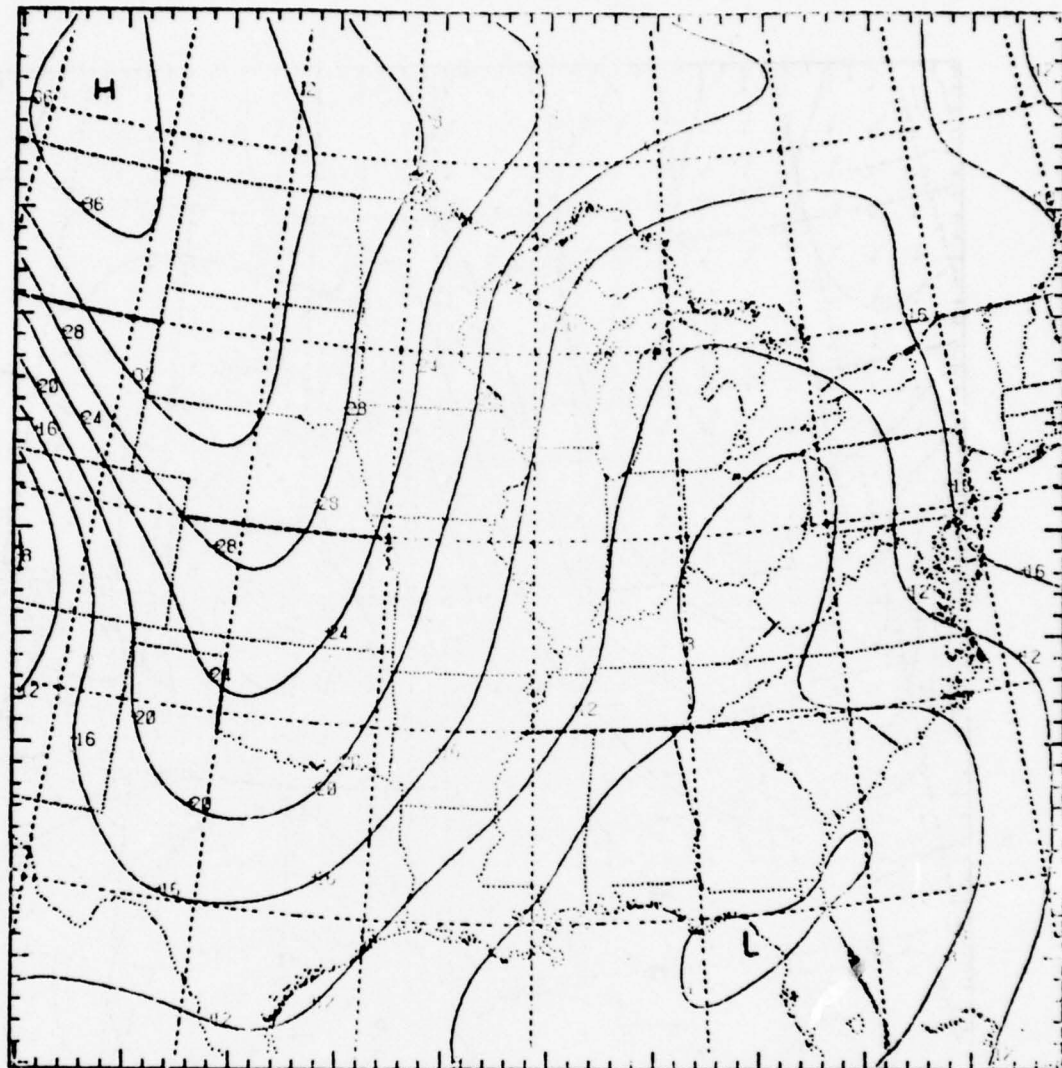


Fig. 23a. Observed SLP-1000 mb for 78030312. The minimum pressure is 1002 mb.

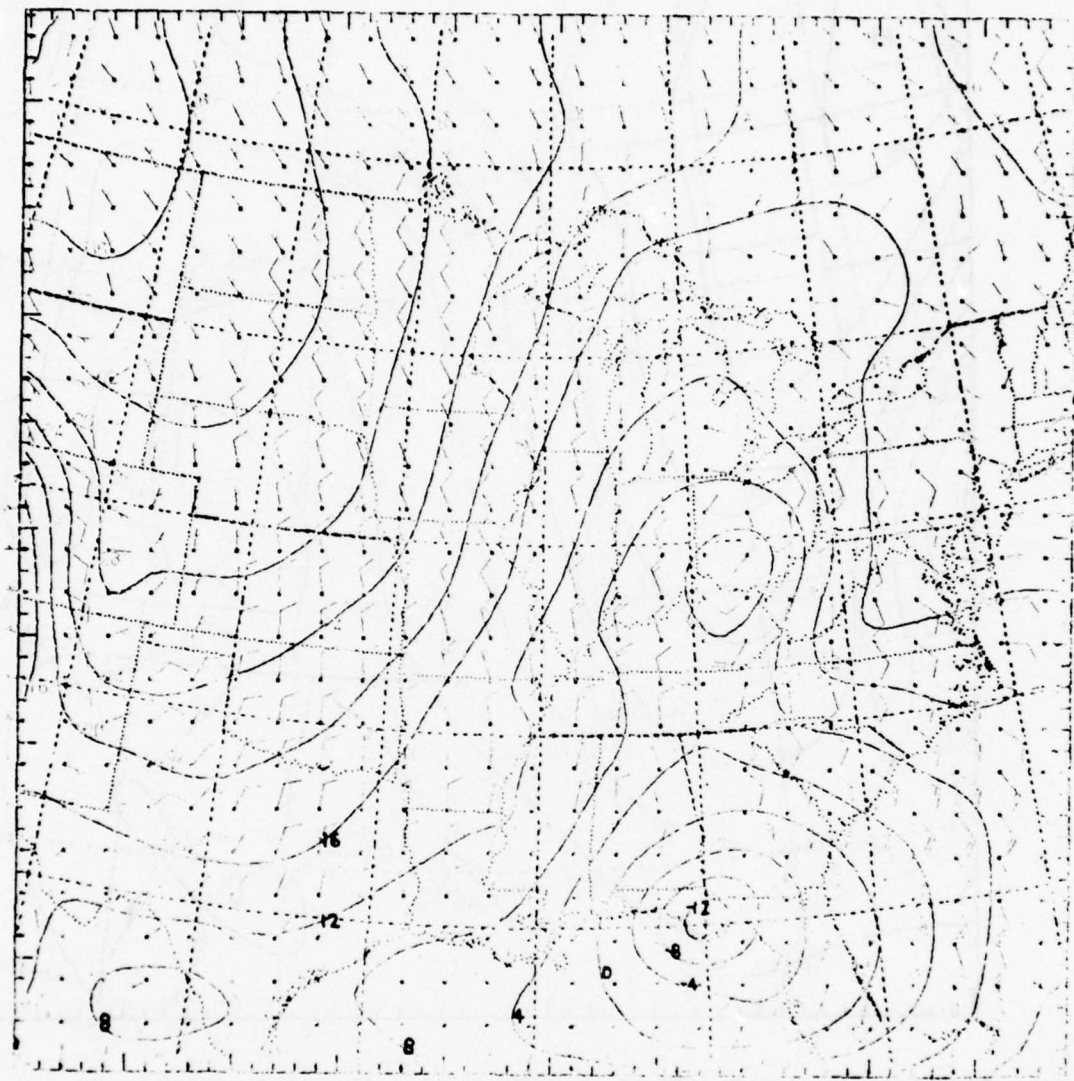


Fig. 23b. 12-h forecast SLP-1000 mb VT 78030312 and winds (m s^{-1}) at $\sigma = 0.925$ for control forecast with latent heating suppressed. The minimum pressure is 986 mb.

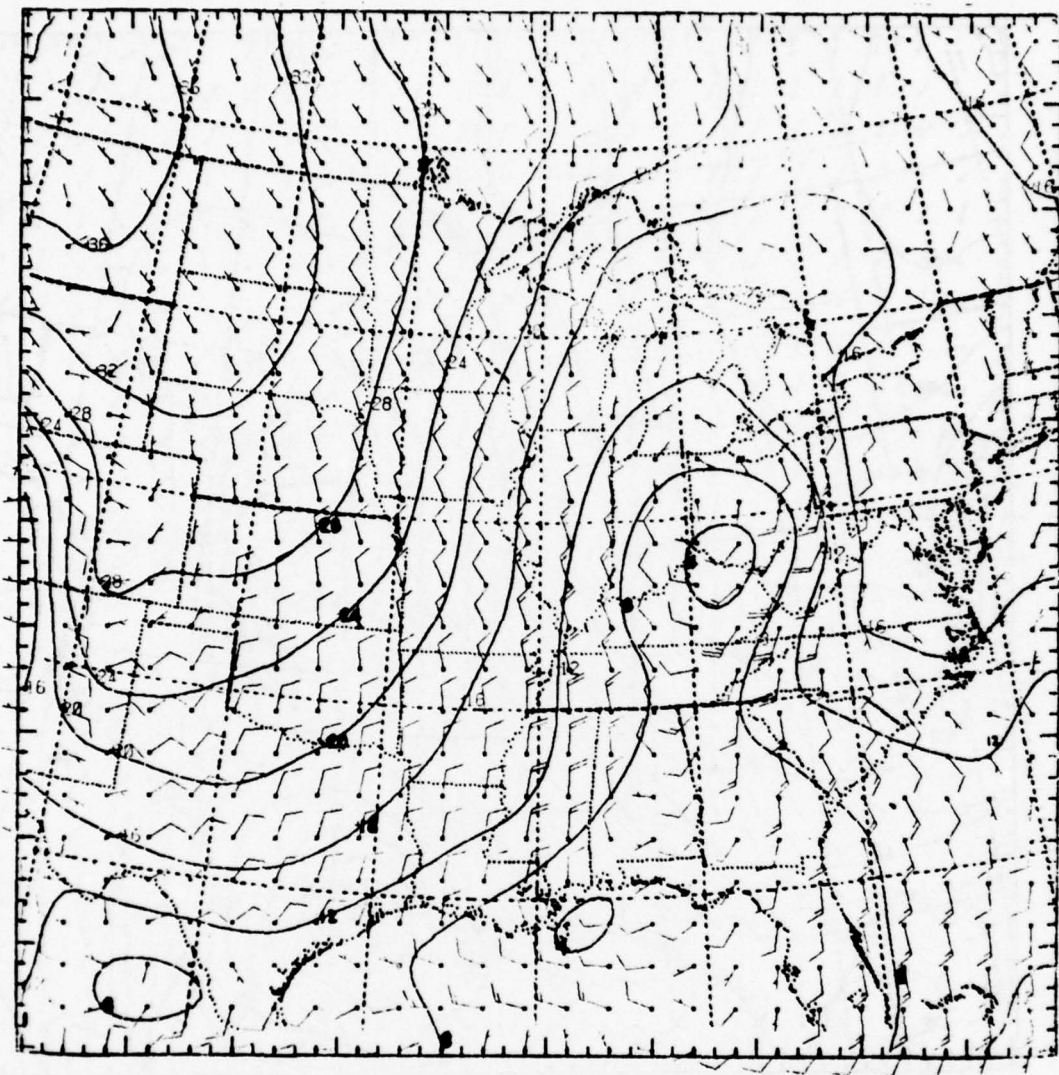


Fig. 23c. 12-h forecast SLP-1000 mb VT 78030312 and winds ($m s^{-1}$) at $\sigma = 0.925$ for control forecast with cumulus parameterization suppressed. The minimum pressure is 1002 mb.

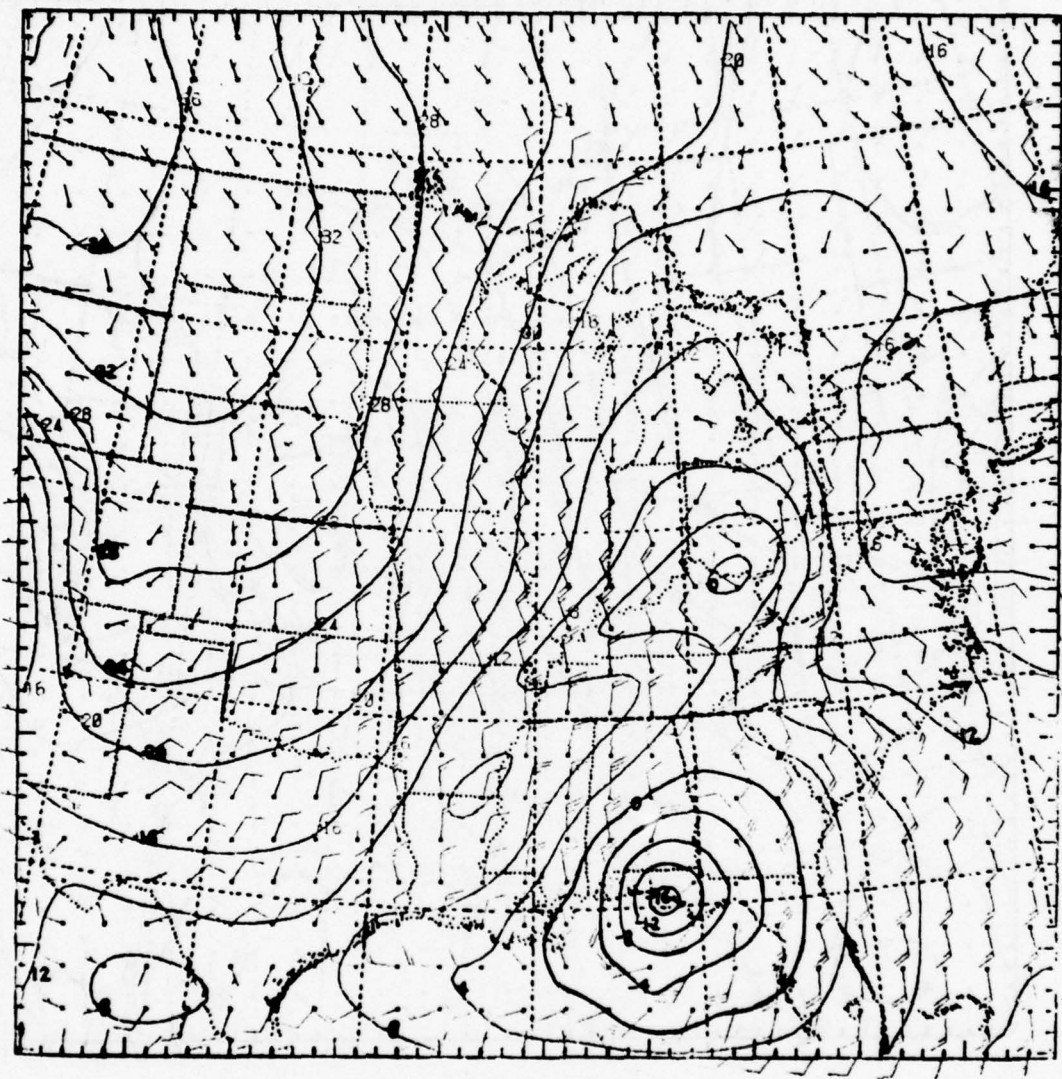


Fig. 23d. 12-h forecast SLP-1000 mb VT 78030312 and winds ($m s^{-1}$) at $\sigma = 0.925$ for control forecast and forecast with revised vertical partitioning of convective heating. The minimum pressure is 983 mb.

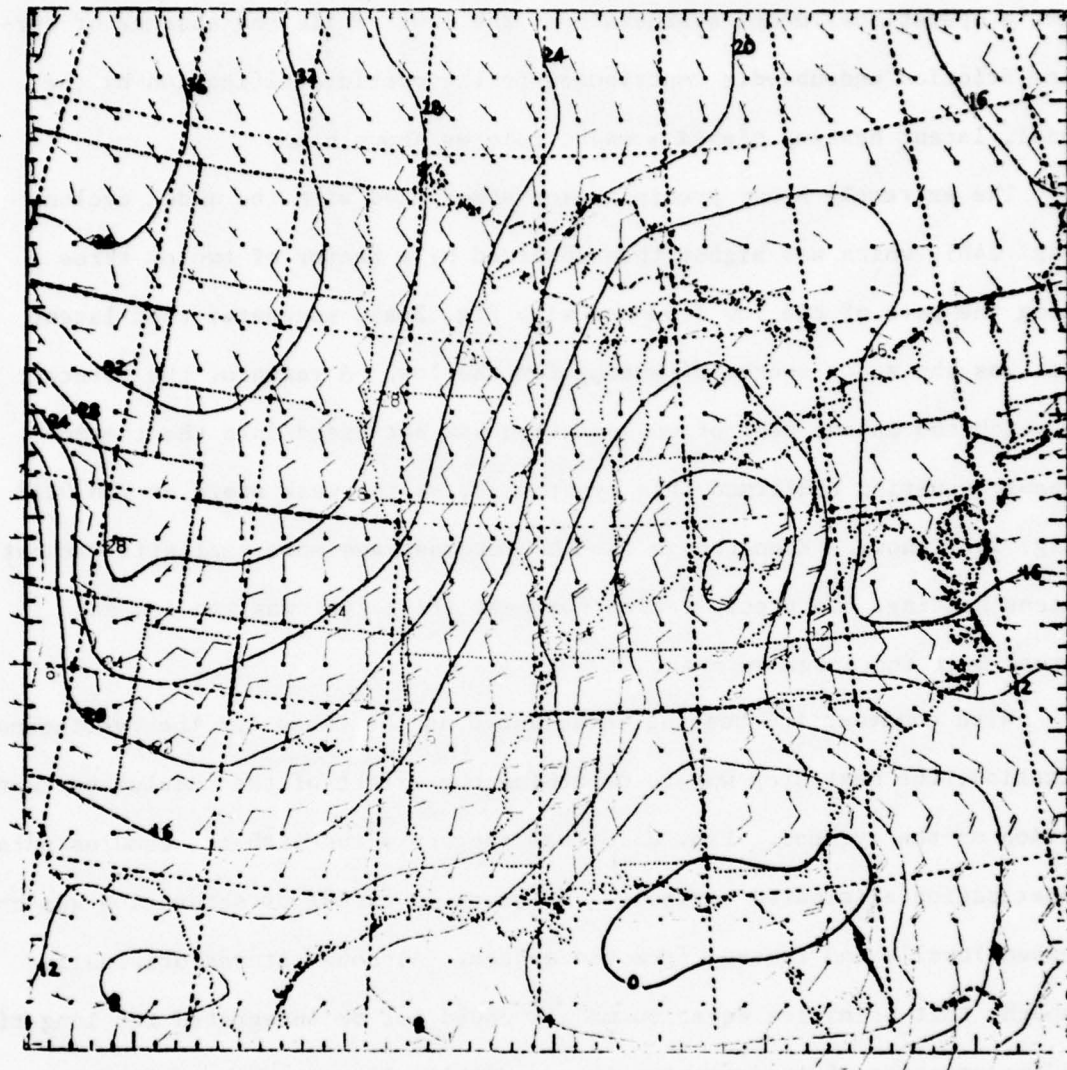


Fig. 23e. 12-h forecast SLP-1000 mb VT 78030312 and winds ($m s^{-1}$) at $\sigma = 0.925$ for control forecast. The minimum pressures is 998 mb.

the New Jersey coast. Neither NMC's limited area fine mesh model nor FNWC's operational model overdeveloped the low. While the absence of surface friction undoubtedly contributed to the overintensification by the model, latent heating played a major role as shown below.

The extremely heavy precipitation associated with the model cyclone (Fig. 24b), which was higher than observed by a factor of two or three along the path of the low (compare with Fig. 24a), suggested that latent heat was the major source of energy for the low. A rerun of the forecast in which the latent heat of condensation was not added into the thermodynamic equation confirmed this hypothesis, as the weak storm at 78030312 (Fig. 23c) shows. Even though the SLP forecast was more realistic without latent heating, the precipitation forecast (Fig. 24c) was too low and spread over too large an area.

With condensation heating established as the cause for the overintensification, the next step was to determine the effect of the cumulus parameterization on the cyclone. Exp. US13B was therefore run with the cumulus parameterization eliminated entirely. Moisture in excess of saturation was condensed locally and removed from the system. Although it was originally thought that primitive equation models could not be integrated for long times in the presence of condensation in a conditionally unstable environment, Rosenthal (1978) has recently shown that vertical transports of heat and moisture by resolvable scales of motion can stabilize the environment without the necessity of cumulus parameterization. In agreement with his results, Exp. US13B proved stable for the 24-h forecast. However, the cyclone at 12 h was more intense than the control (compare Figs. 23d and 23b) and the precipitation forecast was much too high (compare Figs. 24d, 24a and 24b). Apparently the cumulus convective parameterization was acting in the right sense of stabilizing the environment, although its effects were too weak.

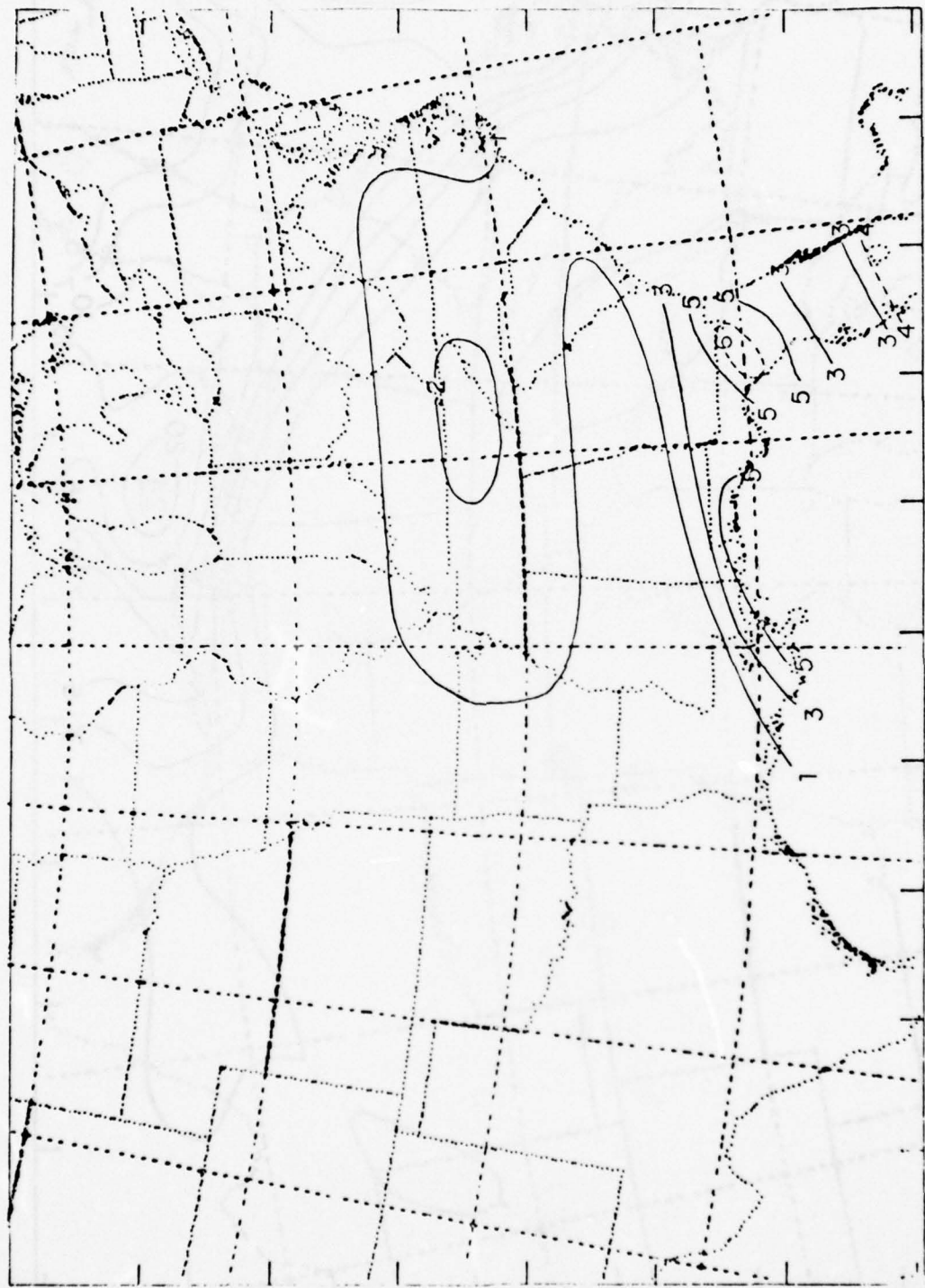


Fig. 24a. Precipitation (cm) for 24 hours ending 78030400.
Observed.

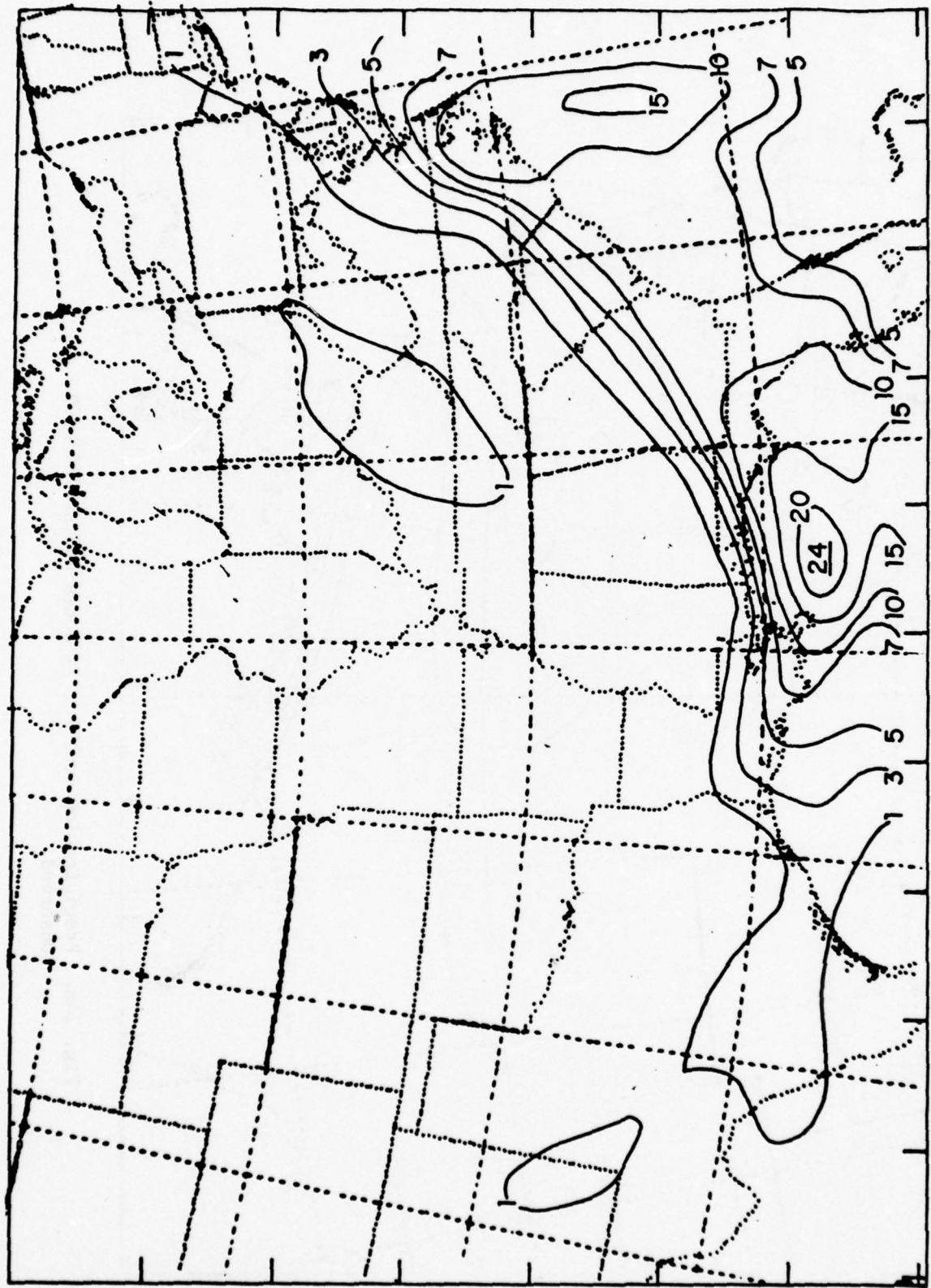


Fig. 24b. Precipitation (cm) for 24 hours ending 78030400.
Forecast (control model).

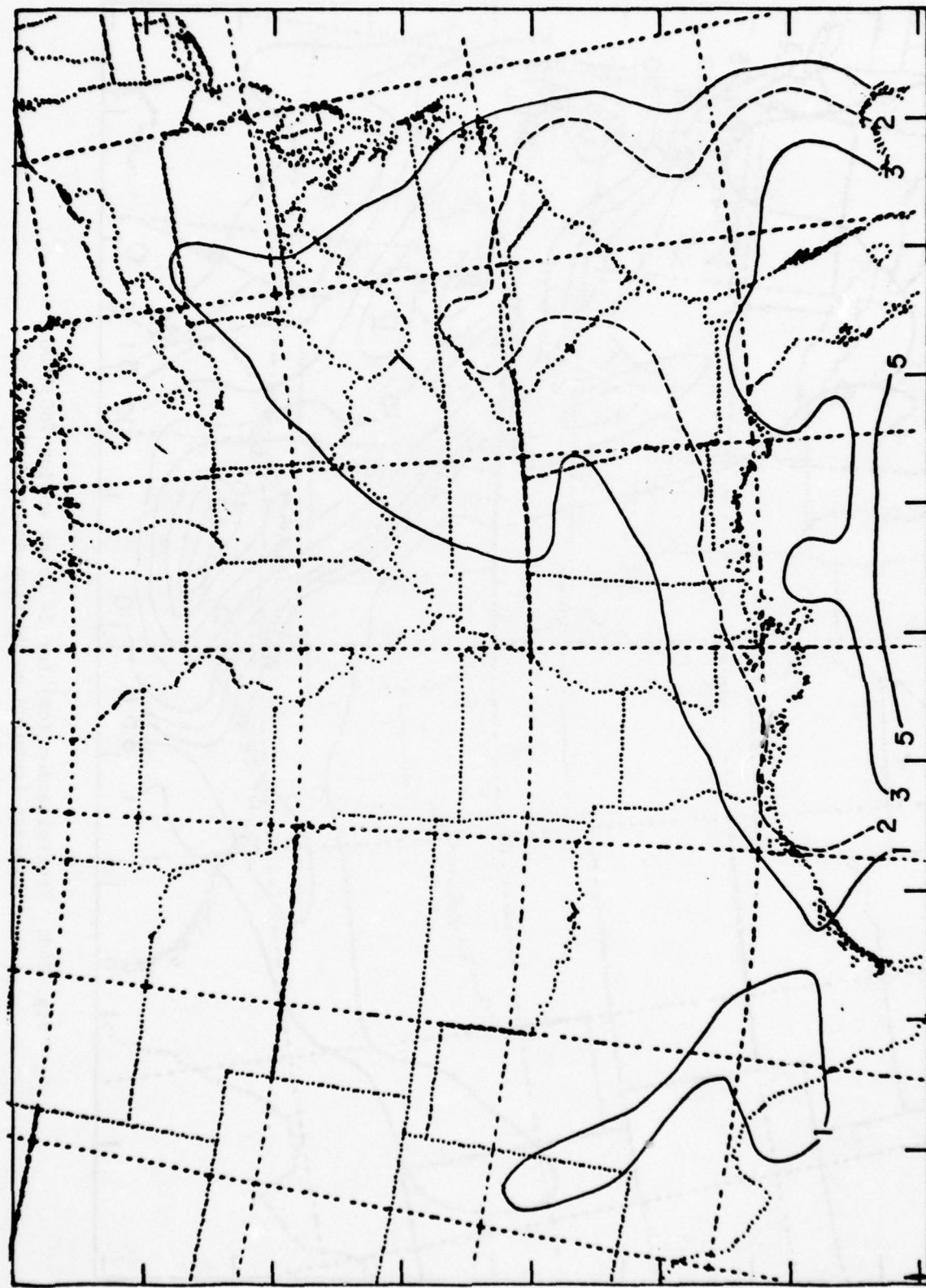


Fig. 24c. Precipitation (cm) for 24 hours ending 78030400.
Forecast (latent heating suppressed).

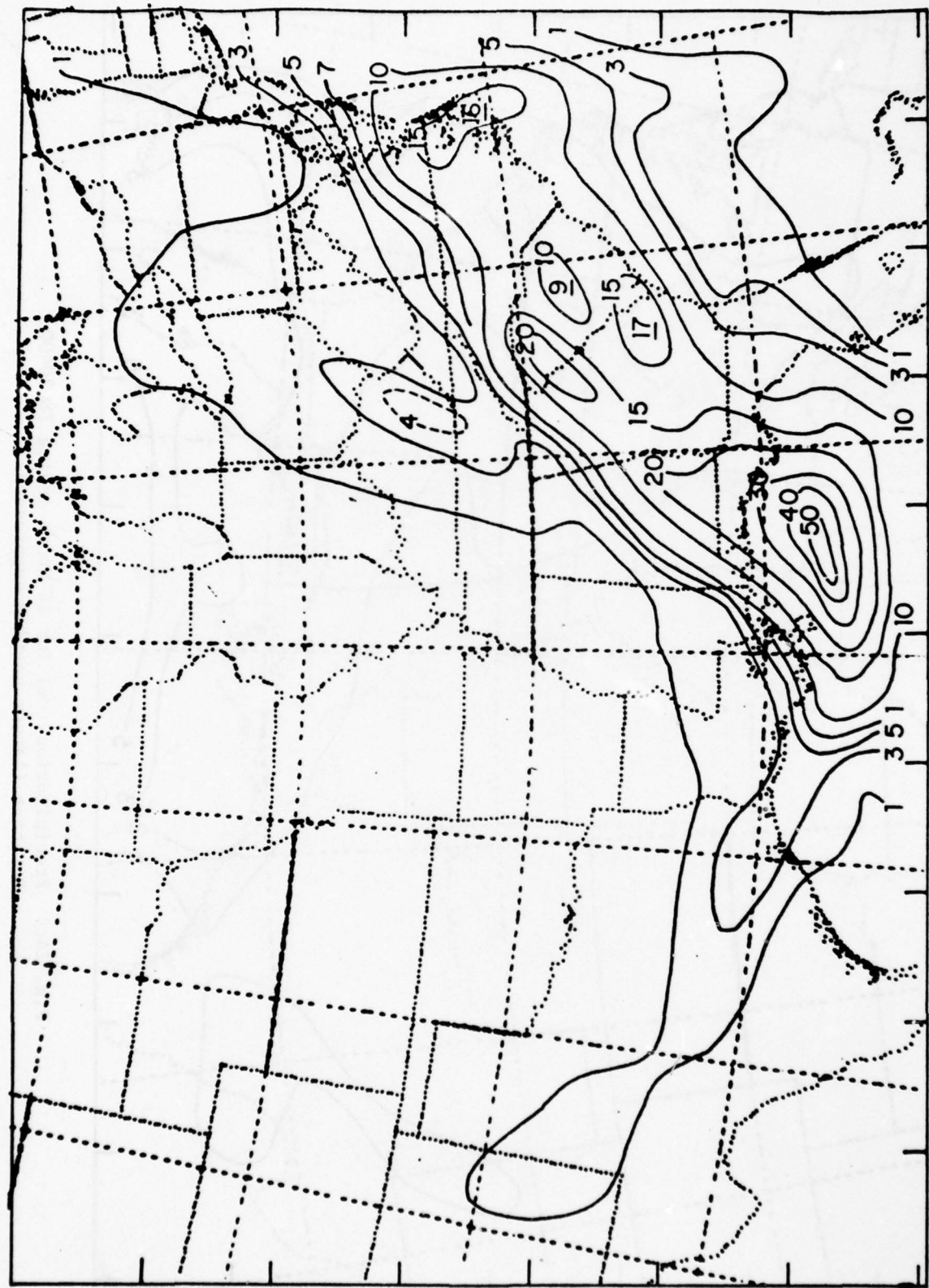


Fig. 24d. Precipitation (cm) for 24 hours ending 78030400.
Forecast (cumulus convection suppressed).

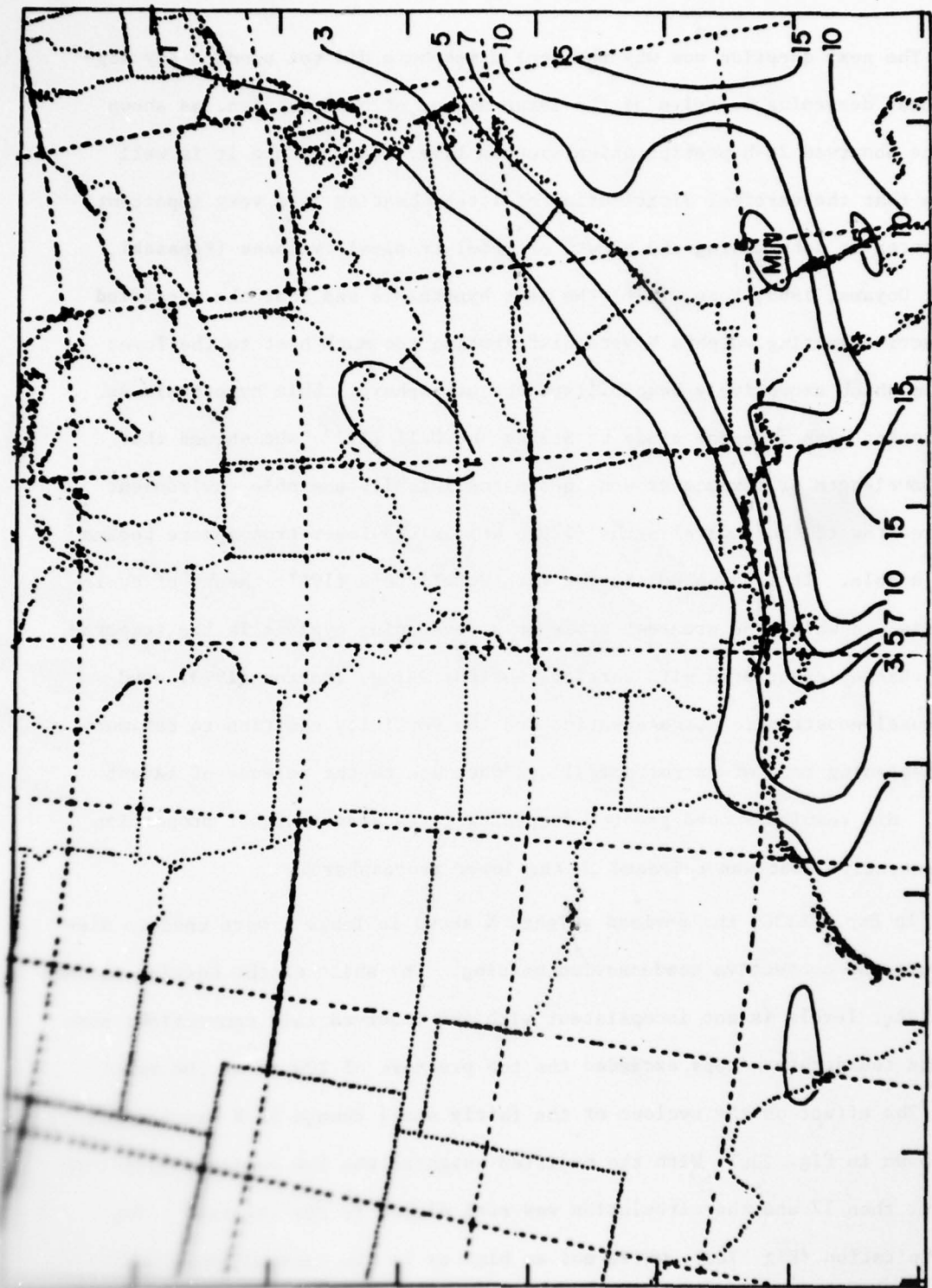


Fig. 24e. Precipitation (cm) for 24 hours ending 78030400.
Forecast (revised vertical partitioning of convective
heating).

The next question was why the real atmosphere did not produce any significant deepening in spite of the large amount of condensation, as shown by the observed 24-h precipitation amounts (Fig. 24a). Since it is well known that the vertical distribution of latent heating is a very important parameter in determining the growth of model tropical cyclones (Yamasaki, 1968; Ooyama, 1969; Koss, 1976) the next hypothesis was that the specified convective heating weights N were distributing too much heat to the lower levels which excessively destabilized the atmosphere. This hypothesis is consistent with a recent study by Staley and Gall (1977) who showed that the wavelength of maximum growth in a baroclinically unstable environment shifted toward short wavelengths (~ 2000 km) as the lower troposphere became less stable. It is also consistent with Sutcliffe's (1947) theory of cyclogenesis, in which the greatest brake on a developing cyclone is the temperature changes associated with vertical motion. Also, Tracton (1973) used the quasi-geostrophic omega equation and the vorticity equation to estimate the deepening rate of extratropical cyclones due to the release of latent heat. His results showed greater deepening rates when a higher proportion of convective heat was released in the lower troposphere.

In Exp. US13C, the revised weights N shown in Table 1 were used to distribute the convective condensation heating. The shift of the heating maximum to higher levels is not inconsistent with the observed tall convection; some of the thunderstorm tops exceeded the top pressure of 200 mb in the model.

The effect on the cyclone of the fairly small change in N was dramatic, as shown in Fig. 23e. With the modified weights, the low deepened only 5 mb rather than 17 and the circulation was much closer to the observed. The precipitation (Fig. 24e), while not as high as in the control experiment (Fig. 24b), was nevertheless very heavy, suggesting that the vertical distribution

of convective heating is as important as the total amount of heating in determining whether a system develops. It is possible that systems which produce heavy rains but do not intensify are stabilized by vertical heating distributions which have high-level maxima.

Some insight into the effect of varying N on the static stability can be seen by comparing soundings taken at the center of the cyclone at 12 and 24 hours into the forecast. Fig. 25 shows that the major effect of the modified N profile given in Table 1 is to cool the lower troposphere so that the static stability in the layer from 800 mb to 400 mb is greatly increased. In the more stable sounding, upward vertical motion produces stronger cooling which inhibits further development. Both soundings at 24-h in Fig. 25 show temperatures that are approximately 5°C too high in the layer from 400 mb to 700 mb. The observed temperature profile was estimated from the NMC analysis over the storm at 78030400. This error is consistent with the overly intense circulation and the excessive precipitation associated with this storm.

The results of experiment US13 and its variations strongly suggest that the treatment of latent heating and cumulus convection is very important in some short-range forecasts of cyclogenesis using fine-mesh models. A proper scheme must be able to discriminate between systems which produce heavy precipitation and yet do not intensify from those in which total heating appears to be responsible for intensification (Tracton, 1973). When we consider the relatively large effect the small differences in N produced, the design of such a scheme appears to be quite challenging.

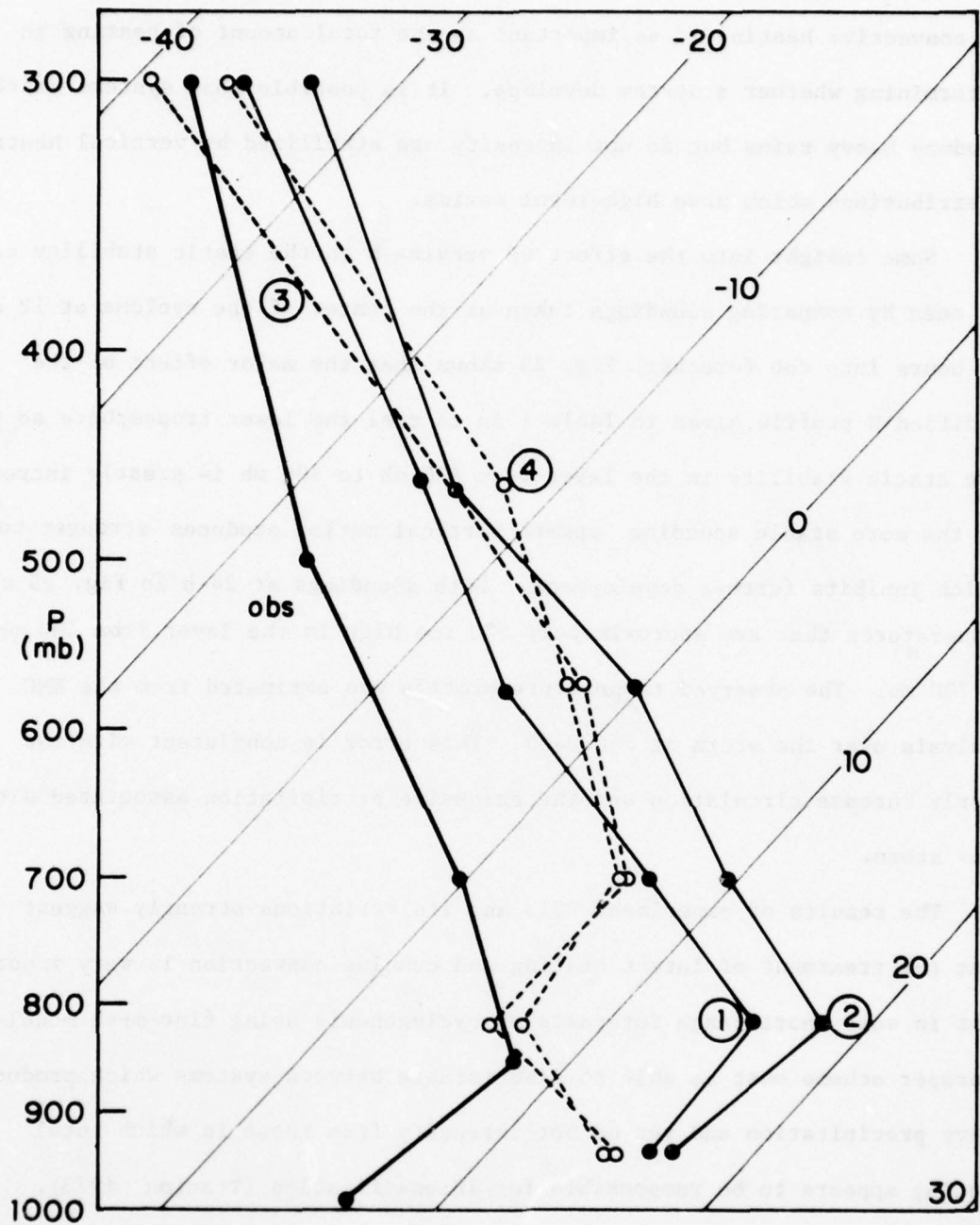


Fig. 25. Temperature soundings in center of model cyclone, initial conditions 78030300.

- 1: 12-h forecast using control model
- 2: 24-h forecast using control model
- 3: 12-h forecast using model with revised vertical partitioning of convective heating.
- 4: 24-h forecast using model with revised vertical partitioning of convective heating.

Observed sounding was constructed from NMC analyses at 78030400.

5. Summary

A total of 32 twenty-four-hour forecasts using a six-layer, 60-km mesh model have been run over western Europe and the eastern United States. The forecasts showed considerable skill in forecasting cyclogenesis in the Mediterranean and over the U.S. The average 24-hour S_1 score for sea-level pressure was 39.1 compared to an average of 45.9 for the FNWC operational model and 73.4 for persistence.

The modifications to the Anthes-Warner (1978) mesoscale model used in these tests were described. These include a simplification of the cumulus parameterization, the use of a ∇^4 rather than ∇^2 horizontal diffusion operator, and the introduction of a weak temporal filter. The noise level of the model was quantitatively assessed and compared to Bleck's (1977) results using an isentropic model.

The unsmoothed model forecasts were verified quantitatively by computing 12- and 24-h S_1 scores for sea-level pressure and by comparing the forecast with the observed minimum pressures associated with the cyclones. The effect of small-scale features in the SLP forecasts on the S_1 score was considered. Removing these features by horizontal smoothing improved the S_1 scores by several points. The model showed considerable skill in forecasting the SLP, although there was a slight bias toward predicting cyclones there were too intense.

Three forecasts were discussed in some detail. The first was a case of cyclogenesis in the Gulf of Genoa which was forecast well by the model. The second was a forecast of the intense Ohio blizzard of January 26, 1978. The model also did reasonably well on this storm. Finally, a case in which the model greatly overpredicted the intensity of a cyclone along the southern coast of the U.S. was presented. Latent heat and the parameterization of cumulus convection were dominant factors in producing the fictitious intensification, as

was shown when the forecast was rerun with changes in the treatment of moisture.

The structure of the PBL in the forecast model was investigated briefly. A high-resolution, higher order closure model of the PBL was supplied with initial and boundary conditions from the forecast model and used to compute a detailed PBL profile of wind and potential temperature. The PBL model indicated that appropriate drag coefficients for use in the quadratic stress law using the mean PBL wind had a value of about 1.0×10^{-3} . This value was considerably lower than the value of 5.0 to 9.5×10^{-3} used over the left half of the domain. Over the right half, C_D was inadvertently zero. Therefore, circulations over the left half of the domain were probably overdamped while those over the right half were underdamped.

The major conclusion from this paper is that significant improvements in 24-hour SLP forecasts were obtained by a model with high horizontal resolution, even though the vertical resolution was coarse and the physics in the model was very simple. They suggest that research should be continued toward developing improved mesoscale models. Aspects of the model that deserve high priority include

- (1) effect of vertical resolution
- (2) improved initialization of mass and moisture fields
- (3) improved treatment of cumulus convection parameterization.

Finally, we note the importance of evaluating the model on a large number of cases. The best forecast of this group would (erroneously) indicate that few problems of forecasting on this horizontal scale remain. On the other hand, the worst forecast might suggest that useful forecasts on this scale are impossible. Only by running the model without changes on many cases can we begin to see patterns emerging which suggest the strengths and weaknesses of the model. In this respect, after evaluation of these forecasts to a greater degree than presented here, we hope to make changes in the model and eventually rerun forecasts using the same data.

References

Anthes, R. A., 1977: A cumulus parameterization scheme utilizing a one-dimensional cloud model. Mon. Wea. Rev., 105, 270-286.

Anthes, R. A. and T. T. Warner, 1978: Development of Mesoscale Model Suitable for Air Pollution and other Mesometeorological Studies. Mon. Wea. Rev., 106, (August issue).

Asselin, R., 1972: Frequency filter for time integrations. Mon. Wea. Rev., 100, 487-490.

Bleck, R., 1974: Short-range prediction in isentropic coordinates with filtered and unfiltered numerical models. Mon. Wea. Rev., 102, 813-829.

Bleck, R., 1977: Numerical simulation of lee cyclogenesis in the Gulf of Genoa. Mon. Wea. Rev., 105, 428-445.

Burk, S. D., 1977: A moist boundary layer with a higher order turbulence closure model. J. Atmos. Sci., 34, 629-638.

Buzzi, A. and R. Rizzi, 1975: Isentropic analyses of cyclogenesis in the lee of the Alps. Riv. Ital. Geofis., Atti del XIII Cong. Intern. Meteor. Alpina, 1, 7-14.

Charney, J. G. and A. Eliassen, 1964: On the growth of the hurricane depression. J. Atmos. Sci., 21, 68-75.

Deardorff, J. W., 1972: Parameterization of the planetary boundary layer for use in general circulation models. Mon. Wea. Rev., 100, 93-106.

Delsol, F., K. Miyakoda and R. H. Clarke, 1971: Parameterized processes in the surface boundary layer of an atmospheric circulation model. Quart. J. Roy. Meteor. Soc., 97, 181-208.

Egger, J., 1972: Numerical experiments on the cyclogenesis in the Gulf of Genoa. Beitr. Phys. Atmos., 45, 320-346.

Hoskins, B. J., 1971: Atmospheric frontogenesis models: some solutions. Quart. J. Roy. Meteor. Soc., 97, 139-153.

Kesel, P. G. and F. J. Winninghoff, 1972: The Fleet Numerical Weather Central operational primitive-equation model. Mon. Wea. Rev., 100, 360-373.

Keyser, D., 1978: An initialization procedure for limited-area models for numerical weather prediction. Naval Postgraduate School Technical Report No. NPS63-78003.

Keyser, D. and R. A. Anthes, 1977: The applicability of a mixed-layer model of the planetary boundary layer to real data forecasting. Mon. Wea. Rev., 105, 1351-1371.

Keyser, D., M. A. Shapiro and D. J. Perkey, 1978: An examination of frontal structure in a fine-mesh primitive equation model for numerical weather prediction. Mon. Wea. Rev., 106, (August issue).

Koss, W. J., 1976: Linear stability of CISK-induced disturbances: Fourier component eigenvalue analysis. J. Atmos. Sci., 33, 1195-1222.

Ludlum, D. M., Weatherwatch January 1978. Weatherwise, 31, 71-74.

McGregor, J. L., L. M. Leslie and D. J. Gauntlett, 1978: The ANMRC limited-area model: consolidated formulation and operational results. Mon. Wea. Rev., 106, 427-438.

Mellor, G.L. and T. Yamada, 1974: A hierarchy of turbulence closure models for planetary boundary layers. J. Atmos. Sci., 31, 1791-1806.

Miyakoda, K., 1975: Weather forecasts and the effects of sub-grid scale processes. Seminars on Scientific Foundation of Medium Range Weather Forecasts, Part II: Reading 1-12 Sept. 1975, 380-593 (European Centre for Medium Range Weather Forecasts).

Miyakoda, K. and A. Rosati, 1977: One-way nested grid models: The interface conditions and the numerical accuracy. Mon. Wea. Rev., 105, 1092-1107.

Ooyama, K., 1969: Numerical simulation of the life cycle of tropical cyclones. Jour. of Atmos. Sci., 26, 3-40.

Orlanski, I. and B.B. Ross, 1977: The circulation associated with a cold front. Part I: Dry Case. J. Atmos. Sci., 34, 1619-1633.

Palmén, E. and C.W. Newton, 1969: Atmospheric Circulation Systems, Academic Press, New York, 603 pp.

Perkey, D.J., 1976: A description and preliminary results from a fine-mesh model for forecasting quantitative precipitation. Mon. Wea. Rev., 104, 1513-1525.

Phillips, N.A., 1978: A Test of Finer Resolution. Office Note 171, National Meteorological Center, Feb. 1978. Unpublished manuscript available from NMC.

Radinović, D., 1965a: On forecasting of cyclogenesis in the western Mediterranean and other areas bounded by mountain ranges by baroclinic model. Archiv fur Meteorologie, Geophys. Bioklimatol., A14, 279-299.

Radinović, D. 1965b: Cyclonic activity in Yugoslavia and Surrounding Areas. Archiv fur Meteorologie, Geophysik und Bioklimatologie, A14, 391-408.

Rosenthal, S.L., 1978: Numerical simulation of Tropical Cyclone development with Latent Heat by the resolvable scales I: Model description and preliminary results. J. Atmos. Sci., 35, 258-271.

Shapiro, M.A. 1974: A multiple-structured frontal zone jet stream system as revealed by meteorologically instrumented aircraft. Mon. Wea. Rev., 102, 244-253.

Shapiro, M.A., 1976: The role of turbulent heat flux in the generation of potential vorticity in the vicinity of upper-level jet stream systems. Mon. Wea. Rev., 104, 892-906.

Shapiro, R. 1970: Smoothing, filtering and boundary effects. Rev. Geophys. and Space Phys., 8, 359-387.

Shuman, F.G., 1957: Numerical methods in weather prediction: I. Smoothing and filtering: Mon. Wea. Rev., 85, 357-361.

Staley, D.O. and R.L. Gall, 1977: On the wavelength of maximum baroclinic instability. J.A.S., 34, 1679-1688.

Sutcliffe, R.C., 1947: A contribution to the problem of development. Quart. Jour. Roy. Meteor. Soc., 73, 370-383.

Teweles and Wobus, 1954: Verification of prognostic charts. Bull. Amer. Meteor. Soc., 35, 455-463.

Tracton, M. Steven, 1973: The Role of Cumulus Convection in the Development of Extratropical Cyclones. Mon. Wea. Rev., 101, 573-593.

Trevisan, Anna, 1976: Numerical Experiments on the Influence of Orography on Cyclone Formation with an Isentropic Primitive Equation Model, J.A.S., 33, 768-780.

Wagner, A. James, 1978: Weather and Circulation of January 1978. Mon. Wea. Rev., 106, 579-585.

Williams, R.T., 1974: Numerical Simulations of Steady State Fronts. Jour. Atmos. Sci., 31, 1286-1296.

Williamson, D.L., 1978: The relative importance of resolution, accuracy and diffusion in short range forecasts with the NCAR Global Circulation Model. Mon. Wea. Rev., 106, 69-88.

Yamasaki, M., 1968: Numerical simulation of tropical cyclone development with the use of primitive equations. J. Meteor. Society Japan, 46, 178-201.

Table 1. Values of $N(\sigma)$ used to distribute convective heat in vertical; cloud updraft velocity, ω_c ; and moisture excess in cloud, $q_c - q$.

σ	0.125	0.325	0.475	0.625	0.775	0.925
N control cases	1.065	1.308	1.356	1.162	0.872	0.194
N modified cases	1.155	1.715	1.540	1.330	0.157	0.0
ω mb/s	0.920	1.160	1.160	0.910	0.520	0.0
q_c g/kg	0.2	1.7	3.5	5.0	4.0	0.0

Table 2. Fraction of initial amplitude remaining after 640 time steps (24h) for various wavelengths $m\Delta s$.

m	
2	3.4×10^{-9}
3	1.9×10^{-5}
4	8.1×10^{-3}
6	0.30
8	0.67
10	0.84
12	0.92
16	0.97

Table 3. Summary of 24-h forecasts: U.S. domain. IC denotes the initial time of the forecast.

<u>Forecast ID</u>	<u>IC</u>	<u>Description</u>
US03	78012212	1034 mb high over Indiana drifts slowly eastward.
US04	78012300	1033 mb high over Ohio drifts off Va. coast.
US05	78012400	1004 mb low forms over Texas, moves to Louisiana, heavy precip Ohio Valley.
US06	78012412	low forms over Texas coast, deepens to 998 mb over Alabama, Heavy precip over Appalachians.
US07	78012500	Low deepens to 980 mb as it moves to eastern Tennessee "Ohio blizzard".
US08	78012512	Low deepens to 958 mb as it moves to southwestern Ontario.
US09	78012600	Low begins to fill slowly as it remains nearly stationary over southern Ontario.
US10	78021300	1002 mb low over Texas deepens to 992 mb over southern Mo. at 12h, then fills to 999 mb over eastern Ky. at 24h.
US11	78021312	992 mb low over srn. Mo. fills to 1000 mb and moves off Va. coast.
US12	77121812	989 low forms off Va. coast, 1001 mb low forms over Oklahoma.
US13	78030300	1000 mb low off La. coast deepens to 994 mb off Va. coast.
US13A		No latent heating.
US13B		No cumulus parameterization.
US13C		Modified vertical distribution of convective heating.
US14	78020600	1016 mb low off N.C. coast deepens to 984 mb off N.J. coast. "Boston blizzard"
US15	78020612	997 mb low off Va. coast deepens to 990 mb off Mass. coast."Boston blizzard"

Table 4 Summary of 24-h forecasts European domain. The minimum pressures are approximate.

<u>Forecast ID</u>	<u>IC</u>	<u>Description</u>
MED01	78011200	998 mb low forms in Gulf of Genoa.
MED03	78012300	1009 mb low in Tyrrhenian Sea deepens to 1007 mb and drifts southeastward.
MED04	78012212	997 mb low over Italy fills, then deepens while remaining nearly stnry.
MED05	78012312	1006 mb low north of Sicily, fills to 1011 mb and moves eastward.
MED06	78012412	1011 mb low south of Greece decays, 1002 mb low forms over Adriatic Sea
MED07	78012500	Weak low forms then decays over Adriatic Sea.
MED08	78020612	998 mb low SE of Greece splits, one low moving NE, another reforming over srn. Italy.
MED09	78021312	999 low ern. Tunisia decays, 998 mb low forms over srn. Italy, moves northeastward.
MED11	78011400	Trough over Ligurian Sea intensifies, 1007 mb low drifts westward toward Spain.
MED12	78011500	1006 mb low off east coast of Spain weakens, moves northwestward over Spain and France.
MED13	78011912	1001 mb low over srn. Italy decays and moves eastward; 992 mb low forms in Gulf of Genoa.
MED14	78012000	1000 mb low over Gulf Genoa deepens to 992 mb and remains stnry.
MED15	77121800	1008 mb low forms south of Sicily.
MED16	77121812	1008 mb low south of Sicily fills to 1011 mb and drifts slowly eastward.
MED17	78030300	1001 mb low south of Greece remains stnry; cyclone intensifies to 997 mb over Pyrenees.
MED18	78030312	1002 mb low south of Greece drifts eastward and weakens; 998 mb low over Pyrenees drifts southeastward to coast of Spain.
MED19	78040200	Rapid development of 993 mb low over Balearic Sea.
MED20	78040212	993 mb low moves from Balearic Sea to Sicily, maintaining its intensity.
MED21	78040300	993 mb low south of Sardinia moves to srn. Italy, maintaining its intensity.

Table 5. Indices of points used in computing S_1 scores. I denotes south-north direction; J denotes west-east direction. Point (1,1) is lower left corner. North latitude is given by ϕ ; west longitude is given by λ .

<u>Point</u>	<u>I</u>	<u>J</u>	<u>ϕ_{US}</u>	<u>λ_{US}</u>	<u>ϕ_{EUR}</u>	<u>λ_{EUR}</u>
1	10	15	31.6	96.5	36.1	2.
2	20	15	37.0	97.0	41.6	3.
3	30	15	42.3	97.8	47.2	4.
4	40	15	48.0	98.6	52.7	5.
5	10	25	31.8	90.0	36.4	-5.
6	20	25	37.2	90.0	41.9	-5.
7	30	25	42.5	90.0	47.5	-5.
8	40	25	48.3	90.0	53.1	-5.
9	10	35	31.5	83.6	36.2	-11.
10	20	35	37.0	83.0	41.7	-12.
11	30	35	42.4	82.3	47.3	-13.
12	40	35	48.0	81.5	52.8	-14.

Table 6. Effect of smoothing on S_1 SLP scores. Smoothing operators are defined by number N of passes and smoothing coefficient v .

		Smoothing operator number:				
<u>Exp</u>		1	2	3	4	5
MED07	12h	25.4	23.9	24.7	23.0	22.6
MED07	24h	46.1	45.3	45.9	42.5	40.0
US08	24h	30.5	30.3	30.4	30.2	30.8
MED01	12h	28.0	27.7	28.1	26.5	25.9
MED01	24h	20.5	19.7	20.4	16.9	16.1
US08	36h	49.6	48.8	49.3	46.8	45.0
Means:		33.4	32.6	33.1	31.0	30.1

1. No smoothing ($N=0$)
2. $N = 1$ $v = 0.5$
3. $N = 6$ $v_i = 0.5$ i odd, $v_i = -0.5$ i even
4. $N = 6$ $v_i = 0.5$ all i
5. $N = 12$ $v_i = 0.5$ all i

AD-A059 905

NAVAL POSTGRADUATE SCHOOL MONTEREY CALIF
TESTS OF A MESOSCALE MODEL OVER EUROPE AND THE UNITED STATES.(U)
AUG 78 R A ANTHES
NPS-63-78004

F/G 4/2

UNCLASSIFIED

NL

2 OF 2
ADA
069905



END
DATE
FILMED
2-78
DDC

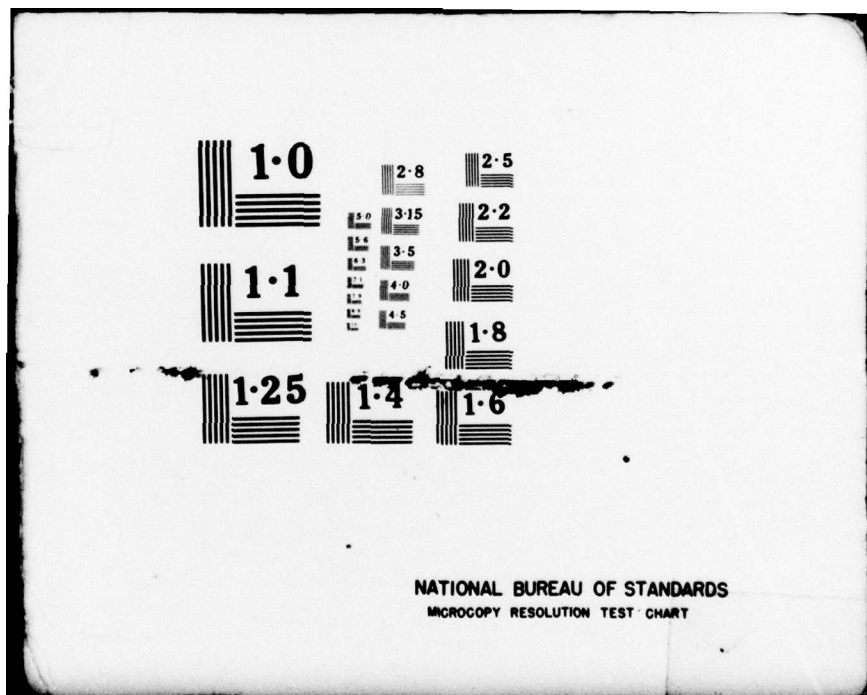


Table 7: S_1 scores for unsmoothed SLP forecasts over U.S.
from fine-mesh model compared to persistence (P)
and FNWC operational hemispheric model.

ID	VT	12-h S_1	12-h P	24-h S_1	24-h P	12-h FNWC S_1	24-h FNWC S_1
US03	78012312	25	24	23	35	25	26
US04	78012400	30	27	27	59	19	31
US05	78012500	26	51	48	85	37	63
US06	78012512	37	59	68	92	29	47
US07	78012600	61	93	35	122	48	48
US08	78012612	34	85	30	96	48	68
US09	78012700	26	62	47	74	31	18
US10	78021400	32	77	46	98	41	63
US11	78021412	32	63	50	86	36	52
US12	77121912	43	63	40	84	56	53
US13	78020400	35	76	51	88	31	50
US14	78020700	28	33	29	40	26	39
US15	78020712	21	22	25	41	22	30
Means:		33.1	56.5	39.9	76.9	34.5	45.2

Table 8. S_1 scores for unsmoothed SLP forecasts over Europe from fine-mesh model compared to persistence P and FNWC operational hemispheric model.

<u>ID</u>	<u>VT</u>	<u>12-h S_1</u>	<u>12-h P</u>	<u>24-h S_1</u>	<u>24-h P</u>	<u>12-h FNWC S_1</u>	<u>24-h FNWC S_1</u>
MED01	78011300	28	67	20	75	24	25
MED03	78012400	26	54	23	70	28	22
MED04	78012312	32	41	41	62	29	37
MED05	78012412	23	52	25	85	21	28
MED06	78012512	28	51	33	62	33	36
MED07	78012600	25	35	46	51	29	37
MED08	78020712	34	31	37	45	39	38
MED09	78021412	33	37	43	50	55	63
MED11	78011500	44	40	52	64	52	58
MED12	78011600	38	46	47	86	40	55
MED13	78012012	45	60	41	73	46	50
MED14	78012100	32	53	25	70	28	20
MED15	77121900	29	41	45	49	35	50
MED16	77121912	40	40	51	53	41	58
MED17	78030400	45	65	61	102	49	75
MED18	78030412	35	63	46	89	56	61
MED19	78040300	53	101	44	112	66	63
MED20	78040312	31	62	31	76	31	57
MED21	78040400	31	56	20	75	40	48
MEANS		34.3	52.4	38.5	71.0	39.0	46.4

Table 9. Distribution of absolute pressure error (mb) for surface cyclones at 24 hours.

Error interval (mb)	Number of cases
0-1	4
2-3	9
4-5	5
6-7	6
8-9	4
10-11	2
12-13	0
14-15	1
over 16	1

Mean absolute error = 5.9 mb

Median absolute error = 2.5 mb

Table 10. Surface stress (τ), depth (H) of PBL, frictional acceleration ($\tau/\rho H$) and drag coefficient (C_D) for 10-m and mean PBL winds as diagnosed from Burk's PBL model. Also shown is C_D appropriate for mean PBL wind obtained by Deardorff's (1972) method.

	$\phi = 36.5^\circ\text{N}$	$\phi = 47.6^\circ\text{N}$
	$\lambda = 80.0^\circ\text{W}$	$\lambda = 80.0^\circ\text{W}$
τ (N m^{-2})	0.774	0.230
H (m)	1000.	600.
H/z_o	3.3×10^3	2.0×10^3
$\frac{\tau}{\rho H}$ (m s^{-2})	7.74×10^{-4}	3.8×10^{-4}
v_m (m s^{-1})	31.8	13.8
v_{10-m} (m s^{-1})	8.8	4.8
$C_D(v_m)$ (Burk)	0.8×10^{-3}	1.2×10^{-3}
$C_D(v_{10-m})$ (Burk)	10.0×10^{-3}	10.0×10^{-3}
$C_D(v_m)$ (Deardorff)	2.3×10^{-3}	2.6×10^{-3}

DISTRIBUTION LIST

	No. Copies
1. Defense Documentation Center Cameron Station Alexandria, Virginia 22314	2
2. Library, Code 0142 Naval Postgraduate School Monterey, California 93940	2
3. Dr. R. T. Williams, Code 63Wu Department of Meteorology Naval Postgraduate School Monterey, California 93940	1
4. Director Naval Oceanography and Meteorology National Space Technology Laboratories Bay St. Louis, Mississippi 39520	1
5. Officer in Charge Navy Environmental Prediction Research Facility Monterey, California 93940	10
6. Dean of Research, Code 012 Naval Postgraduate School Monterey, California 93940	2
7. Commanding Officer Fleet Numerical Weather Central Monterey, California 93940	10
8. Naval Oceanographic Office Library, Code 3330 Washington, D. C. 20373	1
9. AFCRL Research Library Attn: Nancy Davis/Stop 29 L. G. Hanscom Field Bedford, Massachusetts 01730	1
10. Commander, Air Weather Service Military Airlift Command United States Air Force Scott Air Force Base, Illinois 62226	1
11. Dr. A. Arakawa Department of Meteorology University of California Los Angeles, California 90024	1

12. Atmospheric Sciences Library National Oceanic and Atmospheric Administration Silver Spring, Maryland 20910	1
13. Dr. F. P. Bretherton National Center for Atmospheric Research P. O. Box 3000 Boulder, Colorado 80303	1
14. Dr. John Brown National Meteorological Center/NOAA World Weather Building Washington, D. C. 20233	1
15. Dr. C.-P. Chang, Code 63Cj Department of Meteorology Naval Postgraduate School Monterey, California 93940	1
16. Dr. Fred Shuman, Director National Meteorological Center World Weather Building Washington, D. C. 20233	1
17. Dr. R. L. Elsberry, Code 63Es Department of Meteorology Naval Postgraduate School Monterey, California 93940	2
18. Dr. D. Williamson National Center for Atmospheric Research P. O. Box 3000 Boulder, Colorado 80303	1
19. Mr. D. Baumhefner National Center for Atmospheric Research P. O. Box 3000 Boulder, Colorado 80303	1
20. Dr. W. L. Gates Department of Meteorology Oregon State University Corvallis, Oregon 97331	1
21. Dr. R. Somerville National Center for Atmospheric Research P. O. Box 3000 Boulder, Colorado 80303	1
22. Dr. G. J. Haltiner, Code 63Ha Chairman, Department of Meteorology Naval Postgraduate School Monterey, California 93940	5

23. Dr. R. L. Haney, Code 63Ha 1
Department of Meteorology
Naval Postgraduate School
Monterey, California 93940

24. Dr. J. Holton 1
Department of Atmospheric Sciences
University of Washington
Seattle, Washington 98105

25. Dr. B. J. Hoskins 1
Department of Geophysics
University of Reading
Reading, United Kingdom

26. Dr. D. Houghton 1
Department of Meteorology
University of Wisconsin
Madison, Wisconsin 53706

27. Dr. J. Wallace 1
Department of Atmospheric Sciences
University of Washington
Seattle, Washington 98105

28. Dr. Carl Kreitzberg 1
Department of Physics and Atmospheric Science
Drexel University
Philadelphia, Pennsylvania 19104

29. Dr. S. K. Kao 1
Department of Meteorology
University of Utah
Salt Lake City, Utah 84112

30. Dr. A. Kasahara 1
National Center for Atmospheric Research
P. O. Box 3000
Boulder, Colorado 80303

31. Dr. M. G. Wurtele 1
Department of Meteorology
University of California
Los Angeles, California 90024

32. Dr. C. E. Leith 1
National Center for Atmospheric Research
P. O. Box 3000
Boulder, Colorado 80303

33. Dr. J. M. Lewis Laboratory for Atmospheric Research University of Illinois Urbana, Illinois 61801	1
34. Dr. R. Madala Code 7750 Naval Research Laboratories Washington, D. C. 20390	1
35. Dr. J. D. Mahlman Geophysical Fluid Dynamics Laboratory Princeton University Princeton, New Jersey 08540	1
36. Meteorology Library, Code 63 Naval Postgraduate School Monterey, California 93940	1
37. National Center for Atmospheric Research Box 1470 Boulder, Colorado 80302	1
38. Department of Oceanography, Code 68 Naval Postgraduate School Monterey, California 93940	1
39. Office of Naval Research Department of the Navy Washington, D. C. 20360	1
40. Dr. Y. Ogura Laboratory for Atmospheric Research University of Illinois Urbana, Illinois 61801	1
41. Dr. I. Orlanski Geophysical Fluid Dynamics Laboratory Princeton University Princeton, New Jersey 08540	1
42. Prof. N. A. Phillips National Meteorological Center/NOAA World Weather Building Washington, D. C. 20233	1
43. Dr. S. Piacsek Code 7750 Naval Research Laboratory Washington, D. C. 20390	1

44. Dr. J. Smagorinsky, Director 1
Geophysical Fluid Dynamics Laboratory
Princeton University
Princeton, New Jersey 08540

45. Dr. T. Rosmond 2
Naval Environmental Prediction Research Facility
Monterey, California 93940

46. Dr. R. Pielke 1
P. O. Drawer 5508
Charlottesville, Virginia 22903

47. Dr. Chester Newton 1
National Center for Atmospheric Research
P. O. Box 3000
Boulder, Colorado 80303

48. Dr. Harry Orville 1
Institute of Atmospheric Science
South Dakota School of Mines & Technology
Rapid City, South Dakota 57701

49. Professor Yoshi K. Sasaki 1
Department of Meteorology
University of Oklahoma
Norman, Oklahoma 73019

50. Mr. Murray Schefer 1
Naval Air Systems Command 370C
Washington, D. C. 20361

51. Dr. A. Wiin-Nielsen 1
European Centre for Medium Range
Weather Forecasts
Fitzwilliam House, Skimped Hill
Bracknell-Berks U.K.

52. Dr. Donald Johnson 1
Space Science and Engineering Center
University of Wisconsin
1225 West Dayton Street
Madison, Wisconsin 53706

53. Prof. T. Krishnamurti 1
Florida State University
Department of Meteorology
Tallahassee, Florida 32306

54. Dr. Y. Kurihara 1
Geophysical Fluid Dynamics Laboratory/NOAA
Princeton University
Princeton, New Jersey 08540

55. Dr. L. Leslie 1
Australia Meteorology Research Centre
P.O. Box 5089AA
Melbourne, Victoria 3001
Australia

56. Dr. A. Robert 1
Centre Meteorologique Canadienne
2121 Voie De Service Nord, Suite 100
Route Trans Canada
Dorval, Quebec-Canada H9P 1J3

57. Dr. L. Bengtsson 1
European Centre for Medium Range
Weather Forecasts
Fitzwilliam House, Skimped Hill
Bracknell, Berks U.K.

58. Mr. F. Bushby 1
Meteorological Office
London Road
Bracknell, Berks, U.K.

59. Dr. J. Egger 1
Meteorologisches Institut
Der Universitat Munchen
Theresienstrasse 37
D8000 Munchen 2, F.R.G.

60. Dr. J. Hovermale 1
National Meteorological Center/NWS
NOAA World Weather Building
Washington, D. C. 20233

61. Mr. Edward H. Barker 1
Naval Environmental Prediction Research Facility
Monterey, California 93940

62. Terry Tarbell 1
Department of Meteorology
The Pennsylvania State University
503 Walker Building
University Park, Pennsylvania 16802

63. Dr. Thomas T. Warner 1
Department of Meteorology
The Pennsylvania State University
503 Walker Building
University Park, Pennsylvania 16802

64. Daniel Keyser 1
Department of Meteorology
The Pennsylvania State University
503 Walker Building
University Park, Pennsylvania 16802

65. Dr. Richard A. Anthes 20
Department of Meteorology
The Pennsylvania State University
503 Walker Building
University Park, Pennsylvania 16802

66. Richard M. Hodur 1
Naval Environmental Prediction Research Facility
Monterey, California 93940

67. Dr. Donald J. Perkey 1
National Center for Atmospheric Research
P. O. Box 3000
Boulder, Colorado 80307

68. Dr. James E. Hoke 1
11812 South 31st Street
Omaha, Nebraska 68123

69. Dr. Nelson L. Seaman 1
Department of Atmospheric Science
P. O. Box 3038
University of Wyoming
Laramie, Wyoming 82071

70. Patrick C. Gallacher 1
Department of Meteorology, Code 63Ga
Naval Postgraduate School
Monterey, California 93940

71. Dr. Francis Binkowski 2
Research Triangle Park
Meteorology Division
North Carolina 27709

72. Dr. Chandrakant M. Bhumralkar 1
Stanford Research Institute
333 Ravenswood Avenue
Menlo Park, California 94025

73. Dr. Robert F. Adler 1
NASA, Goddard Space Flight Center
Greenbelt, Maryland 20771

74. Dr. Simon Chang 1
JAYCOR
205 S. Whiting Street
Alexandria, Virginia 22314

75. Dr. Rainer Bleck 1
Department of Meteorology
University of Miami Beach
Coral Gables, Florida 33124

76. Dr. Alan McNab 1
Department of Meteorology
The Pennsylvania State University
503 Walker Building
University Park, Pennsylvania 16802

77. Dr. John Cahir 1
Department of Meteorology
The Pennsylvania State University
503 Walker Building
University Park, Pennsylvania 16802

78. Dr. John W. Diercks 1
818 Arlene Avenue
Papillion, Nebraska 68046

79. Dr. William Gray 1
Department of Atmospheric Sciences
Colorado State University
Fort Collins, Colorado 80523

80. Dr. William Cotton 1
Department of Atmospheric Sciences
Colorado State University
Fort Collins, Colorado 80523

81. Dr. Stanley L. Rosenthal 2
National Hurricane and Exp. Lab.
P. O. Box 248265
Coral Gables, Florida 33124